ED-ARCHMAT

PhD Thesis

LASER BASED INTERVENTION ON HISTORICAL STAINED-GLASSES

Evan Maina Maingi

Burgos (Spain), May 2022

Supervisors:
María Pilar Alonso Abad
Rémy Chapoulie
Luis Alberto Angurel Lámban

UNIVERSIDAD DE BURGOS

Université BORDEAUX MONTAIGNE

INMA INSTITUTO DE NANOCIENCIA Y MATERIALES DE ARAGÓN

CSIC Universidad Zaragoza

TABLE OF CONTENTS

Acknowledgements

I would like to express my sincere gratitude to my supervisors and to all who have contributed to the success of this project in one way or the other. I owe very special gratitude to the following people for their consistent support and guidance during the running of this project;

Prof. Luis A. Angurel for his immense support, guidance and overall insight in this complex field of laser conservation, and for making this an inspiring experience for me. Prof. María Pilar Alonso Abad for her advice, support and valuable contributions in the field of history of stained glasses and for availing the important glass samples that have been used in this project.

Prof. Rémy Chapoulie for his invaluable guidance, insights and assistance in correcting the imperfections in this dissertation and for organizing my visit to Maison-Lorin glass conservation workshop to gain that valuable experience first-hand from Elodie Vally, an experienced stained-glass conservator. Dr. Stèphan Dubernet for his enthusiasm for this project, his support and for his contribution to data collection and interpretation. Yannick Lefrais for his support and assistance in data collection for XRF and SEM-EDS.

I also express my gratitude for the funding support from H2020-MSCA-ITN-EJD/ED-ARCHMAT action under the Marie Sklodowska-Curie grant agreement No. 766311. For the partial support obtained from Gobierno de Aragón "Construyendo Europa desde Aragón" (research group T54_20R) and for the availability and the use of the Servicio General de Apoyo a la Investigación at the University of Zaragoza. Also to mention and thank the team working under the framework of the Unidad Asociada de I+D+I al CSIC "Vidrio y Materiales del Patrimonio Cultural (VIMPAC)", INMA (CSIC-University of Zaragoza) and the University of Burgos as well as the team at the Université Bordeaux Montaigne France for all the support.

Finally, to my caring loving wife Priscilla, my lovely daughters Letishia and Aviela; my deepest gratitude. Your encouragement during the tough times has come a long way in making this journey a success.

Abstract

Stained-glass windows form an important part of cultural heritage. Human and environmental factors have subjected these pieces to damage. Mechanical and chemical-based cleaning methods have been used for their restoration and conservation, which have practically not changed much and have overtime become the conventional methods. Ultra-short pulse lasers have opened up new opportunities for safe and controlled decontamination. These types of lasers are promising because they are controllable, safe under certain condition of use and are environmentally friendly among other advantages. In this work, ultra-short picosecond and femtosecond pulsed lasers have been used for developing laser cleaning protocols of the surface of a series of contemporary stained-glasses frequently used in restoration; one of the objectives being to explore the applicability of using these lasers to safely clean historical stained-glass windows and to define safe and effective protocols for laser cleaning of these glasses. Results showed that, even when working with energy values lower that the damage threshold, the limiting factor was the heat accumulation in the coating layer that was being eliminated, subsequently generating significant and destructive thermal stresses. Different laser cleaning protocols have been designed allowing a control of the laser induced local temperature gradients that could deteriorate the glass. Two different alternatives were explored. The first one is based on applying the burst mode when using lasers operating with frequencies in the range of several hundreds of kHz. This protocol is based on limiting the number of pulses in each burst and selecting an adequate time lapse between two consecutive burst runs. The second one is based on reducing the effective frequency to values lower than 20 kHz. The established protocols were applied for laser cleaning of historical stained-glass windows from Cuenca cathedral (Spain) and Chartres cathedral (France). The glasses were analyzed before and after laser cleaning by optical and confocal microscopy, scanning electron microscopy, energy dispersive X-ray spectroscopy, X-ray fluorescence and Raman spectroscopy. It was possible to place the glasses in their historical context as well as to identify the constituent compounds of the crust that had formed on the surface of these glasses. Laser cleaning results showed that the proposed protocol was effective in decontaminating the historical glasses without inducing damage to the grisaille layer or on the glass substrate. Finally, a study was carried out to make a comparison between conventional restoration methods with laser cleaning. It was demonstrated that laser cleaning is an effective, safe, fast, precise and controllable technique for restoration of historical stained-glass windows.

Aims and focus of the research project

The use of laser technology as a restoration technique in cultural heritage has been a subject of research for the last several decades. Some investigations focusing in gaining and broadening the knowledge in laser cleaning of glasses have explored the opportunities associated with this technologies and results have been promising albeit with challenges due to the limitations with the type of lasers used. Pulsed lasers that were used in the near past operated in longer pulse durations and because of that they were deemed inadequate especially in overcoming problems associated with temperature gradients during laser cleaning. However, laser technology has evolved rapidly with the development of short-pulsed (ns) to ultra-short-pulsed (ps) and recently to ultra-short-pulsed (fs) lasers. This has opened up new frontiers for safe and controlled laser restoration of delicate materials such as stained-glass windows. Now pulse durations can be adjusted in the ranges of fs and ps working with frequencies selected from a few kHz to MHz guaranteeing more control when using these lasers. Newer developments in laser technology has also seen the incorporation of galvanometric mirrors that offers the advantage of a high precision of the laser beam movement during laser processing. This work explores the applicability of ultra-short ps and fs pulsed lasers in the restoration of historical stained glasses with cleaning protocols being developed using contemporary stained glasses.

The project aims at making contributions to the knowledge about laser-glass interaction from a conservation and restoration point of view. Several techniques will be applied to realize the final results. In Chapter 1, an assessment of the literature and previous work performed on-site by conservation specialists regarding glass used in historic monuments will be carried out. There will also be a definition and comparison of the state of the art of restoration methods and their influence on selected historic glasses. Chapter 2 shows an initial evaluation of laser-glass interaction, taking into consideration laser emission parameters and material physico-chemical properties. A description of the laser systems, their characteristics and that of the different techniques used to analyze the surface morphology and elemental composition of the glasses before and after laser treatments (optical and confocal microscope, scanning electron microscope (SEM), energy dispersive X-ray spectroscopy (EDS), X-ray fluorescence (XRF) and Raman spectroscopy, temperature recording using a thermocamera) have also been included. In Chapter 3, a description of the contemporary and historical stained-glass samples that have been studied in this work is presented. Chapters 4 shows the importance of heat accumulation during laser cleaning process and a protocol based on the use of a laser burst configuration

is presented. This technique is adequate for systems that can only work with frequencies of the order of hundreds of kHz. Chapter 5 has been devoted to the development of laser cleaning processes using a fs laser. These processes have been applied to clean several historical stained-glass samples. A comparison of laser cleaning and traditional chemical cleaning of a historical stained-glass sample is presented in Chapter 6 and finally, the main conclusions of the work are presented in Chapter 7.

The main purposes of this work have been:

- to investigate the relevance and the influence of laser parameters in laser cleaning of glasses,
- to advance the understanding of laser interactions with historic stained-glasses,
- to develop a practical criterion for the application of laser technology in cultural heritage conservation,
- to develop skills that are necessary for an informed selection and safe operation of lasers in solving problems associated with the removal of corrosion products affecting cultural heritage glasses,
- to carry out experiments to explore the applicability of ultra-short pulsed lasers for the restoration of historical stained glasses and
- to make a comparison between laser based restoration techniques with conventional restoration ones.

The initial laser-glass interaction will be evaluated using contemporary stained-glasses often used for restoration of ancient stained-glass windows. This initial evaluation will lay a foundation for the development of a protocol for the application of laser technology in the restoration of ancient stained-glass windows. The established laser cleaning protocol will be applied in the restoration of selected historical stained-glass windows from Cuenca (Spain) and Chartres (France) Cathedrals. Results obtained with traditional glass restoration techniques (chemical and mechanical) will also be evaluated in comparison with those obtained using laser cleaning techniques.

CHAPTER 1: STAINED-GLASS WINDOWS

1.1. A brief historical perspective

Glass is one of the most intriguing and complex materials found in historic buildings. Its use to produce dazzling displays of colourful light has amazed church-goers for centuries. It is extremely hard, durable and dense, yet it can be transparent, translucent or opaque. Its molecular structure displays the random disorder of a frozen liquid, not the ordered structure of a crystal, which gives it isotropic optical and mechanical properties. Glass can also be produced in a milimetric thin flat surface, and can be easily cut at room temperature. Stained-glasses have been in production for centuries and have formed an important element in human history. Since stained-glasses are multifunctional, they have been utilized both in religious and civil architecture mainly for iconographic support and as light filters on windows (Alberta *et al.*, 2011; N. Carmona *et al.*, 2006; Manuel García-Heras *et al.*, 2005).

Coloured glass pieces, carefully segmented, were assembled together in a lead frame to form what is referred to as a stained-glass window. The artistic appearance of the glass would be enhanced by applying coloured paints, half-tones and/or dark contour lines (Römich *et al.*, 2003b). In the middle ages, stained-glass became the major form of pictorial illustration of the Bible to the people who were largely illiterate.

Coloured glass has been made since ancient times. Both the Egyptians and the Romans manufactured small coloured glass objects. Excavations in the Middle East, particularly in Egypt and Mesopotamia, has led to the recovery of beautiful Pharaonic-era glass artifacts (Elnaggar *et al*., 2010). In Egypt and Israel, glasses seem to have been produced selectively in a few number of production locations during the Late Roman and Byzantine periods (D. Brems & Degryse, 2014; I. Freestone *et al*., 2002; I. C. Freestone *et al*., 2000). During the Hellenistic and Early Roman periods, natron glass was also being produced in the western region of the Roman Empire (Dieter Brems *et al*., 2012; P. Degryse & Schneider, 2008). Stained-glass gained recognition as a Christian art form sometime in the fourth century as Christians began to build churches (tab. 1.1). The spread of Christianity throughout Europe is directly related to the expansion of stained-glass windows across the globe and made stained-glass the dominant art form of the new millennium. One of the oldest known examples of multiple pieces of stained-glass used in a window were found at *St. Paul's Monastery* in Jarrow, England, founded in 686 AD. The oldest complete European

windows are thought to be five relatively sophisticated figures in the 11th century Augsburg Cathedral (fig. 1.1) (Lee, L & Seddon, G. 1976).

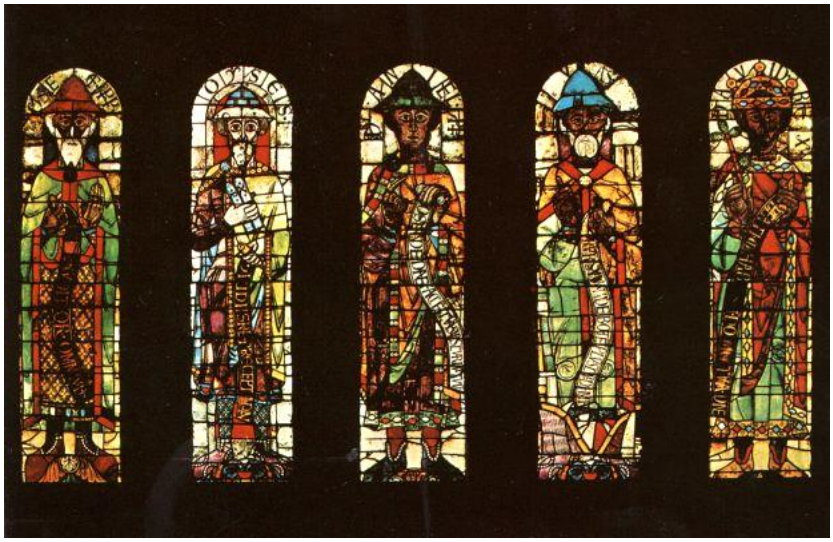

Figure 1.1: *Supposed to be the oldest surviving example of stained-glass windows located at Augsburg Cathedral, Bavaria Germany (c.1065). They depict the portraits of the five biblical prophets David, Jonah, Moses and Hosea. ©Scottish Stained-glass.*

Stained-glass was also produced by Arab architects in the Middle East in the 8th century. Jabir ibn Hayyan, a Persian chemist described 46 original recipes for producing coloured glass in *Kitab al-Durra al-Maknuna* (The Book of the Hidden Pearl) (Al-Hassan, 2009).

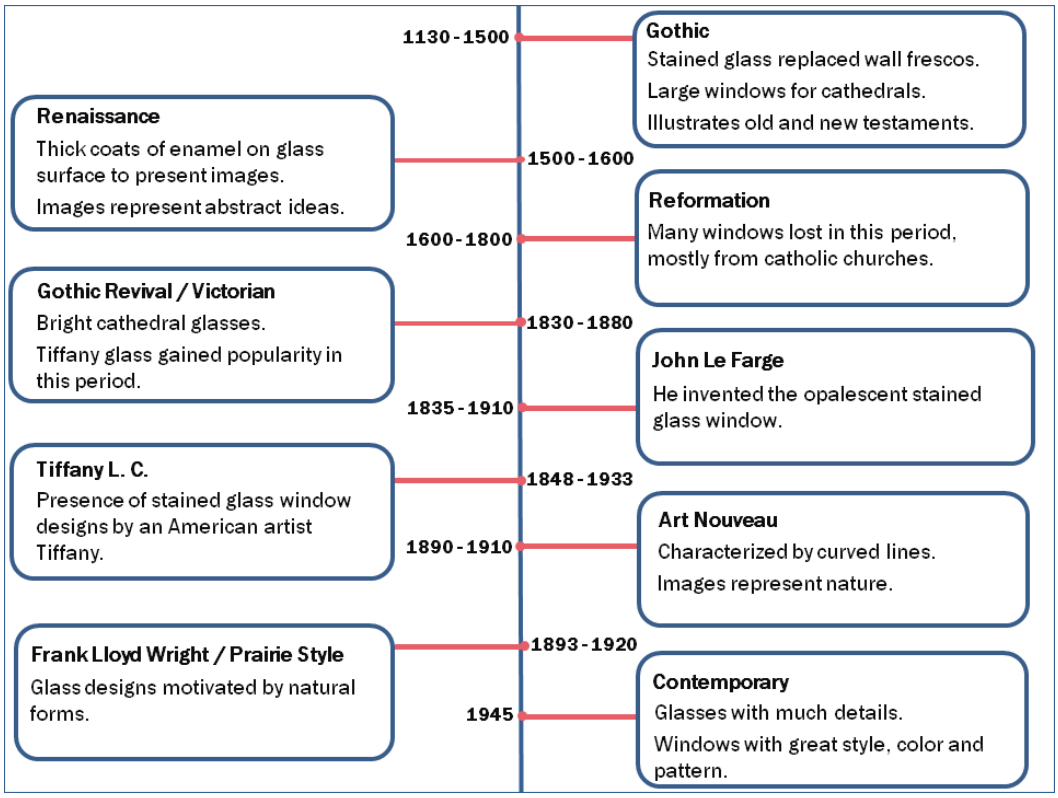

Table 1.1: *A brief timeline of the history of stained-glasses.*

In the European cultural heritage, stained-glass windows form an important part. The most significant stained-glass pieces and the earliest are those from the 12th century (Gothic period), in accordance with the medieval theocentric culture, the new concept and symbolism of light and the technological innovations that allowed to design and build new and spectacular architectural forms. During the Gothic period (the 13th and 14th century) stained-glass history expanded and stained-glass windows took center stage in elaborating monumental cathedral designs. By the mid-1400s, the new realism in painting by the great Spanish-Flemish style and Renaissance artisans, including masters like Jan Van Eyck, Arnao de Flandes, Juan de Valdivielso, etc., led to a decline of traditional stained-glass. The bold lines and strong figures of Gothic styles stained-glass eventually phased out and stained-glass windows evolved into something more like a painting on glass than an architectural element. There has been a variation of stained-glass production techniques exhibited by a change of style in the 15th to the 17th century (Alonso Abad *et al*., 2019; Noemi Carmona *et al*., 2009; Tennent & Newton, 1983).

During the mid-16th century in Spain, a number of glass making workshops arose in cathedrals such as Burgos and Toledo. This was followed by the establishment of independent workshops in Seville and Granada (Nieto Alcaide, 1998). German, Flemish and French glass artists worked and passed their skills in these Spanish workshops (Murcia-Mascarós *et al.*, 2008; Perez-Bueno, 1942). Spain, up to date, has a number of glass art works produced by great Flemish artists. Stained glass was largely a Catholic art form until the 16th century, and many of the valuable art forms were destroyed by order of King Henry VIII after his break with the Catholic Church in the 1600's. Aside from religious instability, the usage of stained glass declined throughout the Baroque period due to the increased use of clear glass. Interiors with exquisite details and rich wall paintings were more popular in architecture. The artisans returned to Gothic style architecture in the late 17th century, sparking a renewed interest in stained glass. The new window openings were authentically Gothic, but the window art was a mix of old and new (www.historyofglass.com/glass-history/stained-glass-history/).

1.1.1. Case study 1: Cathedral of Santa María, Cuenca (Spain)

Figure 1.2: *(Left) Facade of Cuenca Cathedral, Spain. (Right) Old facade of the Cathedral before the collapse of the tower in 1902 (©Alamy Stock Photo).*

This research will mainly focus on stained-glass samples from the Cathedral of Santa María of Cuenca, Spain. Representing some of the earliest Spanish Gothic architecture, Cuenca Cathedral is located in Castilla-La Mancha, a region of south-eastern Spain within the Province of Cuenca. The historic center of Cuenca was listed as a UNESCO World

Heritage Site in 1996, with the cathedral of Santa Maria of Cuenca being the iconic monument (Torrero *et al.,* 2015).

The construction of the Cathedral began in the late 12th century, after the conquest of the city of Cuenca by Alfonso VIII, and it was majorly completed around the second half of the 13th century (Torrero *et al.,* 2015). However, a number of modifications over the centuries have made a huge difference in the appearance of the actual monument in comparison with the original cathedral (fig. 1.2). In 1902, the facade was significantly destroyed after the collapse of the Giraldo tower, thus it has to be rebuilt, this time in a neo-Gothic style.

1.1.2. Case study 2: Cathedral of Notre-Dame, Chartres (France)

Chartres cathedral also referred to as Cathédrale Notre-Dame de Chartres, located in the Centre-Val-de-Loire region (France), is one of the most authentic and complete works of religious architecture of the early 13th century. The Chartres Cathedral was built following a fire that largely destroyed the previous church in 1194, the new choir being completed by 1221 and the whole building consecrated in 1260 as one of the most compelling expressions of the strength and poetry of medieval Catholicism. It was the destination of a pilgrimage dedicated to the Virgin Mary, among the most popular in all medieval western christianity. Because of the unity of its architecture and decoration, the result of research of the first Gothic era, its immense influence on the art of Middle age christianity, Chartres Cathedral appears as an essential landmark in the history of medieval architecture. The cathedral is celebrated for its many outstanding stained-glass windows ensemble, monumental statuary of the 12th and 13th centuries and the painted decorations that have miraculously preserved from the ravages of humankind and time, making Chartres cathedral one of the most best preserved examples of Gothic art (Bernardi et al., 2013; Terry, 2006).

Chartres Cathedral has almost totally conserved its homogeneous decor of stained-glass windows executed between approximately 1210 and 1250. To this must be added the three stained-glass windows of the 12th century above the Royal Portail and the large roses of the 13th century on the three façades: on the west, the *Last Judgement*; on the north, the *Glorification of the Virgin*; on the south, the *Glorification of Christ*. Chartres developed glass of unprecedented quality and was one of the largest manufacturers of glass. Chartres

Cathedral is well known for the atmosphere inside, dominated by the Chartres blue glass, which fills much of the three Rose windows as well as much of the other windows inside. The secret formula of the deep cobalt blue colour that has been termed as Chartres blue has not yet been discovered (Capobianco et al., 2021; Reynolds, 2013; Vondráčková et al., 2016). The cathedral is well-preserved and well-restored: the majority of the original stained glass windows survive intact, while the architecture has seen only minor changes since the early 13th century.

Figure 1.3: *(Left) Exterior side of the Chartres Cathedral, France. (Right) The interior of the cathedral.*

1.2. Stained-glasses: Materials and production processes

Glass, as a solid substance, is composed of long chain molecules forming an unordered structure (Krok *et al.*, 2010). Stained-glass, produced in a flat form, can variously refer to coloured glass as a tangible material or to artistic materials created from it (Richet, 2007). The term, for centuries, has been selectively been used to refer to windows of religious buildings and especially churches. Stained-glass can be referred to as glass whose colour has been altered by adding metallic salts during its production process.

Stained-glass windows are made from pieces of coloured glass arranged together to create

patterns or iconography. Traditionally, these pieces of glass are held together using lead strips and supported by a rigid frame. (M. Corrêa Pinto *et al.,* 2018). A layer of paint is applied on the glass surface and linked to the glass itself by heat treatment on some of the glass pieces for decoration. This glass paint or grisaille is a mixture of metal oxides (PbO, CuO, MnO, CoO, Fe_2O_3), with silicon oxide or sand (SiO_2) in different proportions. This mixture is ground and the final powdered product consists of two different components: the pigment (such as Fe_2O_3) and flux (mostly a highly fusible lead glass).They are usually mixed with a binding agent such as Arabic gum or sugar, and then mixed in water, acetic acid or other suitable solvents (Noemi Carmona et al., 2009; O. Schalm et al., 2003; Bettembourg, 1990; Debitus, 1991). The resultant mixture is then finely ground and spread with a brush on the glass surface. The painted glass is put into a kiln up to about 500-600 ^{o}C to ensure proper attachment of the paint.

The production techniques for stained-glass over the centuries are basically similar to those that were being utilized during the Middle Ages. The earliest available reference to the medieval production process of glass is by Theophilus Presbyter on a 12th century manuscript titled *Diversarum artium schedula* (M. Corrêa Pinto *et al.,* 2018). As much as the production of the glass itself is seen as part of a process handled by a single glass maker, it is important to assume that in reality, the whole production chain was handled by different people, in different locations, each with a unique specialty. The great variation in the condition of medieval glasses today, even within the same panel, supports this assumption. Corrosion of stained-glass is dictated by a number of factors, but from this variation we may conclude that as early as the 13th and 14th centuries, each glass maker's workshop was using different base materials sometimes sourced elsewhere.

According to Theophilus (a 12th century German monk), basic ingredients for producing ancient glasses were washed river sand (silica) and beech-wood ash (potash, an alkali). The mixture was placed in clay pots and then fired in a furnace "for a night and a day" (Hunault et al., 2021; Olivier Schalm et al., 2007). The firing and fusing of these materials fused them to form a viscous glass. Another glassmaking text attributed to a 13th century monk named Heraclius *De artibus romanorum* (or *De colouribus et artibus romanorum*), recommended the addition of powdered metallic oxides to the ash and sand mixture to get different shades of colour on the glass (Patrick Degryse et al., 2014; Olivier Schalm et al., 2007).

During the early periods of stained-glass production grisaille was the predominant painting

media that formed part of the decoration. Grisaille is a mixture of a low melting fine ground glass powder; colouring agents of metallic oxides (e.g. lead, copper and/or iron) and a binding agent. After the application of the grisaille, the glass is fired between 600 and 700ºC. The firing and mixture composition has to be done with care otherwise the grisaille would not adhere well to the glass causing detachment (Murcia-Mascarós *et al.*, 2008). The grisaille was generally applied on the obverse of the glass panel. In the beginning of the 14th century, the use of silver stain on the reverse became popular. From the late 16th century onwards, a vitreous pigment was adopted (M. Corrêa Pinto *et al.*, 2018). In this case enamels from various colours were used, especially for complex heraldic forms: However, the durability of the latter process depends on the firing temperatures.

The starting point for the execution of the panel itself was a sketch. This is necessary from a purely technical point of view and is corroborated by Theophilus. This sketch was very probably drawn onto a wooden panel covered with a chalk whitewash. An example of one such panel from mid-14th century Gerona in Spain has survived. At the same time, sketches made on parchment were in use: these were more easily transportable. Designs and sketches on paper survived in increasing numbers from the late 15th and early 16th centuries (Rauch 2004). The sketch constituted the basis on which the pieces of glass were cut. For each colour desired, a piece of glass was cut out to the correct shape according to its planned outline by means of a hot cutting-iron; the edges were then shaped more precisely with a grozing iron. In subsequent periods, diamond glass-cutters were increasingly used for this purpose. The interior surface was covered in glass-paint (grisaille) and with other washes with various thicknesses to execute a particular design.

The painted glass was then fired in a wood-fired oven. Thereafter, the pieces of glass were assembled into a frame by means of lead cames (fig. 1.4). These cames were cast into H-shaped holders, and in the medieval period these were shaved and cut with a knife to the desired width and height. In later years, the use of lead strips became the norm, whereby the raw material could be cold-worked into the desired profile. When the leading was complete, the joints between the cames were soldered with a lead and tin solder (Rauch 2004; Caldwell, 2019; M. García-Heras et al., 2006; Palomar et al., 2019). It remains unclear whether the panels were then further insulated against wind and rain with putty as was the norm in post-medieval times. There is no mention of putty in contemporary art-technological handbooks and demonstrating the presence of medieval putty on specific objects is quite a challenge. The panels of glass assembled in this manner were usually

installed directly into their intended locations mostly in a groove in the stone window-frame. Wooden frames were probably used during the Romanesque period. However, iron-work frames, comprising of wrought-iron flat bars subdividing the stone-framed openings in the window, were used. Finally, the panels were then secured in the stone frames with mortar and to ironwork with iron T-bars (Rauch 2004; Caldwell, 2019; M. García-Heras et al., 2006; Manuel García-Heras et al., 2004; Palomar et al., 2019). Subsequently, stained-glass windows have gone through a process of change in terms of painting and colour enhancements.

Figure 1.4: *Assembly of glass pieces (left) and soldering lead cames (right). (©Traditional Craft).*

1.3. Stained-glasses: Degradation processes

Stained-glass is lauded as one of the most beautiful and compelling forms of architectural decoration; however, it is also one of the most vulnerable (Brown *et al.*, 2002). The fabric of the glass itself, the paint or stain used to decorate it, and even the metal framework used to hold the design together are all at risk for deterioration, and will likely require conservation work to ensure their long-term survival. Historic glazing is subject to damage caused by continued exposure to pollution and the elements, on top of that resulting from inherent problems, such as the innate fragility of glass and any potential chemical instability of the materials involved (Brown *et al.*, 2002; Rauch 2004). Deterioration does not always occur gradually and may also occur suddenly and catastrophically.

An in-depth understanding of the structure, composition of stained-glasses and mechanisms of degradation is essential for defining and conceiving rational restoration and preventive measures. Background information assessment is also useful for identification of previous interventions on the stained-glass. The proportion of silica in the glass and the additives used in its manufacture affect the durability of the glass. Early

medieval glass made with potash and glass with a low silica ratio are more prone to decay than later 19th and early 20th century glass but the causes of decay remain much the same. The common types of degradation that affect historical stained-glasses include those of physical and chemical nature as well as those caused as a result of organic and human factors. In summary, these factors can be distinguished as follows;

i) Physical factors

Physical degradation includes abrasion, cracking, tearing, and exfoliation of surface layers (grisaille, paint etc.) among other phenomena that are not of chemical nature but which if left unchecked initiates and accelerates damage of chemical nature. Physical damages are mostly due to impact, shock, vibration, abrasion and excessive pressure. Fire is a means of deterioration that can impact glass objects ranging from a potentially minimal amount of damage to a total loss. Problems with fire include burning, soot deposits, and melting, warping, discolouration, embrittlement, cracking, and even shattering. Pests, such as microorganisms, insects, rodents, birds, and bats, are agents of deterioration not as often associated with the problems that occur with glass objects.

Exposure to sunlight over a long period can impact glass in unique ways. While visible light can cause colourful glass to fade, ultraviolet radiation is identified as a non-problematic entity. Infrared radiation does not have a direct effect but can be a cause of heating and therefore subject the glass to problems related to fluctuations in temperature gradients between the inside and outside of the building. Fluctuations in temperatures can lead to possible fractures of glass that has been weakened due to exposure to other agents of deterioration (Becherini *et al.,* 2014; Byrne, 2017; Comite *et al.*, 2020).

Water itself is not a hazard to stable glass, but in the case of a piece with existing weakness due to inherent chemical deterioration, it can accelerate problems associated with it such as weeping. Interestingly, water, whether as rain or condensation caused by variations in temperature and humidity is the principal agent of deterioration of glass; largely in chemical damage (Tennent & Newton, 1983). Rainwater running down the outside of the building and onto the windows slowly deposits particles of the surrounding materials onto the glass surfaces. These deposits include lime scale from render, mortar and limestone; and rust from ironwork. Over time they form a thin but very tough patina. On stained-glass windows this usually just mellows the intensity of the sunlight passing through the glass but on clear windows a dense patina can be quite intrusive.

Airborne particles can attach themselves to the glass surface and to the leads. Heavy traffic or industrial pollution can deposit thick crusts, which are most visible in those areas that are protected from direct rain, such as at the top of a lancet, in small tracery panels or under a horizontal bar. These crusts can be quite loose and flaky, but they can also be extremely hard. Tree sap may regularly coat a window in sticky droplets, which then allow dust to adhere to the glass. Over time, this can result in similar crusts (Maingi *et al*., 2022; Garcia-Vallès *et al.*, 2003; Römich & Weinmann, 2000; Kontozova-Deutsch *et al.*, 2011).

Figure 1.5: *(Left) Fatigue crack in lead came. ©Geoffrey Wallace Stained-glass. ©stainedglassausitn.com. (Right) Crusts formation on stained-glass window. Cartuja de Miraflores Burgos. ©Maria Angeles Villegas.*

ii) Chemical factors

Chemical degradation occurs generally as a result of contact with external catalysts or due to inherent instability of the glass, thus causing damage. In principle glass is a durable material especially when stored in a dry and unpolluted environment. Generally, the initial step of glass corrosion can be described as the attack of humidity on the glass surface. In all glasses, sodium and potassium oxides are hygroscopic and therefore attract water (Brill, R. *et al.,* 2021; Fearn *et al.,* 2004). The deterioration process which moisture initiates is complex but it usually involves the diffusion of hydrogen ions from water within the glass network. One hydrogen ion (H^+) from the water molecule displaces the sodium (Na^+) or potassium (K^+) ions from the network, leaving a hydroxide ion (OH^-). The by-product of this displacement is sodium or potassium hydroxide, both highly reactive alkalis which leach from the surface of the glass, depleting the body of the glass as a result. The

accumulation of water on the glass surface will continue to produce a build-up of alkaline corrosion products which attack the silica network of the glass causing surface decay (Bellendorf *et al.*, 2010; Corrêa Pinto *et al.*, 2019; Delgado *et al.*, 2017; Drewello *et al.*, 2000; Guiheneuf *et al.*, 2017; Römich *et al.*, 2003a).

In addition, the deposition of atmospheric particles initiates the deterioration of stained-glass panels and leads to the formation of a deposition crust on the glass normally composed of carbonates and sulfates and other opaque weathering products. The corrosion will increase, taking the form of pitting or crusting. Pitted glass surfaces are often strikingly uniform in size across a corroded area. These pits, depending on a number of factors, may range from 0.1 mm in diameter to much larger, perhaps around 2.0-4.0 mm. Pits can become linked together and crusts form within them so the difference between pits and crusts become slightly ambiguous (Corrêa Pinto et al., 2019; Drewello et al., 2000; Garcia-Vallès et al., 2003; Koob & Davison, 2004; Ngo et al., 2021; Roemich et al., 2003; Tang, 2009). In the most severe cases, pitting and crusting can reduce the glass to a very fragile state often depleting the thickness of the glass, and in extreme cases, pitting may even produce holes.

iii) Biological factors

Deterioration can also be of biological nature (fig. 1.6). Organic growth such as algae and lichens can also be found on the outside of windows. Even if a window is not leaking, water in the form of condensation will regularly run down the inside surface and can create thick whitish-grey deposits. Soot from decades of burning candles can gradually cause window glass to darken. Algae, fungi and molds are more often found on the inside of a window, as there they have a regular supply of condensation water but are not washed away by rain and are shielded from direct sunlight. Soft deposits that attract and hold water on the surface, and particularly organic growth, can actively damage the glass by keeping it damp. Birds excrements, for instance, get dissolved, accumulate and feed the development of microorganisms such as bacteria, moss, lichens etc. Organic growth often has acidic metabolic by-products and, over time, can trigger corrosion damage even on post-medieval glass, further reducing the transparency of the glass (Ngo *et al.*, 2021; Brill *et al.*, 2021; Wittstadt *et al.*, 2008; Fearn *et al.*, 2004; Corrêa Pinto *et al.*, 2019; Drewello *et al.*, 2000; Koob & Davison, 2004; Roemich *et al.*, 2003; Schalm *et al.*, 2011; Maingi *et al*., 2022).

Some glass types are more prone to damage than others and medieval glass is particularly vulnerable. Some deposits can be harmful to the glass while others are not. Patina and some hard crusts, although they can be unsightly, are unlikely to cause damage to the underlying glass. Stained-glasses with decoration are particularly at a higher risk. Grisaille or glass paint is similar to a pottery glaze and is fused to the glass surface in a kiln before the window is assembled. Windows of all ages can have problems with poorly fired, damaged or decaying grisaille (Brill *et al.*, 2021; Fearn *et al.*, 2004).

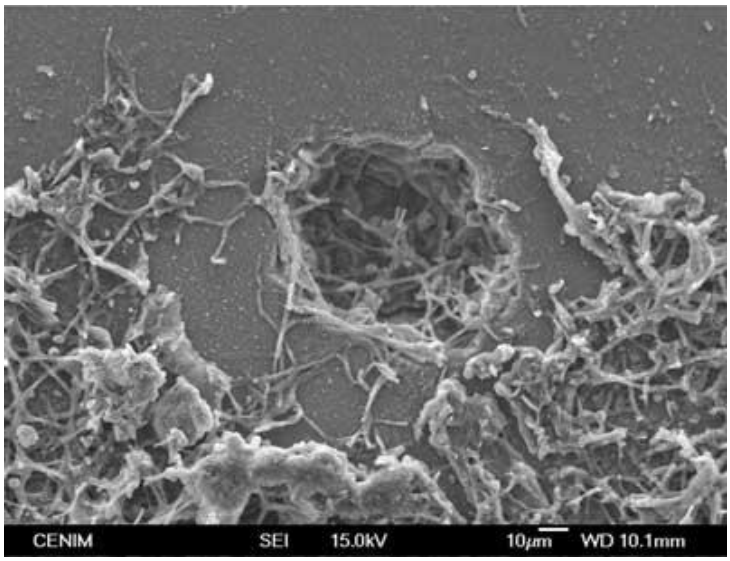

Figure 1.6: *SEM micrograph of a crater and filaments due to bio-deterioration. Cartuja de Miraflores, Burgos Spain. ©María Angeles Villegas.*

iv) Human actions

Human actions have played a major role in the deterioration of glass windows. These human actions include errors in the use of materials, ignorance of conservation/restoration techniques when an intervention is being carried out, lack of vigilance in conservation, vandalism, or malicious damage, for instance, during wars and conflicts (Brown *et al.*, 2002; Vogel & Achilles, n.d.). There have been evidence of people damaging glass by etching names and signatures on the windows found in historic buildings. Glass breakage is also a serious form of deterioration of glass, and this manly occurs because of carelessness and improper handling of these delicate materials. This form of damage mostly happens during cleaning or moving of the glass windows. Acts of vandalism has led to damage and loss of glass windows and these pieces end up in the black market for

cultural heritage materials. An example of vandalism include that of the windows of a church in Hornow (dated to 1902) in the German State of Brandenburg that underwent restoration after it had been heavily damaged by vandals (Byrne, 2017; Koob & Davison, 2004; Op & Halogen-free, 2019; Tennent & Newton, 1983).

1.4. Conservation of historical stained-glass

Conservation of stained-glass refers to the protection and preservation of historic stained-glass for the present and future generations. It involves any and all actions devoted to the prevention, mitigation, or reversal of the processes of deterioration that affect such glass works and subsequently inhibit individuals' ability to access and appreciate them, as part of the world's collective cultural heritage. It functions as a part of the larger practices of cultural heritage conservation (which includes restoration) and architectural conservation. Any conservation work should be handled with great sensitivity, and the conservator of historic stained-glass must be able to appreciate all the many messages which it brings to us from the past i.e. the painted scene, the style, the technique used in the iconography, the choice of colours, the type of glass, the use of silver stain and grisaille, the documentation about the contract, promoter, possible sketches, etc. All these information must be interpreted and passed on to the future generation with utmost care (Murcia-Mascarós *et al.*, 2008; Tennent & Newton, 1983).

Owing to the delicate nature of the materials, and the incalculable historic and aesthetic value of stained-glass work, any and all treatments should be planned and performed by professional conservators and craftspeople that have been specially trained in the peculiarities of the medium. While preservation is the shared responsibility of all involved, including visitors, caretakers, and other stakeholders, it is imperative that professionals are consulted to ensure the continued integrity of the physical materials and their associated significance. Three ethical principles are essential; any intervention must be the minimum necessary, it must be carried out with respect and with certainty that the intervention will be adequate for the integrity of the whole window, and it should be reversible, in case anyone in the future needs to undo the treatment. In an emergency situation, however, only the minimum necessary work should be done. For this reason, all projects should begin with a conservation plan that incorporates research in such topics as the history of the windows or building, the materials involved, and past alterations, as a key element of all conservation decisions. The type of performed conservation treatment should reflect this

research, as well as the needs of the building as a whole, and should always be documented for reference in the future (Bernardi et al., 2013; Römich et al., 2003a; Tennent & Newton, 1983).

Historical stained-glasses are mostly affected by formation of an obstructing crusted layer on its surface due to continuous exposure to the environment. The state of conservation that the external and internal surfaces of the stained-glass present is usually very different. As the paint layers (grisaille etc.) deteriorate, the overall graphic image of the stained-glass window becomes increasingly hidden (O. Schalm et al., 2003). Also, the paint layers are very different. Most of the painting is on the inside of the windows and the crusts are mainly outside. This dictates the cleaning actions to be taken, for instance, to restore transparency it is necessary to clean the crusts on the outside. One of the biggest challenges faced in conservation of historical stained-glasses and windows is the delicate removal of these accumulated crusts (Murcia-Mascarós *et al.*, 2008; Verita *et al.*, 2006). Stained-glass, for centuries, has been subjected to cleaning using mechanical methods (scalpels and brushes), and chemicals such as acidic and alkaline solutions. It is worth noting that cleaning methods have evolved over time and each has been improved by incorporating the advances in technological knowhow.

1.4.1. Mechanical cleaning

Mechanical cleaning, also referred to as dry method, is based on the application of energy with different tools to break and displace the bonding between surface deposits and substrate by impact, cutting or friction. Friction is considered the smoothest mechanism allowing greater control during treatment, although its effectiveness is usually restricted to thin and/or slightly compact surface deposits (Iglesias-Campos, 2014; Tennent & Newton, 1983).

Glass-fiber brushes are an example of tools that were utilized. They were used by skilled operators with good control over the cleaning action, and cleaning could be stopped as soon as the crust was nearly gone. Scalpels, steel brushes, sand paper and other specialized tools such as dental drills and the Cavitron descaler were and are still used occasionally (Murcia-Mascarós *et al.*, 2008; Striova *et al.*, 2021). An air-abrasive machine has been in use as well and it was found to be effective in removing the hardest crusts but careful control by a skilled user was required. To minimize damaging the glass while using this

technology, it was necessary to change several processing parameters such as the hardness and size of the grit, the size and shape of the nozzle, the air pressure or the period of application. Grinding the deposited crust from the glass, leaving a smooth surface, and then giving it a high polish, greatly improved the transparency of badly crusted glass (Iglesias-Campos, 2014; Tennent & Newton, 1983). However, there was a risk of losing all traces of any previous painting from the glass surface if the crust being removed had formed over a painted area.

Over the past several centuries, stained-glass windows have been cleaned using mechanical cleaning, which basically involves scraping and scratching of the surface. Mechanical cleaning has been shown to cause damage by the formation of pits on the glass as a result of scratches thus exposing the material to other deterioration agents (Murcia-Mascarós *et al.*, 2008).

1.4.2. Chemical cleaning

An alternative to the mechanical cleaning method is cleaning with liquids such as water-based solutions, acids and alkaline solutions. The chemical cleaning takes advantage of reagents and solvents capability of modifying the nature of materials to be removed, either by loosening or solubilizing the unwanted materials (Striova *et al.*, 2021). The loosened or solubilized materials can then be removed using the mechanical methods.

It has previously been observed that a shorter time of wetness does not allow a chemical balance leading to glass leaching (Murcia-Mascarós *et al.*, 2008; Verita *et al.*, 2006). Insoluble salts could be removed by using a convenient solution volume during a short time. The type of solution and concentration for cleaning stained-glass should be chosen according to the composition of both the glass and the accumulated crusts. Most crusts that have been analyzed have a composition consisting of silica, SO_3, CaO and K_2O (Murcia-Mascarós *et al.*, 2008; Romich *et al.*, 2000). Poorly soluble salts, which darken the glass, are mainly hydrated silica, gypsum $CaSO_4$ $2H_2O$, basanite $CaSO_4$ $^1/_2H_2O$, arcanite K_2SO_4, syngenite $K_2Ca(SO_4)_2 \cdot H_2O$, palmierite $K_2Pb(SO_4)_2$, anglesite $PbSO_4$ and calcite $CaCO_3$ and are difficult to dissolve. Other carbonates, nitrates and other sulfates do not form crusts as they are more soluble (Murcia-Mascarós *et al.*, 2008). Grisailles are as well affected by encrustations, mainly consisting of $CaCO_3$, $CaSO_4$ and/or $PbSO_4$.

Water is the most commonly used liquid for cleaning. Water is the simplest cleaning

liquid, even though it attacks glass slowly, it is widely available, although distilled water or deionized water is preferred; very 'hard' water is not recommended. According to Newton (Tennent & Newton, 1983), in the early 1970s it was recommended that stained-glass panels should be soaked in pure water but by mid 1970s there were doubts about the safety of using water because of its high surface tension which could lift off some of the loosely attached paint works.

Detergents have been suggested as well but highly alkaline ones have caused damage. Ammonia has also been used especially as an agent in ultrasonic cleaning baths. Before the 1970's, acids were widely recommended before it was realized that glasses made from beechwood ash with a high lime content were soluble in mineral acids. Hydrofluoric acid was another cleaning agent that was in use by many restorers but its use was abandoned due to risks involved (Tennent & Newton, 1983).

Murcia (Murcia-Mascarós *et al.*, 2008) proposed an optimized solution to dissolve calcium carbonates and lead sulfates crusts from Avila Cathedral (Spain) glass windows: a system designed to dissolve these crusts utilizing a diluted solutions of $NaNO_3$ in deionised water with a pH between 5.5 and 6.1 at a temperature of 15 ^{o}C with a controlled laminar rate of flow. This system was tailored to control pH, temperature, conductivity and concentration of Ca^{2+}. Continuous on-line analysis of these parameters allowed monitoring of the cleaning process. In particular, the Ca^{2+} concentration in the cleaning solution was controlled by means of a Ca^{2+} ion selective analyzer. This proposed method allowed cleaning only unpainted sides of the stained-glass being restored, avoiding any intervention on the damaged grisaille.

Using water or any other solvent as a cleaning agent has been seen to be effective when combined with mechanical cleaning method. However, studies have indicated that this combination approach of cleaning i.e. applying a solvent followed by scrubbing leads to damage, since the gel layer is softened and detached when dampened.

1.4.3. Laser cleaning as a conservation technique

Laser cleaning, as a conservation technique, is gaining momentum though it has been a research topic for the last four decades or so (Bartoli *et al.*, 2006; Cooper, 2007; Paraskevi Pouli *et al.*, 2008; Siano *et al.*, 2012). After the first laser was developed, its potential for

material removal and decontamination was recognized. Main limitation for broader studies of laser cleaning application was because of technological limits, low reliability and high costs. From 1980's onwards, a small number of research works were reported regarding laser cleaning of cultural heritage objects. From the beginning of 1990's onwards, interest and research on laser conservation started to grow again (Siano *et al.,* 2012; Zanini *et al.,* 2018). This is mainly due to various collaborations between different research institutions and support for research of innovative technologies deriving from European Framework Programs and various National Innovation ones. Stepping stone for further development of laser conservation was the foundation of LACONA (Laser in the Conservation in Artworks) and the organization of the first international conference dedicated to application of laser in cultural heritage in Crete, 1995 (Römich & Weinmann, 2000; Siano *et al.,* 2012). From there until now, numerous studies have been published dedicated to broadening the knowledge in laser cleaning of various materials. These scientific studies have led to laser techniques gaining a prominent position in the field of heritage conservation and restoration (Striova *et al.,* 2021).

The relatively high price of laser systems and cost of maintenance has led to research on laser to be mostly confined in Europe. Laser research and development in Europe is mainly financed by cultural heritage institutions supported by national and international government funds (Cooper, 2007). Even though the extensive progress that has been achieved in this field, part of conservation community considers laser conservation (laser cleaning particularly) as an experimental and not as a consolidated conservation technique (Aiello *et al.,* 2006). Nevertheless, laser cleaning has been utilized on numerous artifacts and objects of historical importance and conservation complexity. Some of the examples are cleaning of Parthenon west frieze (Frantzikinaki *et al.,* 2007), *Porta del Paradiso* in Florence (Matteini *et al.,* 2003; Salimbeni *et al.,* 2005; Siano *et al.,* 2012), terracotta decorations on the Cathedral of Seville (Oujja *et al.,* 2005), the Nickerson mansion in Chicago (Dajnowski *et al.,* 2017), removal of a shellac layer from mural painting mock-ups to demonstrate the effectiveness of lasers in the gradual removal of organic layers (Striova *et al.,* 2021), the removal of biological patina on volcanic scoria of the rock-hewn churches of Lalibela Ethiopia (Gemeda et al., 2018) among others.

As a result of the benchmark studies from the 1980's to the 1990's that led to greater interests and research on laser conservation (Siano *et al*., 2012; Zanini *et al*., 2018), a good number of papers and patents arose focusing on how lasers can be applied to both industrial and cultural heritage conservation problems. Some of these research works were, and

continue to be directed to laser cleaning of glassware and transparent materials (Bilmes *et al*., 2018; Fekrsanati *et al*., 2000, 2001; Joyce & Kane, 2006; Lu *et al*., 1994; Römich *et al*., 2003a). Examples of these works include the use of pulsed lasers (YAG, N_2 and CO_2 lasers) to clean a glass surface (Ueda *et al*., 1991), use of a YAG laser in the cleaning of a glass sample in the Jordanian museum (Al Sekhaneh *et al*., 2015), removal of unwanted surface deposits from a Roman glass bowl excavated in the Roman necropolis of Sisapo Spain using two Nd:YAG laser devices (SFR and LQS) (Elnaggar et al., 2010), removal of biogenic surface crusts on a historical glass window models using an excimer laser device (Drewello *et al*., 2000) among other approaches that include using different wavelengths to investigate the potential of laser cleaning of glass materials (Fekrsanati *et al*., 2001).

Laser technology has evolved tremendously in the last few decades and new ultra-short pulsed lasers (picosecond and femtosecond) are now available. The interaction of ultra-short ps and fs pulsed lasers with glass (Maingi *et al*., 2022), and these lasers' potential to the cleaning of cultural heritage glass are explored in this work.

CHAPTER 2: PROCESSING AND CHARACTERIZATION TECHNIQUES

2.1. Working principles of laser cleaning

The word LASER is an acronym for Light Amplification by Simulated Emission of Radiation. Because of its unique properties, such as mono-chromaticity, directionality and coherence, laser has been considered a technological advance in all its areas of application (Mahamood, 2018). When laser reaches a material surface, the incident radiation may be transmitted, reflected, scattered or absorbed (fig. 2.1). The percentage of each component is determined by different operational parameters of the laser radiation and physical properties of the material. Scattering and absorption contribute to attenuation and spatial diffusion of the laser energy. The absorption of laser radiation can lead to ablation, which is the main phenomenon involved in laser cleaning. Ablation involves the ejection of material from a laser irradiated surface, sometimes accompanied by the formation of plasma when intense laser irradiation is used (Bartoli *et al.*, 2006; Cooper, 2007; Koh, 2006; Paraskevi Pouli *et al.*, 2008).

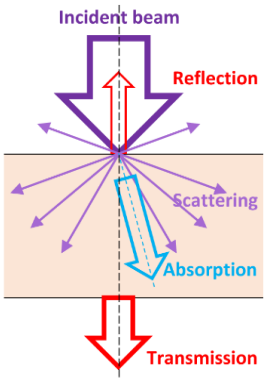

Figure 2.1: *Schematic illustration of the interaction between a laser incident beam and material surface.*

Three main types of interactions may occur during the process of laser ablation, which are; photo-thermal, photo-chemical, and photo-mechanical. The exact interaction mechanisms depend on the laser parameters and on the physical and chemical properties of the target material. The thermal properties of the material (i.e. thermal conductivity and heat capacity) are significant parameters to evaluate both the volume of the material affected

by laser irradiation and the maximum temperature reached in the process. Strong absorption of energy leads to rapid heating of the material (Merino et al., 2021), followed by its thermal expansion and the propagation of a thermal shock wave, which causes ablation at the surface. The minimum energy density required to achieve ablation is called the ablation threshold. When the ablation threshold of the material to be removed (crust in fig. 2.2) is lower than that of the original substrate, the removal process can be performed within safe parameters, selecting a level of laser energy higher than the crust ablation threshold but lower than that of the substrate one. In this situation, the energy density deposited onto the sample surface is sufficient to clean the contaminants but not enough to damage the substrate material. Unless a laser beam is at least absorbed, it can have no effect on the irradiated surface, this process of ablation and vaporization with controlled parameters has been described as a "self-limiting" process (Koh, 2006; Mateo *et al.*, 2005; Papanikolaou *et al.*, 2008). By contrast, when the crust ablation threshold is higher that the substrate one, the energy level required to eliminate the contaminant can damage the substrate as soon as the laser reaches it. In this case, it is important to establish the amount of contaminant that is eliminated and assure that the laser does not reach the substrate.

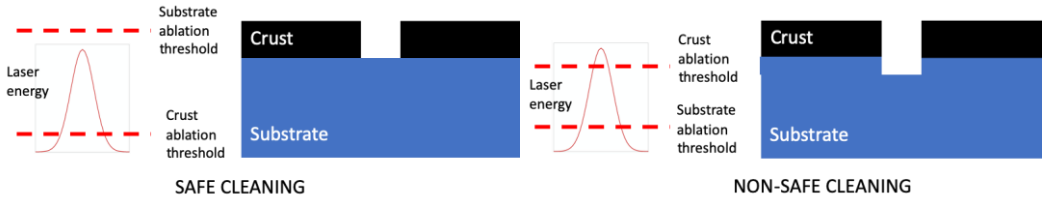

Figure 2.2: *Scheme of the conditions when safe and non-safe cleaning processes are expected.*

2.1.1. Laser cleaning parameters

There are a number of important parameters that should be considered when planning to use laser systems for cleaning. In order to determine the adequate set of parameters affecting the cleaning outcomes, laser parameters, material parameters and the surrounding environment have to be taken into consideration. The first selection is the type of laser considering its wavelength (Aiello *et al.*, 2006; Andreotti *et al.*, 2006; Dajnowski & Dajnowski, 2017; Mateo *et al.*, 2005; Oujja *et al.*, 2005; Papanikolaou *et al.*, 2008; Paraskevi Pouli *et al.*, 2008; Maingi *et al.*, 2022). The wavelength fixes the energy of photons involved in the reaction, being more energetic when wavelength is lower. Usually,

infrared radiation generates more thermal processes, while UV radiation can generate chemical modifications on the material surface. Various materials exhibit different reactions and absorbance values when interacting with different wavelengths. For example, in the case of cleaning of marble surface contaminants, laser cleaning done with near-IR laser with a wavelength of 1064 nm generates an alteration of the original surface, called "yellowing effect", while cleaning with UV, 355 nm, avoided this problem (Frantzikinaki *et al.*, 2007). In the case of removing aged varnish or other contaminants from the painting, the best results are obtained with UV laser (Bordalo *et al.*, 2006; Fekrsanati *et al.*, 2001; Georgiou *et al.*, 1998; Teule *et al.*, 2003). For paper, parchment and other biogenetic sensitive materials, cleaning with 532 nm lasers is recommended (Arif & Kautek, 2015; Kautek & Pentzien, 2005).

Another crucial laser parameter is the pulse width, also called pulse duration. The fast evolution of the very short picosecond (ps; 10^{-12} s) or femtosecond (fs; 10^{-15} s) pulsed lasers is opening new possibilities for laser cleaning. The shorter the pulse duration, the higher the reached peak power intensity and the produced shock waves are stronger. But the interaction time is shorter and the thermal component is lower and more localized on the sample surface. These properties facilitate to prevent heat accumulation of the substrate (Koussi et al., 2020). The thermal side effects are negligible when pulse duration is less than the thermal conduction time (Bartoli *et al.*, 2006; P. Pouli *et al.*, 2007; Paraskevi Pouli *et al.*, 2008). Choosing the right optimal pulse duration is therefore necessary.

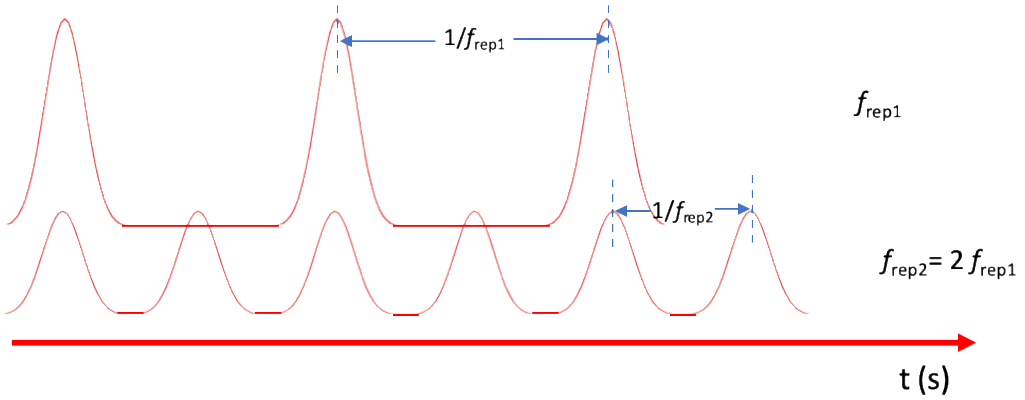

Figure 2.3: *Scheme of the influence of f_{rep} on the energy per pulse for a given output power.*

Pulse repetition rate describes the number of emitted pulses per second (fig. 2.3). If multiple pulses are applied, repetition rate, f_{rep}, should be lowered to avoid cumulative

heating of the substrate. In most of the laser systems, average output power is fixed and, in consequence, the total average output energy is defined. f_{rep} determines the number of pulses for a given time. In consequence, for a given output power, higher is the frequency, lower is the energy of each pulse. Considering these facts, higher frequency values should be selected if heating and melting processes at the surface of the material are desirable. By contrast, low frequency values are more adequate for ablation processes. It is also important to have in mind that too low frequencies also mean that the time to clean an area is higher.

Another important point is how to move the laser beam over the sample surface. Nd:YAG lasers equipped with an optical fiber or articulated mirror arm for beam delivery are the most common commercial laser systems used in conservation (Asmus, 2010; News *et al.*, 2017). A big step for the conservators was the introduction of short pulses Nd:YAG lasers with wavelength multiplied laser radiation, providing emissions from IR to UV wavelength (K. Dickmann *et al.*, 2005; Klaus Dickmann *et al.*, 2001). The advantage of spatial maneuverability can also be a disadvantage, since the exact irradiation point is not known due to non-achromatic optics and the beam cannot be manipulated automatically (Lentjes, 2007). Movement of a fiber or arm from the focal spot changes the amount of irradiance emitted on the surface. Additionally, it is not possible to control the overlap of pulses, which results in over-under exposed area or to thermal accumulation. This is also problematic when sensitive, fragile objects need to be cleaned with precision. Klaus Dickmann *et al.*, 2001 have used a webcam and image processing for obtaining coordinates for each emitted pulse.

Automatic cleaning with self-limiting capabilities is not applicable to all materials. This is a hindrance to the use of lasers coupled with articulated arms. As it was presented in figure 2.2, when ablation threshold of contaminant layer is higher than of the substrate, object can be over-cleaned and damaged by radiation (Lentjes, 2007). As it has been mentioned, in these cases, the cleaning process can be performed by removing contaminated surface layer by layer and this is more feasible when ultra-short laser pulses are used because interaction is more localized at the sample surface.

Another advantage of laser scanning systems is high precision that allows uniform cleaning regardless of corrosion's morphology. Carrying out controllable ablation is possible with laser systems that operates on bases of laser scanning while taking into account geometric parameters. Defining cleaning parameters in this configuration requires

the adjustment of pulses overlap. These include spot size, interlining, scanning speed and repetition rate. All of the named parameters are reciprocative. Spot size, repetition rate and scanning speed define overlap in one direction, while in the perpendicular one overlapping is determined by interlining. The adjustment of the geometric parameters allows high precision and control of the cleaning treatment by avoiding over-radiation and thermal incubation.

2.1.2. Characterization of a laser beam

Laser cleaning is achieved when the amount of power or energy per unit area is sufficient enough for removal of targeted corrosion products without damaging the underlying original substrate of an object. Some of the most important parameters are irradiance, *I* (laser peak power per unit area) and fluence, *F* (the energy density per unit area).

Considering that the energy of a given pulse is given by:

$$E = \frac{P}{f_{rep}}$$

where *P* is the average output power and f_{rep} is the repetition rate. If the spot area is *A*, the average fluence is calculated using the equation:

$$F = \frac{E}{A} = \frac{P}{f_{rep}\,A}$$

Irradiance is determined:

$$I = \frac{P}{f_{rep} A t_p} = \frac{F}{t_p}$$

where t_p is pulse duration. Both magnitudes are used for quantifying laser radiation, but in most of the laser induced processes it is more appropriate to use irradiance (*I*) rather than fluency (*F*) (Bäuerle, 2011, p. 4), because it considers the effect of pulse duration that determines pulses peak intensity besides the average energy of a pulse.

Quantitative studies of laser-materials interactions require absolute calibration of laser-energy fluence. This calculation only can be done if the dimensions of the beam size are known. In the case of a beam with a gaussian energy distribution, this is not evident. The measurement of the laser-beam spot size is essential to determine these parameters and a cleaning protocol that can be used with another laser. A number of methods have been used to measure the beam profile (Winer, 1966; Yariv, 1975). In 1982, Liu (Liu 1982) described a simple technique for measuring pulsed Gaussian beam spot sizes and

determine the damage threshold to produce a modification in the material surface. In the original work, this technique was used for characterizing the spatial profiles of focused, intense laser beams based on optically induced phase changes on silicon surfaces. Moreover, this method provided a simple technique to diagnose the energy distribution of high-power pulsed-laser beams by direct imaging the contour of specific-threshold energy fluences on large silicon wafers. Liu (1982) suggested that this technique can also be applied to inexpensive and more-sensitive film materials that permit a precise determination of the laser-spot size. According to Liu (1982) this technique is convenient and accurate for *in situ* measurements of laser beams focused on a sample surface.

Liu propose that the spatial distribution of the fluence assuming a circular gaussian profile (fig. 2.4) given by

$$F(r) = F_{max} \exp\left[-2\left(\frac{r}{r_0}\right)^2\right]$$

With this definition, the beam size is associated with r_0, point where the energy is F_{max}/e^2 ($1/e^2$ criterium). Other works also propose the 1/e or the FWHM criteria. If the energy distribution is integrated, it is derived that the maximum fluence value at the centre of the gaussian is two times the average fluence value, $F_{max}=2F$.

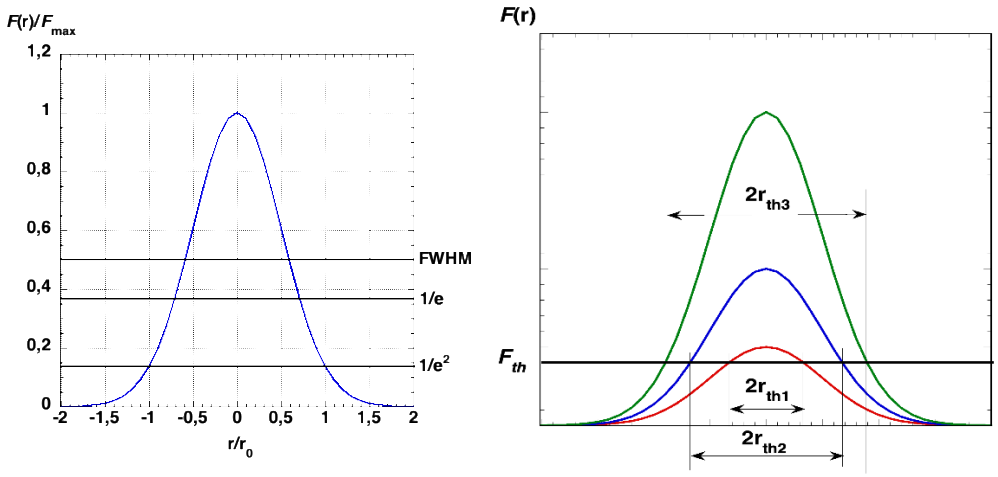

Figure 2.4: *(Left) Spatial energy distribution of a gaussian energy profile. (Right) Evolution of the footprint size as the fluence of the beam increases.*

Given a value of F_{max}, the size of the footprint generated on the surface of the material is related with the size of the region where a fluence higher than the damage threshold, F_{th},

is reached (fig 2.4):

$$F_{th} = F(r_{th}) = F_{max} \exp\left[-2\left(\frac{r_{th}}{r_0}\right)^2\right]$$

$$\frac{F_{th}}{F_{max}} = \exp\left[-2\left(\frac{r_{th}}{r_0}\right)^2\right] \qquad 2\left(\frac{r_{th}}{r_0}\right)^2 = ln\left(\frac{F_{max}}{F_{th}}\right) = ln\left(\frac{E}{E_{th}}\right)$$

$$r_{th}^2 = \frac{r_0^2}{2} ln\left(\frac{E}{E_{th}}\right) \qquad D_{th}^2 = 2r_0^2 ln\left(\frac{E}{E_{th}}\right) = 2r_0^2 lnE - 2r_0^2 lnE_{th}$$

In consequence, measuring different footprint size increasing the pulse energy and plotting D_{th}^2 as a function of ln$E$ it is possible to obtain a linear dependence. The slope is associated with the size of the laser beam and the the intercepts of these lines with the horizontal axis provides the damage threshold. Figure 2.5 shows an example of this analysis, that appears in the original work of Liu. This study was performed on Si samples showing two different types of damage and on a Polaroid film. In both cases, as expected, the spot size is very similar. Also, Figure 2.5 shows another example that has been done in this work to measure the spot size of the 800 ps near-infrared laser. These results were obtained in stained steel surface.

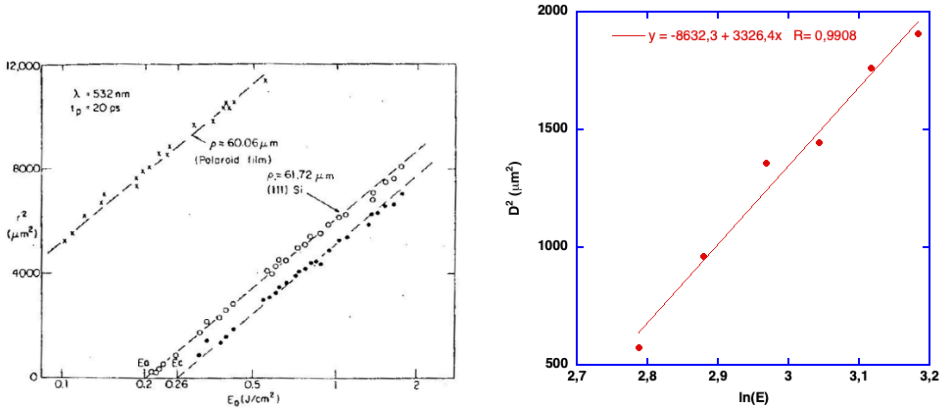

Figure 2.5: *(Left) Semilog plots of the energy dependence of the outer radii (o) and inner radii (●) of the amorphous ring patterns on a (111) silicon surface and the radii of the burn spots (X) on a Polaroid film, induced by 20-psec pulses at 532 nm. p is the experimentally determined (l/e) intensity radius of the green beam at the focal spot (J. M. Liu, 1982). (Right) Results obtained in this work on stained steel samples to measure the beam size of the 800 ps near infrared laser.*

This technique proposed by Liu (1982) has some advantages such as its simplicity and rapidity in measuring the spot size directly, freedom from errors introduced by

uncertainties from characterizations of the beam and the optical arrangement, and also *in situ* measurements that can be performed directly on the sample surface during an experiment if working out of focus is required.

2.1.3. Modes in laser processing

In this work, surface laser scanning was performed in two different modes; the beam scan and burst.

i) Beam scan mode

In the beam scan mode, the laser scans the surface at a given speed while controlling the distance between two consecutive scan lines thus covering a surface uniformly. In addition, it is possible to control the scanning direction. When this protocol is used, it is important to have in mind that when the laser beam reaches the border of the irradiation region, it has to move its way back or start from the other side. In consequence, there is a region of the sample, where the scanning speed has been reduced until stopping the laser and where the treatment has been stronger. This can cause localized defects on the surface that can be very relevant in Cultural Heritage. If it is possible, the scanning has to be performed over areas higher than the sample size or to use some kind of masks or a shutter (Strassl *et al.*, 2008).

The scanning can be performed using an uni-directional or a bi-directional configuration (fig. 2.6). In the bidirectional scanning pattern, the laser moves in a zigzag way across the sample surface. In the unidirectional one, the laser always starts from the same side of the irradiation region. Different scanning patterns would cause different phenomena. In the bidirectional case, it is important to consider that the laser starts a line in a region that is close to the region that has just processed at the end of the previous line, and that can still be hot, increasing even more the effect of the laser on the border of the scanned area and the differences between center and border. By contrast, when the unidirectional configuration is used, the time between two equivalent positions in two lines is the same in all the line and only the effects of stopping the laser have to be considered. Sometimes the effect of the laser treatment increases during the line because the temperature of the sample is lower at the starting position and higher at the end of the line.

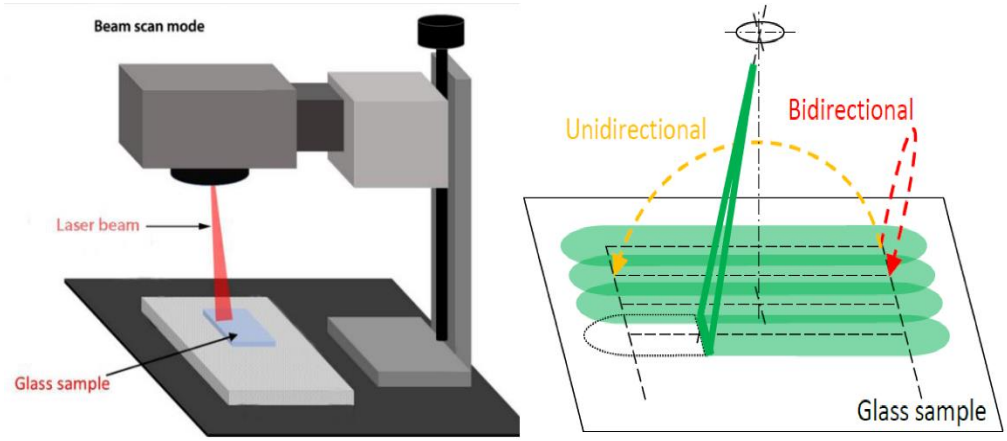

Figure 2.6: *Schematic diagram illustrating the beam scan mode*.

In this configuration, it is important to select the laser parameters in order toFor instance, when the laser scans one line in the *Y*-direction, a series of discrete gaussian pulses reaches the sample. The distance between two consecutive pulses, $\delta_{pulses}= v_L/f_{rep}$, is fixed by the laser scanning sped, v_L, and f_{rep}. Figure 2.7 shows the distribution of the energy along the line x=0 for different δ_{pulses}/r ratios. It is observed that when this ratio is small enough ($\delta_{pulses}<0.9r$), the energy distribution can be considered uniform in the *Y*-direction with differences between the maximum and the minimum at x=0 lower than 1%. In the *X*-direction, also a gaussian distribution is obtained, given by the expression:

$$F(x) = F_{centre1D} exp\left[-2\left(\frac{x}{r}\right)^2\right] = 1.588\ \frac{\pi\, r}{2\,\delta_{pulses}}\ F_{av} exp\left[-2\left(\frac{x}{r}\right)^2\right]$$

where, $F_{centre1D}$ is the maximum fluence in the centre of the line, $F(x=0)$.

Consider $\delta_{pulses}/r<0.9$ and a time interval $\Delta t>>1/f_p$. In this period of time, the laser emits $N= f_p\,\Delta t$ pulses and covers a rectangle with an area given by $(2\,r)\,(v\,\Delta t)>>\pi r^2$. It is possible to define the effective number of pulses, N_{eff1D} as:

$$\langle F_{1D}\rangle = \frac{N\,E}{2\,r\,v\,\Delta t} = \frac{f_p\,E}{2\,r\,v} = \frac{f_p\ \pi\,r\,E}{2\,v\ \pi r^2} = \frac{\pi\,r}{2\,\delta_{pulses}}\,\frac{E}{\pi r^2} = N_{eff1D}\,F$$

where $N_{eff1D} = \frac{\pi\,r}{2\,\delta_{pulses}}$

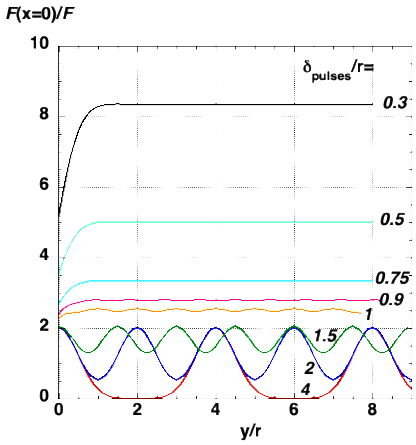

Figure 2.7: *Normalized fluence distribution along the centre of the line (x=0) when the laser beam scans in the Y-direction*

A similar analysis in the perpendicular direction determines that the distance between two scanning lines should also be lower than 0.9*r*.

ii) Burst mode (pulse mode)

The burst mode consists on a spot-by-spot scanning process with adjustable laser parameters. In burst mode, the laser system produces a sequence of a defined number of pulses (a burst) with a high intra-burst repetition rate (Kerse *et al.*, 2016). A single burst is incident at a given position and the distance between these positions can be set by software. It is also possible to adjust the number of pulses in a burst and the energy of each individual pulse, which would provide more flexibility and convenience in the cleaning process. This process is slower than the continuous mode because the laser stops at every point.

2.2. Laser systems used to define the cleaning protocols

Laser treatments were performed using three different lasers. Details are presented in table 2.1. A picosecond (ps) near-infrared laser (PowerLine Pico 10-1064, Rofin-Sinar, Germany) with a wavelength of 1064 nm, a pulse duration of 800 ps and a maximum output power of 8W, coupled with a galvanometer mirror system. The pulse repetition rate

can be modified between 250 and 800 kHz and the waist diameter of the laser beam ($1/e^2$ criterium) is approximately 80 μm, as deduced following the D^2-method proposed by Liu (J. M. Liu, 1982) and was presented in figure 2.5.

The second laser system used in this study was a UV laser, and in particular to observe the response of the glass samples to UV radiation for optical characterization. This UV laser (Power Line Pico, Rofin-Sinar, Germany) has a wavelength of 355 nm, a pulse duration of 300 ps and a maximum output power of 3 W coupled with a galvanometer mirror system. The pulse repetition rate can be modified between 250 and 800 kHz. The laser beam has an elliptical shape and the laser beam waist axes dimensions ($1/e^2$ criterion) are approximately 34 and 29 μm.

Treatments were also carried out using a femtosecond (fs) laser (Carbide model, Light Conversion, Lithuania), also coupled to a galvanometer mirror system (Direct Machining Control, UAB, Vilnius, Lithuania). Treatments were performed in this case at 1030 nm, with a variable pulse duration that can be changed between 228 fs and 10 ps, a maximum output power of 40 W and a beam diameter of 100 μm. Pulse frequency can be modified between 1 kHz and 1 MHz and the system offers the possibility of selecting the final frequency using the pulse peak divider option. This laser also emits with the third harmonic, at 343 nm. The maximum power is 11 W and the pulse duration can be modified between 238 fs and 10 ps. The beam has an elliptical shape with main axis 41 and 30 μm.

Laser Type	Maximum Power	Wavelength	Pulse Duration	Frequency	Beam Diameter
Picosecond IR	8 W	1064 nm	800 ps	250-800 kHz	80 μm
Picosecond UV	3 W	355 nm	300 ps	250-800 kHz	34-29 μm
Femtosecond IR	40 W	1030 nm	238 fs to 10 ps	1kHz-1 MHz	100 μm
Femtosecond UV	11 W	343 nm	238 fs to 10 ps	1kHz-1MHz	41-30 μm

Table 2.1: *Laser systems used and their specifications.*

2.3. Optical and surface analysis techniques

Characterization of the samples microstructure and of the changes generated during laser cleaning have been performed using the following characterization techniques.

i. Technical photography

Generally, photographic imaging is the first step taken in documentation and evaluation of surface morphology and conservation status of glass pieces, as well as complementing optical microscopy examination. Technical photography is used to closely analyse aspects related to the production processes and conservation status of materials. Photographic documentation can be performed under different types of illumination; reflected light, transmitted light, oblique light and UV light. The obtained information allows detailed evaluation of the surface of the object under study and to check for any topographical and morphological changes of interest. Ultraviolet (UV) light is a form of electromagnetic radiation (Webb, 2020; Zheng *et al.*, 2014) commonly used for the examination of objects. Typically, the wavelength of UV ranges from 100 to 400 nanometers and can be divided into regions such as longwave, mediumwave and shortwave ultraviolet radiation (Shugar *et al.,* 2017). UV radiation which is not visible to the human eye causes the emission of visible light (fluorescence) from a substance under examination.

In this study, general morphological aspects were documented and evaluated by photography under standard reflected light using a Canon EOS 400D digital camera.

ii. Optical Microscopy

Optical microscopy is a quick method for identifying a broad range of materials. It is used to magnify small objects in order to provide information on the structure and morphology otherwise not detectable with the naked eye. Optical microscopy involves the interaction of light with a sample and can operate up to more or less 1000 times magnification (Murphy, 2001). A resolution of about 0.5 μm is possible, depending on the limits of the instrument and the nature of the sample being examined.

There is a variety of light microscopy techniques that may be used to examine materials. Samples may be examined with transmitted light, reflected light as well as stereomicroscopy where a three-dimensional image is obtained. There are also different imaging modes that may be used. Bright field is the normal mode of operation in optical microscopy. With transmitted light, the contrast is based on variations of colour and optical density in the material. With reflected light, if the bright field mode does not provide adequate contrast, then the dark field mode may be employed. This mode excludes un-

scattered light, the background light becomes approximately zero and a high image contrast is possible. Short wavelength radiation can also be used to induce fluorescence in a sample, resulting in the emission of longer wavelengths.

A microscope basically comprises two parts: a mechanical part which acts as the support and the optical part consisting of the objective and eyepiece. The resolution of the image is a function of wavelength of light and the numerical aperture of the objective. The numerical aperture is basically the amount of light at a solid angle (and resolution) that an objective can gather from an object (Murphy, 2001; Vandenabeele, 2007).

To optically assess morphological features and degraded areas of the glasses in this work, a portable loop microscope and a ZEISS SteREO Discovery.V8 (8:1 manual zoom range) microscope were used (fig. 2.8).

Figure 2.8: *ZEISS SteREO Discovery.V8 optical microscope used in the surface morphological observation of the glasses. INMA-CSIC University of Zaragoza, Spain.*

iii. Confocal Microscopy

A confocal microscope provides information about the topography of a surface. This is achieved by excluding most of the light from the specimen that is not from the microscope's focal plane. The image has less haze and better contrast than that of a conventional microscope and represents a thin cross-section of the specimen. Furthermore, confocal microscope allows user to build three-dimensional (3D) reconstructions of a

volume of the specimen by assembling a series of thin slices taken along the vertical axis (Peterson, 2010).

In confocal microscopy, a coherent light emitted by the laser system passes through a pinhole aperture that is situated in a conjugate plane (confocal) with a scanning point on the specimen and a second pinhole aperture positioned in front of the detector. As the laser is reflected by a dichromatic mirror and scanned across the specimen in a defined focal plane, secondary emitted from points on the specimen (in the same focal plane) pass back through the dichromatic mirror and are focused as a confocal point at the detector pinhole aperture. Because only a small fraction of the out-of-focus emission is delivered through the pinhole aperture, most of this extraneous light is not detected by the photomultiplier and does not contribute to the resulting image. Refocusing the objective in a confocal microscope shifts the excitation and emission points on a specimen to a new plane that becomes confocal with the pinhole apertures of the light source and detector (Conchello & Lichtman, 2005; Paddock, 1999; Peterson, 2010).

A dual microscope Sensofar PLμ2300 (fig. 2.9) was used combining confocal and interferometer adapted for the surface characterization of materials. All confocal images were taken with Sensofar PLμ2300 equipped with 10x/0.935, 20x/0.623 and 50x/0.350 objectives.

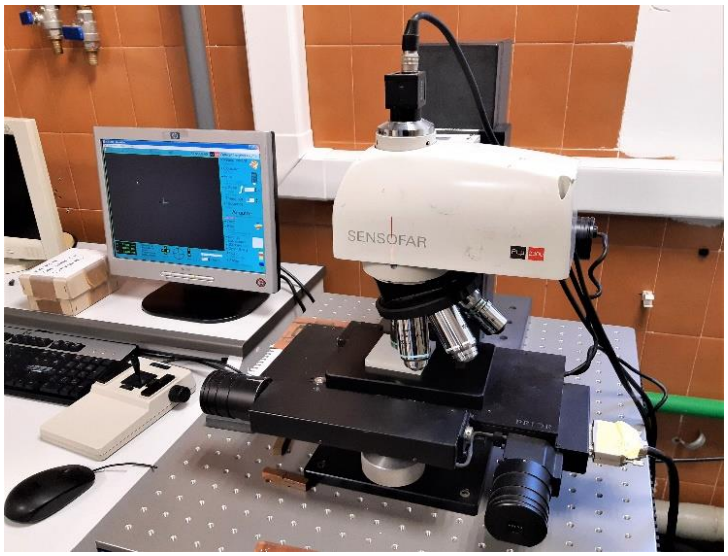

Figure 2.9: *Sensofar PLμ2300 confocal microscope used for surface and profile characterization of the glasses. INMA-CSIC University of Zaragoza, Spain.*

iv. Optical properties measurements (Spectrometer and power meter)

The differences in colour between the glasses suggest that they can exhibit different absorption properties at the emission wavelength of the laser. The transmittance and absorption values in the UV-Vis-nIR range, in particular between 300 and 1100 nm, were characterized using a StellarNET Miniature Spectrometer in transmittance mode (fig. 2.10). A SL1-CAL light source, 0.6 mm in diameter and a cone angle of 25.4º at the output of the optical fiber and specifically configured for irradiance calibrations in the 300-1100 nm range, was used. Transmittance tests were carried out with an integration time of 5 ms, averaging 100 scans.

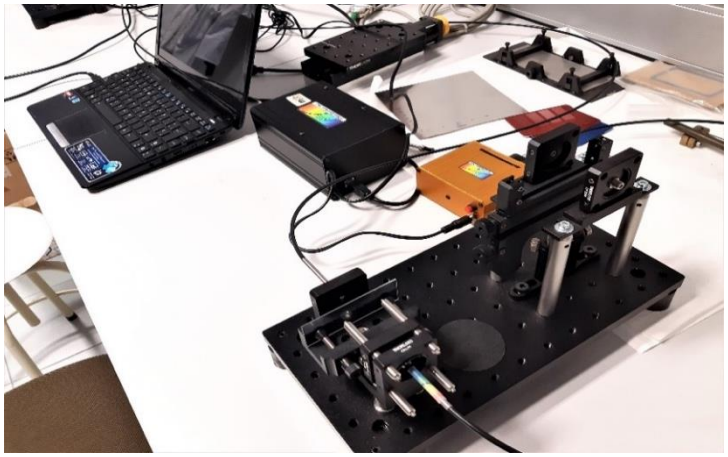

Figure 2.10: *Spectrometer setup used to measure the transmittance of the glasses. In the foreground is a glass piece in the sample holder. INMA-CSIC University of Zaragoza, Spain.*

Transmittance measurements were also performed using the processing lasers with power levels similar to those used in the cleaning experiments. For a given nominal power, the laser reaches a thermopile power sensor (LM10 Coherent), first directly and, in a second run, through the glass that was being characterized.

v. Scanning electron microscopy and Field emission scanning Electron microscopy with energy dispersive X-ray spectroscopy

Scanning Electron Microscopy (SEM) is a powerful technique in the examination of materials. High magnification images, with a good depth of field, are obtained through SEM using a beam of electrons rather than the traditional visible light. An electron beam

that strikes a target sample will cause the emission of characteristic X-rays, which, with the aid of high-magnification, high-resolution imaging can show the distributions of the chemical elements within the sample (Murphy, 2001; Vandenabeele, 2007). Other important signals produced by SEM equipment include backscattered electrons (BSE) and secondary electrons (SE). Secondary electrons produce an image showing the surface morphology and features while backscattered electrons provide information on elemental chemical distribution within the sample (Danilatos, 1986; McMullan, 1995; Smith & Oatley, 1955; Stokes, 2008).

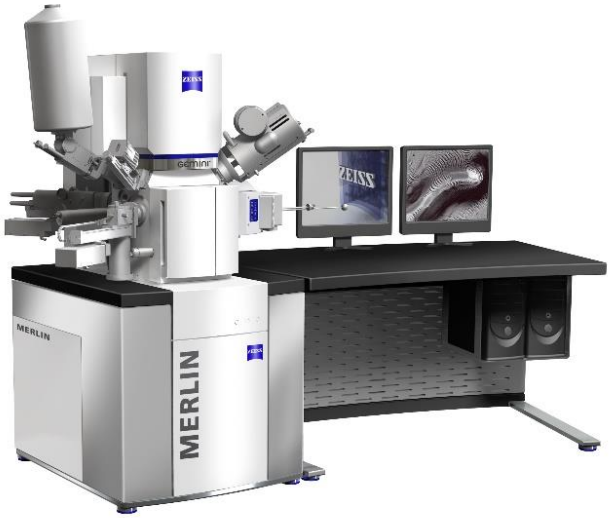

Figure 2.11: *FE-SEM equipment used in this work. ©ZEISS Microscopy, Germany*

The elemental composition of a region of the sample can be determined and spectra generated when SEM is coupled with energy-dispersive X-ray spectrometer (EDS) (McMullan, 1995; Stokes, 2008). It is important to note that SEM-EDS rely upon an electron beam to stimulate elements within a sample to fluoresce X-rays unlike other techniques such as XRF which use electromagnetic radiation. A typical scanning electron microscope operates at a high vacuum, although recent developments have come up with low pressure or environmental SEM (ESEM) which is best suited for biological samples (Stokes, 2008; Suzuki, 2002). The interest of an ESEM for heritage materials lies in the absence of a deposit of a conductive layer on the surface to be observed, which reduces the resolution of images and maps obtained in that mode due to the interactions between electrons and X-rays with the remaining air molecules.

The sample surfaces in this study were observed before and after the laser treatment with a JSM 6360-LV Scanning Electron Microscope (SEM). Images were taken in a vacuum mode at 20 Pa. Polished transverse samples were also analysed using a Field Emission Scanning Electron Microscope (FE-SEM, Carl Zeiss MERLIN) (fig. 2.11). Samples without coating were also observed in this work using low electron acceleration voltages. Semi quantitative elemental analysis of the glass samples was performed using Energy Dispersive X-ray Spectroscopy (EDS, INCA350, Oxford Instruments) with acquisition times of 500 s.

vi. SEM-Cathodoluminesence (SEM-CL) spectrometry

The CL system used in this work is installed on a FESEM (Field Emitting SEM) JEOL IT500 (fig. 2.12). To collect SEM-CL spectra, a Gatan MonoCL3 system equipped with a retractable mirror was used. The collected light was directed to a monochromator and then to a high-sensitivity PMT. The spectral range was set to 350–900 nm with acquisition time of 2 nm/sec.

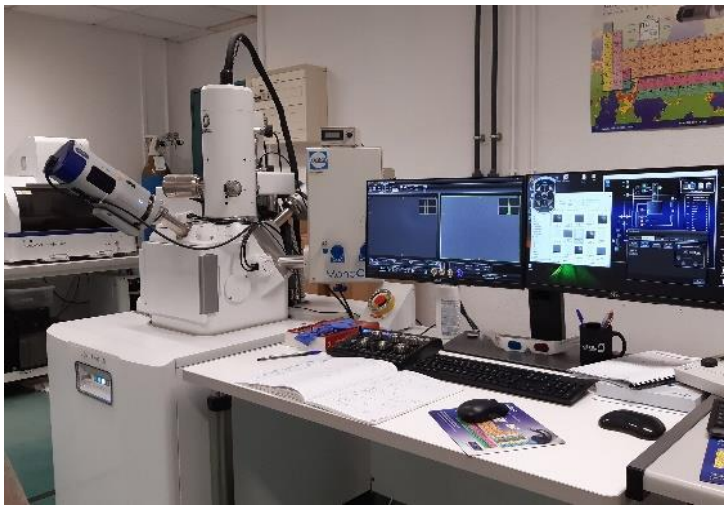

Figure 2.12: *FESEM-EDS equipment utilized for surface analysis. This equipment is also equipped with a cathodoluminescence detector. Archéosciences Bordeaux, Université Bordeaux Montaigne, France.*

The acceleration voltage was 20 kV, with current density of around 20 nA. No carbon or metal coating was needed. High voltage for the PMT (photomultiplier tube) was 1200 V.

vii. X-ray fluorescence (XRF)

X-ray fluorescence (XRF) is the emission of characteristic secondary (or fluorescent) x-rays from a material that has been excited by bombarding with high energy short wavelength radiation (e.g. X-rays or gamma rays). Its characterization capabilities are due in large part to the fundamental principle that each element has a unique atomic structure allowing emission of X-rays that are characteristic of an element's atomic structure to be identified uniquely from each other. Since the energy differences between electron shells are known and fixed, the emitted radiation always has a characteristic energy, and the fluorescence X-rays that arise can be utilized to determine the abundances of elements in the sample (Janssens *et al*., 2000; Legrand *et al*., 2019; Shackley, 2011; Van der Snickt *et al*., 2016). The phenomenon is widely used for elemental analysis in the investigation of a wide range of materials such as metals, glass, ceramics, photographs and building materials. XRF can be used to analyze historical stained glass to determine the composition of the materials used to manufacture the glass, to identify surface deposits and corrosion and degradation products among other important details. X-ray maps to determine the elemental distribution on the glass surface and on the grisaille were acquired at a voltage of 15kV and 40kV, with a current of 1000 μA, a collimator measuring 0.5 x 0.5 mm and frame accumulation counts set at 5.

viii. Raman spectroscopy

Raman spectroscopy is a non-destructive photonic technique and one of the most powerful tools for molecular and structural investigation of materials. Raman spectroscopy relies on the scattering of radiation rather than absorption. A sample is illuminated with a monochromatic laser beam which interacts with the molecules of the sample leading to a scattered light. This Raman scattering occurs as a result of a weak interaction between the radiation and the molecules. Though most of the wavelength of the scattering radiation is the same as that of the incident light, due to Rayleigh scattering, photons are occasionally scattered with more energy, or less energy. This Raman scattering produces spectral lines that are distinct for each molecule. This phenomenon allows individual components of a substance to be identified from a single spectrum. Raman scattering constitutes only a fraction of the scattered radiation that has a frequency different from the frequency of the incident radiation (Bumbrah & Sharma, 2016; Daher *et al*., 2010; Davies *et al*., 2008; Ferrer & Torres, 2013; Vandenabeele, 2013).

The equipment that has been used in this work is a Renishaw type RM2000 equipped with three lasers at 785-633-532 nm with two monochromators (grating at 1200 gr/mm and 1800 gr/mm). The system is coupled with a Leica LM-DM microscope holding 4 objectives (x5, x10, x20 for global approach, x50 long and short focal) (fig. 2.14). System works with a motorized stage with a step accuracy of 1µm. The detector is a 576x576 pixels CCD cooled by Peltier effect. The spatial resolution is $8\mu m^3$ (2x2x2µm) and the spectral shift resolution is $1cm^{-1}$.

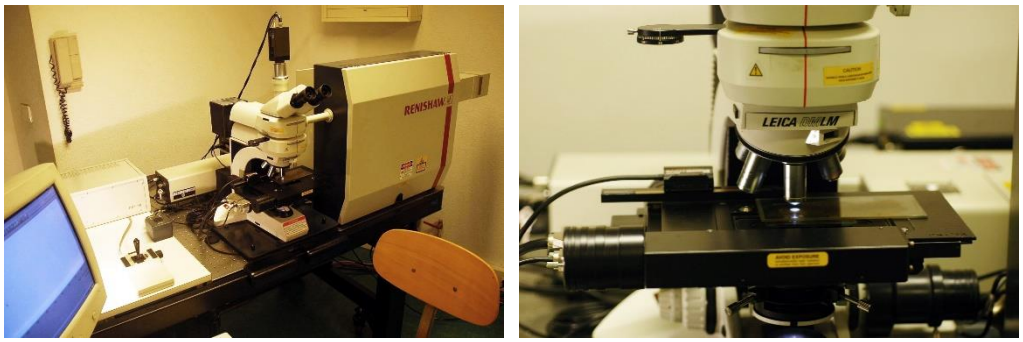

Figure 2.13: *Raman spectroscopy system used in this work. Archéosciences Bordeaux, Université Bordeaux Montaigne, France.*

ix. Thermal camera

It is important to have a real-time control of temperature of the surface subjected to laser radiation in combination with a preliminary setting of laser parameters to prevent immediate and long term damages (Striova *et al.*, 2021). Previous studies have shown the exploitation of thermocouples to detect temperature gradients during laser irradiation in medical and commercial fields. De Cruz *et al*. (de Cruz *et al.*, 2014) applied a similar approach to monitor the effects of an Er:YAG laser irradiation in the cultural heritage field (Striova *et al.*, 2021). Other temperature monitoring studies during laser treatment were devised by Osticioli *et al*. (Osticioli *et al.*, 2017) in which they used a thermopile sensor and an optical circuit to monitor the effects of the laser irradiation on a target surface.

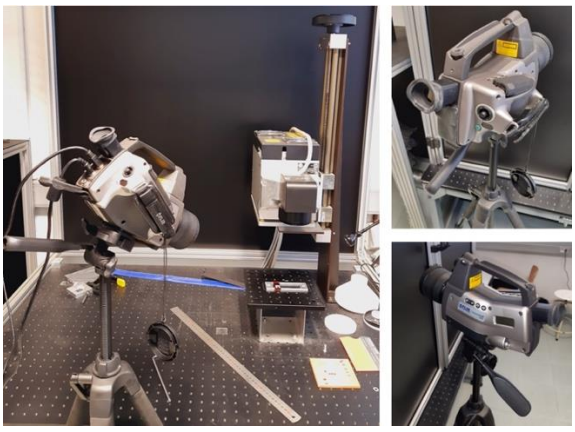

Figure 2.14: *Thermocamera set-up used to monitor temperature rise on the glass surfaces. INMA-CSIC University of Zaragoza, Spain.*

Here, in this work, the glass average temperature increase was monitored and recorded using a thermocamera (Thermo Cam P25, Teledyne FLIR Systems, USA) during representative laser treatments (fig 2.15).

CHAPTER 3: GLASS CHARACTERISTICS

3.1. Contemporary glass samples

3.1.1. Description of the samples

Various contemporary glass items of different colours and chemical composition were incorporated in the experimental process for comparisons. A total of 49 contemporary stained-glass samples from the glass factory of *Verrière de Saint-Just* (Saint-Just-Saint-Rambert, Loire France) were sourced for this experiment. The *Verrière de Saint-Just* glass factory was founded about 189 years ago. Their expertise in the art of glass making, blown glass to be specific, has been handed down from generation to generation. Currently, Verrière de Saint-Just glass maker is the reference supplier of glass and stained-glass in Europe (https://www.archiexpo.com/soc/verrerie-de-saint-just-62271.html).

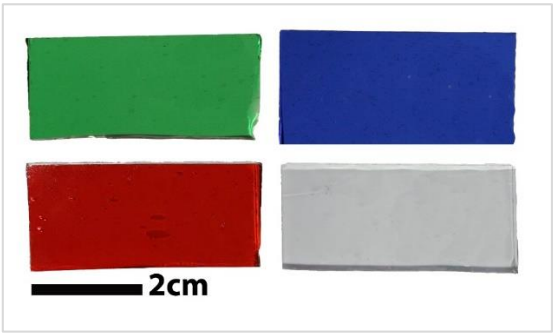

Figure 3.1: *Modern glasses from Verrière de Saint-Just factory used for the experiments.*

The samples were of different colours and were cut into rectangular samples of approximately 4 cm x 1.5 cm x 2 mm. The selection of the contemporary glasses was narrowed down to four pieces (fig. 3.1) that represented the different shades of colour from the 49 glasses. The four were green, blue, red and colourless pieces.

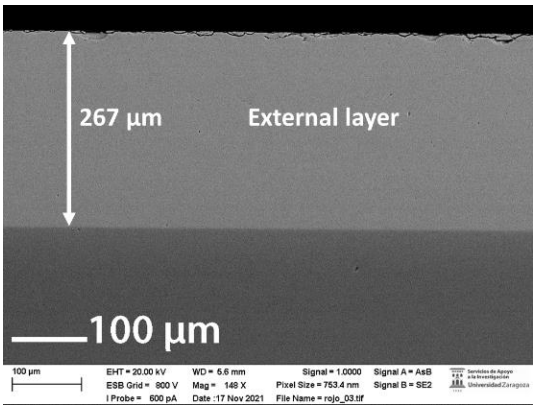

Figure 3.2: *FESEM image of the red glass showing the external layer (approximately 267 µm in thickness) that has been observed in one of the sides. See Table 3.1 for elemental composition of this layer.*

Glass	O	Si	Na	Ca	Mg	K	Al	Cr	Cu	As	Zn	Ba	Co
Green	57.8	25.2	12.3	3.3	1.0	0.1	-	0.1	0.1	-	-	-	-
Colourless	58.3	25.5	11.7	3.3	0.9	-	0.2	-	-	0.2	-	-	-
Red	58.3	25.6	11.5	3.4	1.0	0.1	0.2	-	-	0.2	-	-	
Red (surface)	57.7	27.1	7.0	-	-	5.6	-	-	-	-	2.1	0.5	-
Blue	57.8	25.1	12.6	3.4	1.0	-	-	-	-	-	-	-	nd

Table 3.1: *Modern glasses from Verrière de Saint-Just factory. EDS elemental analyses (at%, acquisition time 500 s) obtained on the four contemporary glasses subjected to this study.*

Elemental chemical compositions were determined by EDS analyses and are presented in table 3.1. The major components found in the green, colourless and blue glasses include SiO_2, Na_2O, CaO, and MgO. Differences in colours are reflected in the presence of small amounts of other elements, as for instance Cr and Cu in the green glass. The red glass differs from the previous ones. In this case, the glass exhibits an external layer of 267 µm with a different composition in one of the sides, as can be observed in figure 3.2. The bulk composition of this glass is similar to that of the other glasses, but its external layer includes SiO_2, Na_2O and K_2O as main components, as well as important amounts of Zn and Ba oxides.

3.1.2. Analysis of the optical properties

Figure 3.3 shows the transmittance spectra that correspond to the different types of studied contemporary glasses. For each sample, spectra were acquired in three different positions, in order to obtain information about the homogeneity of the optical response in each glass. In all the cases, differences lower than10% are only observed in the regions of the spectra with transmittance values higher than a 70%. These differences have been associated to

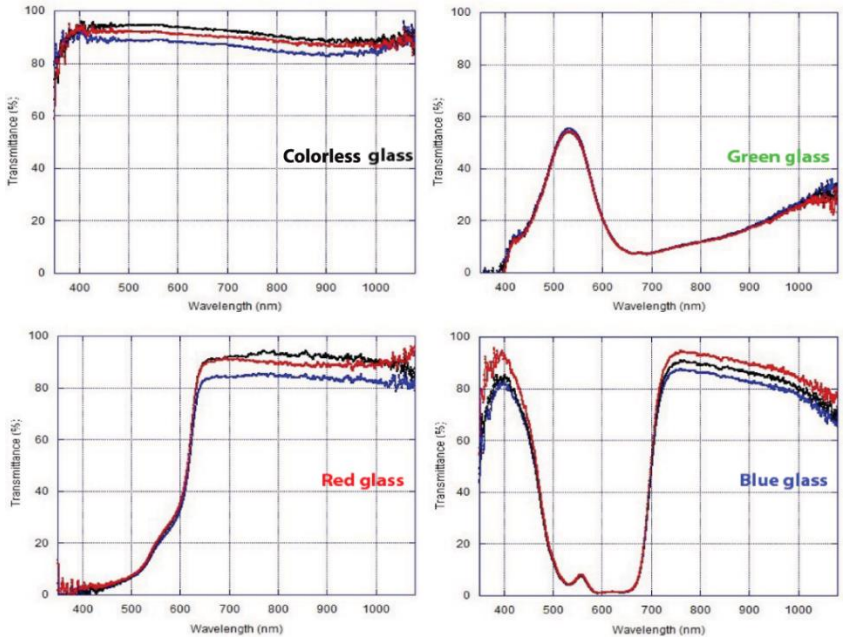

Figure 3.3: *UV-Vis-nIR transmittance spectra recorded in three different positions of each type of contemporary glasses from Verrière de Saint-Just factory.*

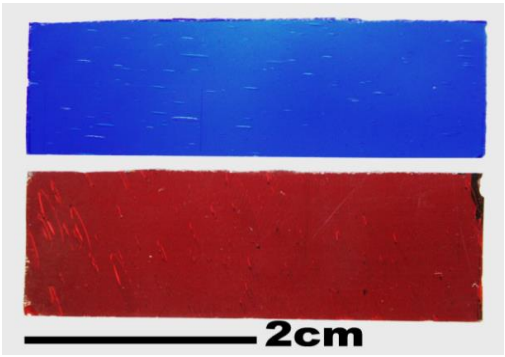

Figure 3.4: *Photograph of blue and red modern glass from Verrière de Saint-Just factory showing the presence of micro-bubbles inside the glasses.*

the distribution of micro-bubbles inside the glass (fig.3.4) in the illuminated area (approximately 1 cm in diameter).

As expected, the differences in colours generate very different transmittance spectra. For example, in the spectral range close to 1064 nm colourless, red and blue glasses absorb less than 20%. The amount of energy that is absorbed by the green glass, however, increases to values approaching 70%. In the region of the spectrum close to 530 nm, corresponding to the emission of green lasers, it is also observed that the amount of absorbed energy is very high in the three coloured glasses and only the colourless one presents high transmittance values. Finally, the four glasses, in particular the green and red ones, exhibit lower transmittance values in the proximity of 355 nm, a characteristic emission wavelength for third harmonic (UV) solid state and rare-earth fiber lasers. Red and green ones are opaque for radiations with wavelength lower than approximately 400 nm. By contrast, colourless and blue glasses show the typical cut-off response in the UV region with a strong reduction in the transmittance values when radiation wavelength penetrates in the UV range of spectra.

These experiments were performed with a light source in which the irradiance level (power density) is very low. In order to check if this behaviour is similar when the direct laser radiation is used, a set-up was built in which the energy that reaches a thermopile power sensor is recorded when the laser is focused directly on it (direct incidence), or through each one of the different glasses. Table 3.2 collects the transmittance values measured for each sample, using the 800 ps n-IR laser and the 300 ps UV laser as emitter sources, with the samples being placed at the laser beam focal distance. Results presented in table 3.2 and in figure 3.3 correlate very well, confirming that both types of measurements are equivalent for these materials.

	n-IR laser λ = 1064 nm, t_p = 800 ps		UV laser λ = 355 nm, t_p = 300 ps	
	Recorded power (W)	**% transmittance**	**Recorded power (W)**	**% transmittance**
Direct incidence	2.35	-	0.29	-
Colourless	2.05	87	0.15	52
Green	0.76	32	0	0
Red	2.01	86	0	0
Blue	1.72	73	0.13	45

Table 3.2: *Transmittance values obtained with a laser power meter, directly or through the different contemporary glasses from Verrière de Saint-Just factory used for this study and using near-IR and UV laser sources with the specified emission.*

The above results seem to indicate that laser treatments on colourless, blue and red stained-glass windows using IR radiation can be safer than using UV radiation because, once the IR laser radiation reaches the glass sample, the percentage of transmitted radiation is higher. But IR radiation effects have a strong thermal component and, in consequence, if absorbed by the glass or the external layer that is being removed, the sample temperature increases locally, inducing thermo-mechanical stresses on the glass that can generate micro-cracks in the sample. Due to these differences on the optical properties, the response of the green glass to IR radiation and the associated phenomenology are expected to be different.

This has also been observed during these transmittance measurements. The laser power meter used in these experiments determines the laser power by measuring the temperature at its sensor. From this measurement, the temperature evolution at the surface of the sensor is observed to reach a stable value after several seconds. Within this time frame, the higher absorption values observed in the green glass led to further heating and higher temperature gradients between the incident laser spot and its surroundings. This led to the fracture of the green sample during these optical transmittance studies when the IR laser radiation was used.

3.2. Historical glass samples

A number of historical stained-glasses pieces of different colours were used to develop new laser cleaning protocols. The pieces include three glass samples from the Cuenca Cathedral in Spain and three from Chartres Cathedral in France (Cathédrale Notre-Dame Chartres). The glasses exhibit different degrees of deterioration that had accumulated due to exposure to different environmental conditions over the centuries.

3.2.1. Description of the samples from Cuenca Cathedral (Spain)

Potash-lime silica glass was used for window panels in Europe, north of the Alps, in the medieval era. Glass produced during this period (11^{th}-15^{th} centuries) shows a different chemical composition from ancient soda-lime-silica glass probably as a result of unavailability of raw materials. The common glass composition of this era had a significantly high amount of potassium and calcium and a low concentration of silica which made this glass have a lower chemical stability in comparison to glass from other periods such as the soda-lime-silica glass (Navarro, 1991; Schreiner, 1991).

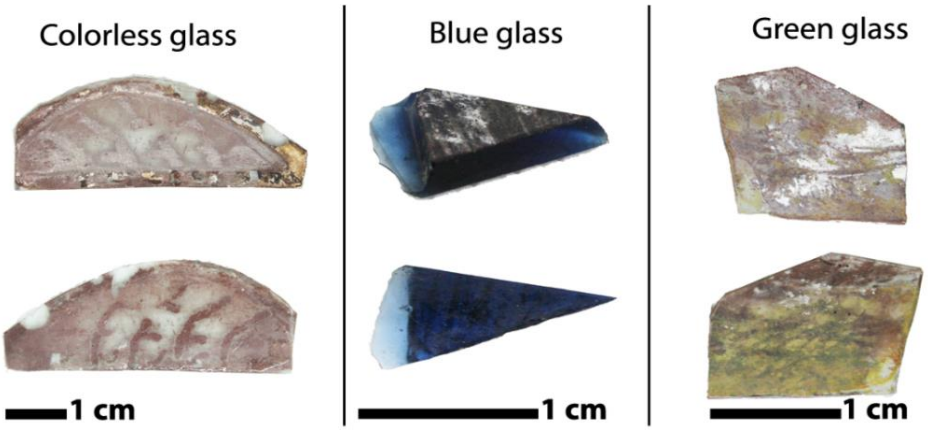

***Figure 3.5**: Photographs of the colourless, blue and green stained-glasses from the Cuenca Cathedral Spain. Top images show the faces with grisaille and the bottom images are for the opposite faces.*

Figure 3.5 shows the three glasses from Cuenca Cathedral that were studied. They were photographed in normal reflected light using a Canon EOS 400D digital camera. Images were captured of both the internal rough side (with paint layer) and of the external

smoother side of the glass pieces. The three glasses exhibit different levels of conservation with all the pieces showing presence of red-brown grisaille and localized white-coloured contamination crust on the internal face. Differences between the three glasses were studied with scanning electron microscopy.

Colourless glass

On this glass, the grisaille appears to have been applied in striated patterns that could possibly have been part of a larger iconography. This grisaille layer was well adhered to the bulk glass. The surface corrosion crust was spread mostly on the painted layer with thinnest crust forming on the glass surface itself. This glass piece had remnants of yellow-coloured putty on one of the edges, and this putty layer was approximately 600 μm in thickness.

Table 3.3 shows the composition of the glass obtained by EDS analysis. These values are the average of six measurements obtained in areas of approximately 100 x 25 μm^2 distributed in the cross section of the sample. The amount of SiO_2 reaches 63.9%wt, 11.5% of CaO, 7.5% of K_2O and 8.5% of Na_2O. The composition of this historical glass exhibits an important amount of K_2O, confirming that it is a soda-potash-lime silica glass, with similar content of soda and potash. Other oxides have also been detected, such as the network forming Al_2O_3 (4.2%wt), and the network stabilizer MgO (4.6%wt). This is a relatively high amount of Al_2O_3. The increase in viscosity and creation of surface tension is enhanced by the addition of aluminium compounds to the glass network, which in turn makes the glass to have a greater resistance to thermal shock (Navarro J.M. 1985; Pinto *et al.*, 2018).

Observing the cross-section with high magnification, small precipitates have been detected inside the glass, as it can be observed in figure 3.6. Comparing the composition of these regions with the rest of the glass, Mn has been detected.

% at	**O**	**Si**	**Ca**	**Na**	**K**	**Al**	**Mg**	**Cl**	**Fe**
	57.9	*23.4*	*4.5*	*6.0*	*3.5*	*1.8*	*2.5*	*0.4*	*0.1*
% wt	**SiO_2**	**CaO**	**Na_2O**	**K_2O**	**Al_2O_3**	**MgO**			
	63.9	*11.5*	*8.5*	*7.2*	*4.2*	*4.6*			

Table 3.3: *Colourless glass from Cuenca cathedral. Elemental composition (%at) determined by EDS on the glass and % wt of the main oxides.*

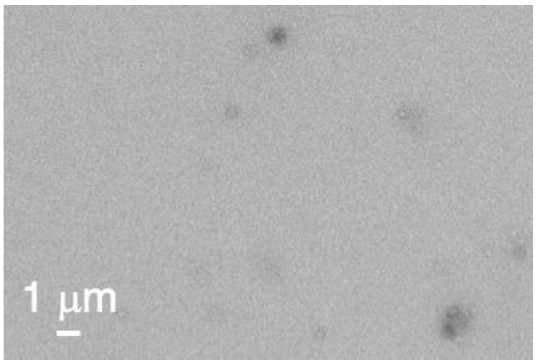

***Figure 3.6**: Small precipitates that have been detected in the cross section of the colourless glass from Cuenca cathedral.*

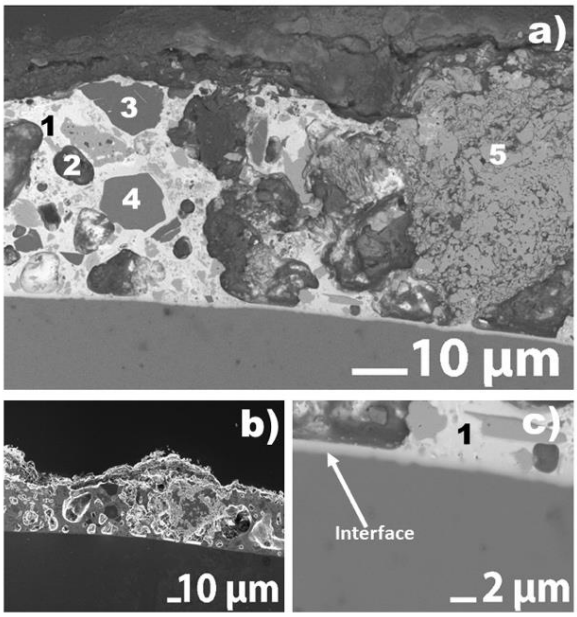

***Figure 3.7:** Colourless glass from Cuenca cathedral. (a) Cross-section on the region with grisaille, (b) topography in this layer, and (c) detail of the interface between the glass and the grisaille.*

Figure 3.7 shows the cross-section of the grisaille layer. It has a thickness that ranges between 45 and 75 µm. The layer has different components (fig. 3.7a) and high porosity, as it can be observed in figure 3.7b. Elemental analysis of the different phases is presented in table 3.4. Grisaille consists on a matrix (region 1) of lead silica glass, as the glass phase, and iron oxide (Fe_2O_3) as the pigment. Region 2 corresponds to a grain of iron oxide, while region 5 shows oxides particles with a higher porosity. Also, aluminium and potassium-aluminium silicates are detected. Other important issue is the good adherence between the

grisaille and the glass, observing a diffusion layer of approximately 750 nm thick.

	O	Si	Ca	Na	K	Al	Mg	Fe	Pb
1	*57.7*	*21.8*	*1.1*	*1.5*	-	*0.8*	*0.7*	*2.6*	*13.8*
2	*57.4*	-	-	-	-	-	-	*42.6*	-
3	*63.4*	*31.2*	-	-	*1.5*	*3.7*	*0.3*	-	-
4	*59.1*	*22.3*	-	-	*8.8*	*9.8*	-	-	-
5	*57.4*	-	-	-	-	-	-	*41.6*	-
Interface	*58.1*	*24.1*	*2.6*	*1.9*	*1.2*	*0.9*	*1.7*	*2.0*	*7.5*

Table 3.4: *Colourless glass from Cuenca cathedral. Elemental composition (% at) determined by EDS on the different regions indicated in figure 3.7*

Figure 3.7 shows that the grisaille structure suggests a combination of Pb and Fe oxides with the latter forming particles with a higher porosity. This type of combination and formation is an indication that during the production of the grisaille, the ideal temperature to allow the grisaille to adhere to the glass was reached (roughly 600-750^{o}C), as it can be observed in the interface presented in fig. 3.7.c, but it was not enough to allow the complete melting of Fe (Fernandes *et al*., 2008).

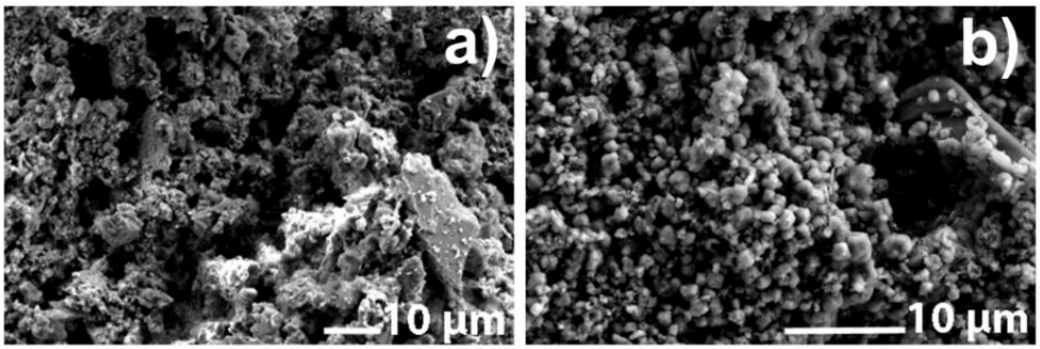

Figure 3.8*: Micrographs of the surface of the crust layer in two regions of the surface crust of the colourless glass from Cuenca cathedral.*

	O	Si	Ca	Na	K	Al	Mg	P	Fe	Pb	S
Crust (1)	*74.1*	*6.6*	-	*0.9*	-	*3.0*	*1.2*	-	*2.5*	*2.8*	*8.7*
Crust (2)	*75.8*	*0.9*	*12.4*	-	-	*0.3*	*10.4*	-	-	-	*0.2*
Crust (3)	*71.8*	*13.8*	-	*1.2*	-	*3.9*	*1.8*	*1.1*	*4.4*	*0.8*	-

Table 3.5: *Elemental composition (% at) determined by EDS on different regions of the crust layer observed in the colourless glass from Cuenca cathedral.*

All the glass surface is covered by a white layer. As it can be observed in figure 3.8 and in table 3.5, this layer is not uniform. SEM analysis shows that the morphology of this layer is different when the surface morphology is observed on top of the grisaille (fig. 3.8a) and on top of the glass (fig. 3.8b), where regular submicrometric particles are observed. EDS analyses also show that different regions have different compositions. In one case, the composition showed an important amount of S, while in the other case, the crust showed a relatively rich concentration of Ca and Mg which could infer to the presence of calcite ($Ca_2(CO_3)_2$) or calcium magnesium carbonate ($CaMg(CO_3)_2$) and the initial formation of anhydrite ($CaSO_4$) or gypsum ($CaSO_4 \cdot 2H_2O$). In other regions, P was also detected, indicating the presence of phosphate compounds.

This analysis has been completed with Raman spectroscopy. Like EDS analysis, different Raman spectra are different depending on the region where they have been recorded. Figure 3.9 collects the different types of spectra that have been identified. Figure 3.9.a shows a Raman spectrum that it is usual in carbon-based compounds. Generally, the Raman spectrum of these carbon-based compounds comprise of a narrow peak at about 1580 cm^{-1} known as G band and another peak at about 1350 cm^{-1} known as D band often referred to as the 'disorder' band (Tomasini *et al*., 2015). Both spectra exhibit these two broad and almost overlapping peaks with intensity reaching a maximum of approximately 1340 ± 12 cm^{-1} and 1582 ± 5 cm^{-1}. This order of spectra with two broad and strongly overlapping peaks typical of carbon has been observed for different types of compounds such soot, lamp black, carbon black, bistre, etc.(Marucci *et al*., 2018; Sadezky *et al*., 2005; Tomasini *et al*., 2015). In this glass, it has been observed that the external layer of the crust has a darker colour, that could explain this type of spectra. Furthermore, in figure 3.9.a a broad band was observed around 617 ± 7 cm-1, an indication of the presence of iron oxide, and this correlates with the analysis of this glass by EDS (Tables 3.3 and 3.4).

In other regions (fig. 3.9.b), in addition to the carbon-base compound, the Raman analysis further revealed a heterogeneous corrosion product composed of hydrated and anhydrous sulfates. In addition, apatite was also identified. Raman spectra for anhydrite show the SO_4 symmetric stretching mode at 1015 cm^{-1}. The symmetric bending and asymmetric stretching modes of SO_4 tetrahedra appear in two bands i.e. 420 cm^{-1} and 496 cm^{-1} and the other one at 1122 cm^{-1} and 1159 cm^{-1}. The bands seen at 628 cm^{-1} and 671 cm^{-1} are attributed to the to the asymmetric bending vibration mode (White, 2009). A band with a weak intensity can be seen at 608 cm^{-1}, and according to Liu *et al*. (2009) this band is due to the asymmetric bending mode of SO_4.

Finally, figure 3.9.c shows that in other regions, gypsum is detected. In this case, the strongest peak at the Raman spectrum is observed at 1010 cm^{-1} and this peak relates to the symmetric stretch vibration mode of the SO_4 tetrahedra. At approximately 420 cm^{-1} and 497 cm^{-1} double symmetric bending exhibited by presence of gypsum is observed. Peaks assigned to the asymmetric bending vibration modes of sulfates appear at about 623 $cm^{-1}$and 673 cm^{-1}, with the peaks observed at 1118 cm^{-1} and 1155 cm^{-1} being assigned to the asymmetric stretching modes. Since the Raman spectra were acquired in the spectral range 200-2000 cm^{-1}, the characteristic bands for the stretching vibration modes of water in gypsum were not confirmed. These bands have previously been reported by White (2009) and Bhagavantam (1938) as appearing at 3406 cm^{-1} and 3494 cm^{-1}.

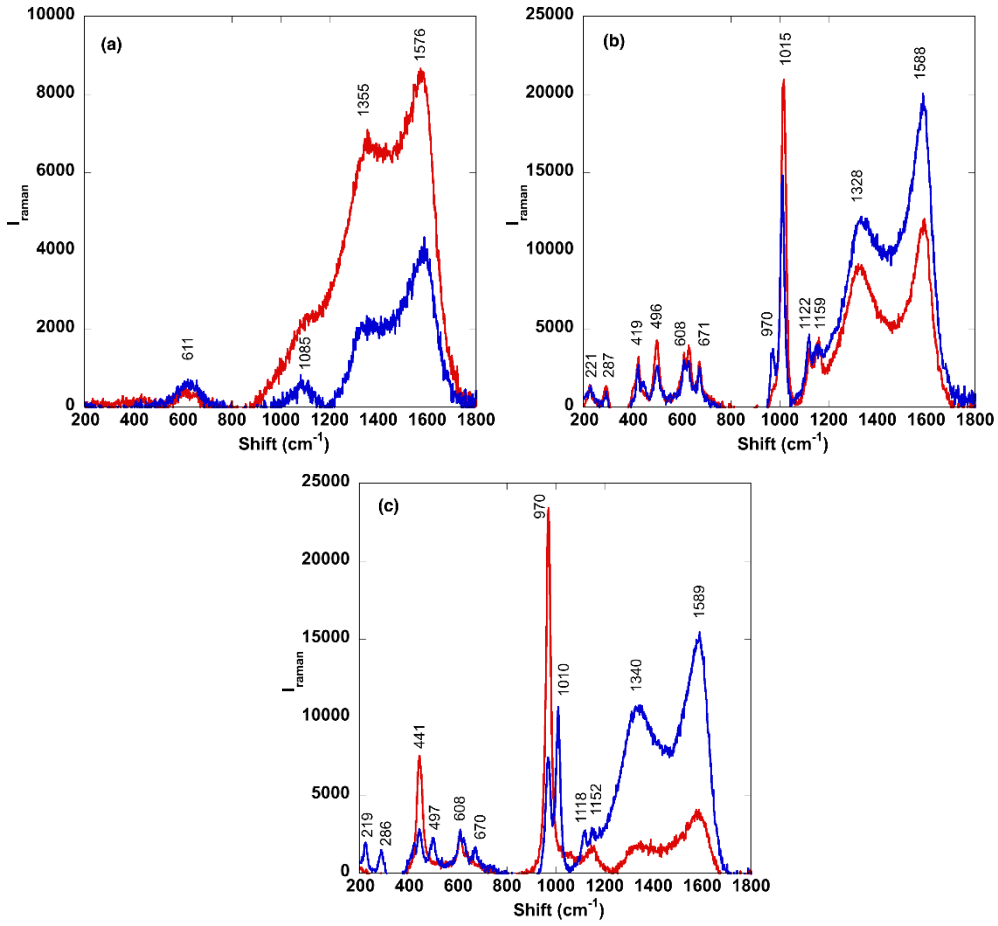

Figure 3.9*: Raman spectra in different regions of the surface of the colourless glass from Cuenca cathedral.*

In addition, Raman analysis identified presence of apatite as part of the crust covering the colourless glass surface. The typical single peak of apatite can be observed at 970 cm^{-1} in figures 3.9.a and 3.9.b and which is consistent with previous measurements presented in the literature (Litasov & Podgornykh, 2017). A peak corresponding to symmetric bending of PO_4 appear at about 440 cm^{-1} while the asymmetric bending mode peak can be observed at about 608 cm^{-1}.

Green glass

This glass is also a glass with similar contents of Na_2O and K_2O (tab. 3.6). The main difference with the colourless one is the low content of CaO. It also shows a deterioration associated with the formation of a white layer on top of the glass surface. The layer has a high level of non-uniformity showing regions where the crust layer is very thin (fig. 3.10) and others with a bigger thickness (fig. 3.11). In this crust layer, the crystals have a needle-like shape as it can be observed in figure 3.11. EDS analysis (tab. 3.7) allowed the identification of this compound as either gypsum ($CaSO_4 \cdot 2H_2O$) or anhydrite together with a formation of calcite (calcium carbonate). Also in this case, the red-brown grisaille used on the three Cuenca glass indicated use of lead silica glass, as the glass phase, and iron oxide (Fe_2O_3) as the pigment.

% at	**O**	**Si**	**Ca**	**Na**	**K**	**Al**	**Mg**	**Cl**	**Fe**	**Pb**
	64.3	*25.1*	*1.8*	*4.1*	*2.9*	*2.0*	*1.2*	*0.4*	*-*	*0.7*
% wt	**SiO_2**	**CaO**	**Na_2O**	**K_2O**	**Al_2O_3**	**MgO**				
	69.2	*4.6*	*5.8*	*6.3*	*4.7*	*2.2*				

Table 3.6: *Green glass from Cuenca cathedral. Elemental composition (%at) determined by EDS on the glass and % wt of the main oxides.*

	O	**Si**	**Ca**	**Na**	**K**	**Al**	**Mg**	**Cl**	**Fe**	**Pb**	**S**
Grisaille	*64.7*	*17.5*	*3.1*	*6.5*	*1.4*	*1.3*	*2.3*	*-*	*0.9*	*2.4*	*-*
Crust	*76.3*	*0.7*	*10.6*	*-*	*-*	*-*	*-*	*-*	*-*	*-*	*11.9*

Table 3.7: *Green glass from Cuenca cathedral. Elemental composition (%at) determined by EDS on the different regions observed in this glass.*

Figure 3.12 shows the interface between the grisaille and the glass in this sample. It was determined that the maximum thickness of the paint layer was approximately 51 µm. By contrast with the colourless glass (fig.3.7), in this case a strong interaction with the glass is observed in many regions of the glass surface, generating some bubbles on it. The size

of these pores ranges between 3.5 µm and 7.5 µm. These bubbles deteriorate the glass surface as it was observed in figure 3.13.

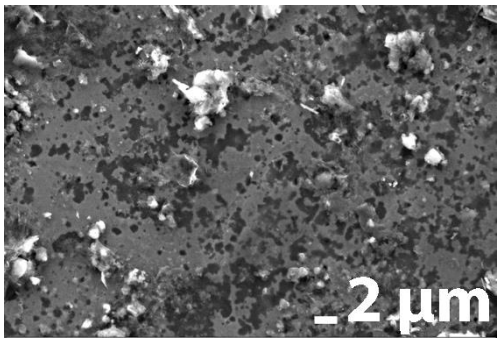

***Figure 3.10**: Green glass from Cuenca cathedral. Micrograph of the surface of the green glass in regions where the crust layer is thinner, revealing a flat surface (seemingly original and corroded surface)*

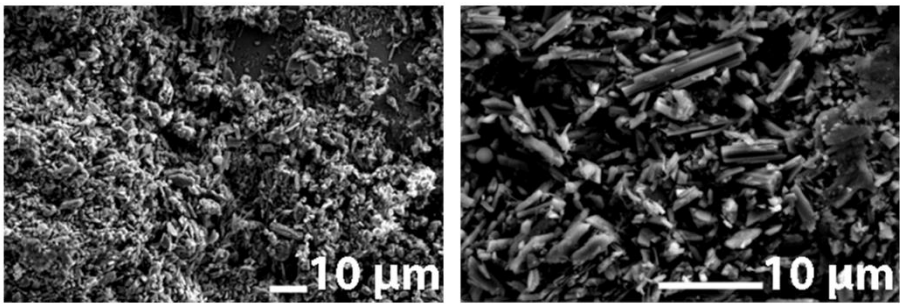

***Figure 3.11**: Green glass from Cuenca cathedral. Micrographs showing the variations of the thick crust forming on the surface of the green glass.*

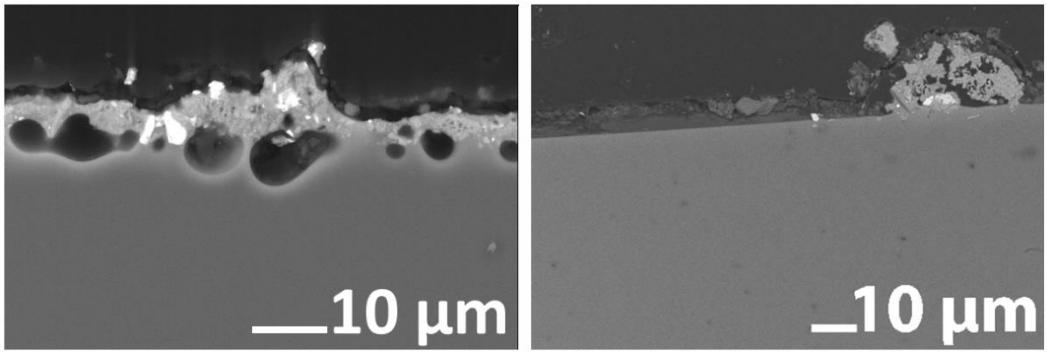

***Figure 3.12**: Green glass from Cuenca cathedral. Detail of the interface between grisaille and glass.*

An X-ray mapping to determine the elements constituting the green glass substrate and the grisaille was also performed using XRF. The area of the glass from which the X-ray maps were obtained, measured 17 x 14 mm^2, as it is seen in figure 3.13. The composition of the glass was identified by the detection of significant amounts of homogenously distributed Si, Ca, Al and K. As observed in figure 3.13, Si, K and Al were mostly distributed in sections of the glass that had a thinner layer of grisaille and crust. Ca can also be detected in the glass, but with higher concentrations on the regions where the amount of crust is higher, in accordance with the EDS analysis of the crust layer presented in table 3.7.

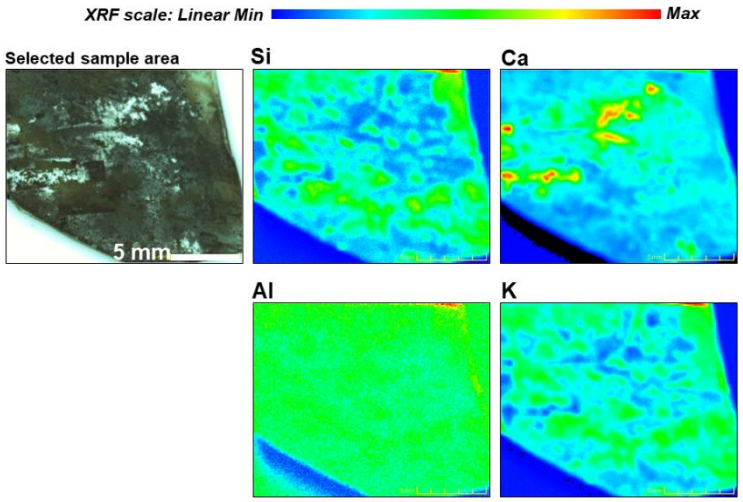

Figure 3.13: Green glass from Cuenca cathedral. XRF elemental map distribution of the glass forming elements.

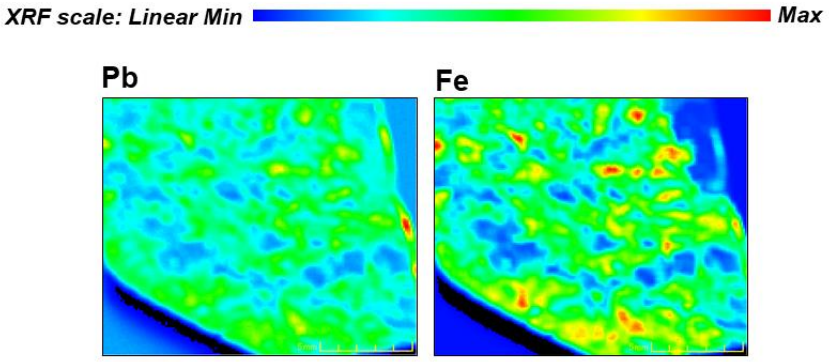

*Figure 3.14**:** Green glass from Cuenca cathedral. XRF elemental map distribution of the grisaille layer.*

Also, in this green glass, the red-brown grisaille used indicated the use of lead silica glass, as the glass phase, and iron oxide (Fe_2O_3) as the pigment and this is confirmed in figure 3.14 with the identification of Pb and Fe as well as by previous EDS analysis from the same glass (tab. 3.7). From figure 3.14, it can be seen that the distribution of these two elements (Pb and Fe) on the glass surface follows the regions covered with grisaille.

Figure 3.15 shows the X-ray maps of the main elements identified in the crust layer. Where the crust layer is thicker, the higher concentrations of S, Ca and P are detected. The microstructure of these areas with high S and Ca amount corresponds to the SEM observations presented in figure 3.11. Finally, with the detection of P observed in the X-ray map in figure 3.15, there was an indication of the presence of phosphate compounds as well in the crust.

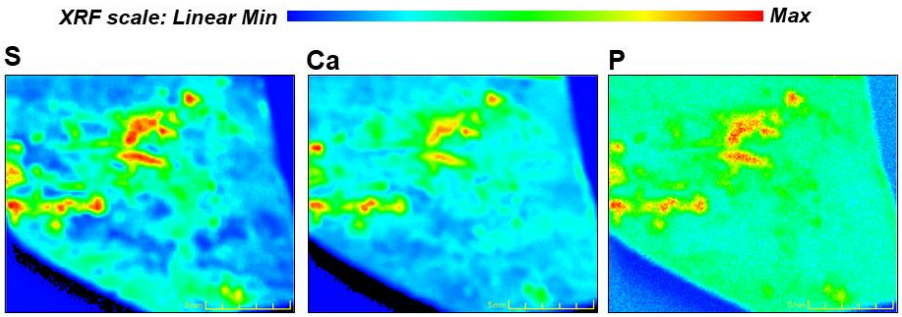

Figure 3.15: Green glass from Cuenca cathedral. XRF elemental map distribution of the crust forming compounds.

All these results have been complemented with a study of the Raman spectroscopy response of the sample. Raman spectra were obtained from areas covered by white crust. In particular, region indicated as Z1 in figure 3.16 was analysed. Five different spectra measured in five different points of this regions are presented in figure 3.17. Clearly, the detail presented in Figure 3.17.c shows the presence of two different compounds. Spectra recorded at positions 1 and 3 (Figure 3.18) show the fundamental bands of calcite which appear at 281 cm^{-1}, 712 cm^{-1} and 1086 cm^{-} (Ferrer & Torres, 2013; White, 2009). Calcite is the crystallographic form of calcium carbonate (Fernandes *et al*., 2008; Ferrer & Torres, 2013) and it has typical needle-shaped crystals previously identified by SEM in this work and presented on the right image in figure 3.11.

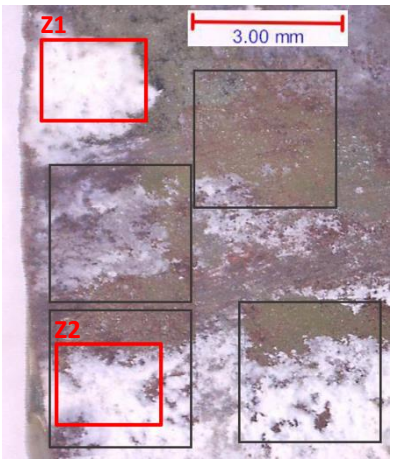

Figure 3.16: *Green Cuenca glass. The Raman spectra were collected on zone Z1.*

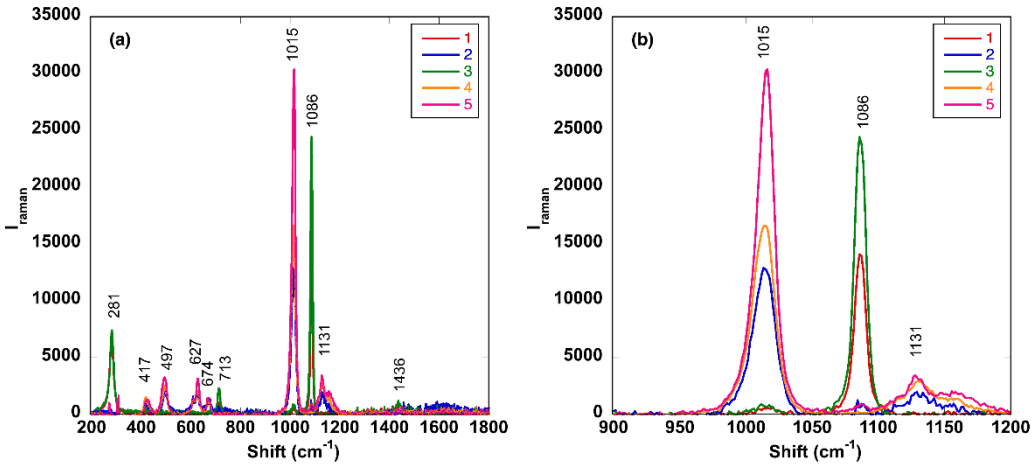

Figure 3.17: *Green Cuenca glass. (a)Spectra collected in five positions of the crust on this glass (b) Detail in the regions 900-1200 cm^{-1}.*

Raman spectra in positions 2, 4 and 5 (fig. 3.17) identify the presence of hydrated and/or anhydrous calcium sulfate. Figure 3.22 presents the Raman spectrum of anhydrite and gypsum. Raman analysis on the surface crust further revealed a heterogeneous corrosion product composed of hydrated and anhydrous sulfates. Figure 3.19 presents the example of the spectra measured at positions 2 and 5. In this case, the main peak is located at 1014 cm^{-1} and it is associated to the symmetric stretch vibration mode of the SO_4 tetrahedra. The symmetric bending and asymmetric stretching modes of SO_4 tetrahedra appear at 417 and 495 cm^{-1}. The additional peaks at 628 and 673 cm^{-1}can be assigned to asymmetric bending vibration modes of sulfates (White, 2009). A band with a weak intensity can be seen at 610 cm^{-1}, and according to Liu *et al.* (2009) this band is due to the asymmetric bending

mode of SO_4 that often appear at 609-612 cm^{-1}. The peaks at 1131 cm^{-1} and 1159 cm^{-1} to the asymmetric stretching modes. A band at 1108 cm^{-1} had been reported by Bhagavantam (1938) and in figure 3.19.b, this band seem to have been overlapped by the 1129 cm^{-1} band.

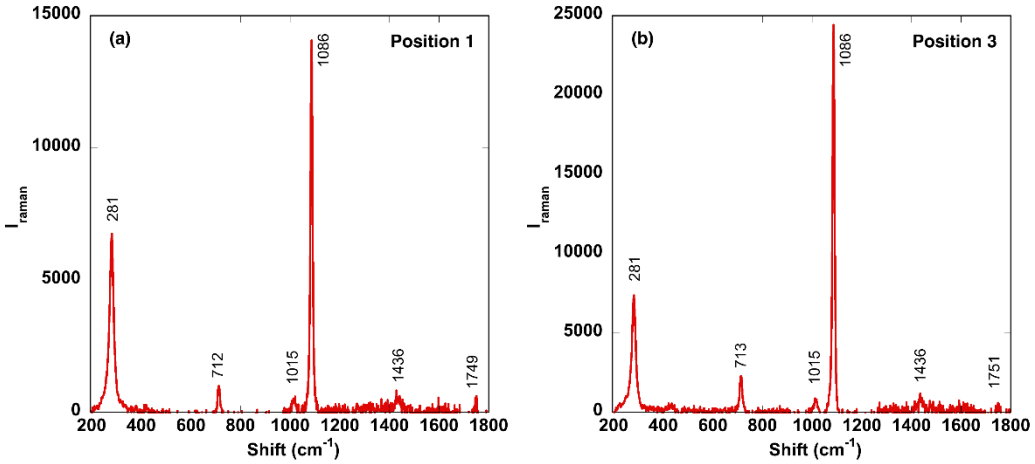

Figure 3.18: *Green Cuenca glass. Plots showing the fundamental bands of calcite which appear at 281 cm^{-1}, 712 cm^{-1} and 1086 cm^{-1} in the spectra recorded at positions 1 (a) and 3 (b).*

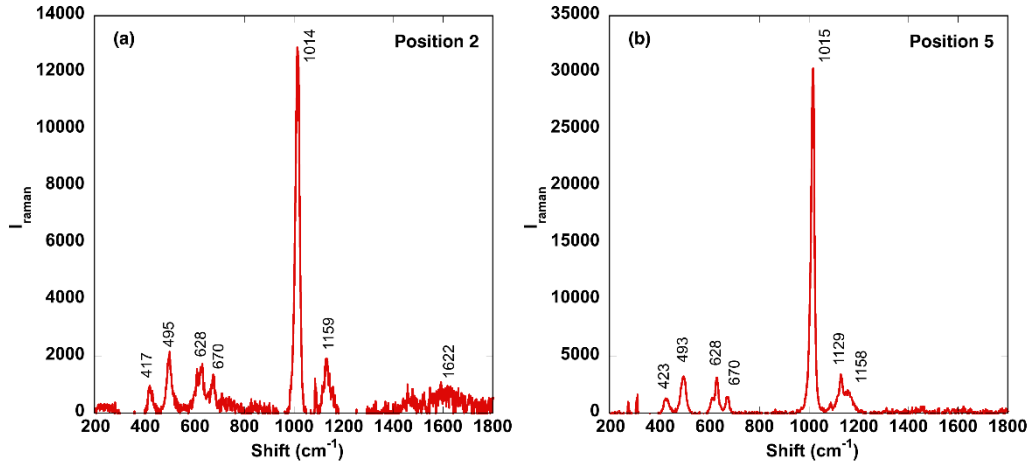

Figure 3.19: *Green Cuenca glass. Calcium sulfate spectra recorded in positions 2 (a) and 5 (b).*

It is not easy to differentiate between gypsum and anhydrite in these spectra. The internal bands of the SO_4 group produce similar spectra in both materials. In anhydrite the asymmetric stretching mode is split in about three bands and this can be explained by the distortion of SO_4 tetrahedra. In this case, in the SO_4 groups the oxygen atoms are in

different crystallographic environments. Within anhydrite, the oxygen atoms are linked with two calcium atoms while in gypsum with a calcium atom and two water molecules. As a result, the variations in the vibrational modes of the sulfate group could be a consequence of the dehydration process (Buzgar *et al*., 2009; Popović *et al*., 2003). The spectral range reached in this acquisition (200-2000 cm^{-1}) did not allow the recording of the characteristic bands for the stretching vibration modes of water in gypsum that typically appear at 3406 cm^{-1} and 3494 cm^{-1} (Bhagavantam, 1938; White, 2009).

Blue glass

The composition of the blue glass is different from the colourless and green glasses. As it can be observed in Table 3.8, the composition is the typical soda-lime glass, indicating that probably this glass was fabricated in a different period compared to the other two glasses. Looking at the cross section of the sample with higher magnification it is possible to detect a nanostructure of particles with a darker contrast in the images obtained with back-scattered electrons (fig. 3.20). Due to the size of these particles it is not possible to quantify their composition, but it was detected a higher amount of Al and lower amount of Na in comparison with the glass matrix. The amount of these particles is lower in the regions close to the sample surface. The grisaille (fig. 3.21) follows the same trends observed in the other two glasses, the use of the lead silica glass as the glass phase, adapted to the composition of the glass, and the use of iron oxide as pigment (seen as white particles in fig. 3.22). In the grisaille of this glass, the amount of lead is lower than in the other two glasses. It is worthy taking into consideration the heterogeneity of glass paints, given that variations in flux to pigment ratio is a common thing (Bernady *et al.*, 2018). Figure 3.24 shows the interface between the grisaille and the glass. As it was observed in the green glass, the reaction between both materials is high generating big bubbles on the glass surface, reaching sizes in the range of 3 µm and 23.5 µm.

% at	**O**	**Si**	**Ca**	**Na**	**K**	**Al**	**Mg**	**Cl**	**Fe**	**Pb**
	61.2	*24.8*	*3.9*	*10.0*	-	-	-	-	-	-
% wt	**SiO_2**	**CaO**	**Na_2O**	**K_2O**	**Al_2O_3**	**MgO**				
	73.8	*10.8*	*15.4*	-	-	-				

Table 3.8: *Blue glass from Cuenca cathedral. Elemental composition (%at) determined by EDS on the glass and % wt of the main oxides.*

	O	Si	Ca	Na	K	Al	Mg	Cl	Fe	Pb	S
Grisaille	*54.5*	*33.4*	*4.7*	*4.4*	-	-	-	-	*1.3*	*1.7*	
Crust	*74.7*	*0.5*	*11.7*	-	-	*0.2*	*0.3*	-	-	-	*12.6*

Table 3.9: *Blue glass from Cuenca cathedral. Elemental composition (%at) determined by EDS on different regions with grisaille and crust observed in this glass.*

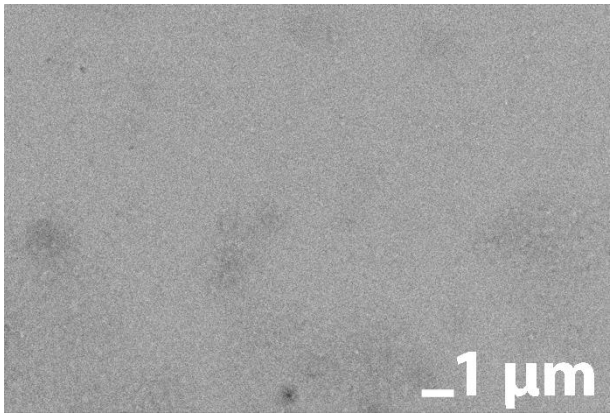

Figure 3.20*: Blue glass from Cuenca cathedral. Detail of the glass structure in cross-section.*

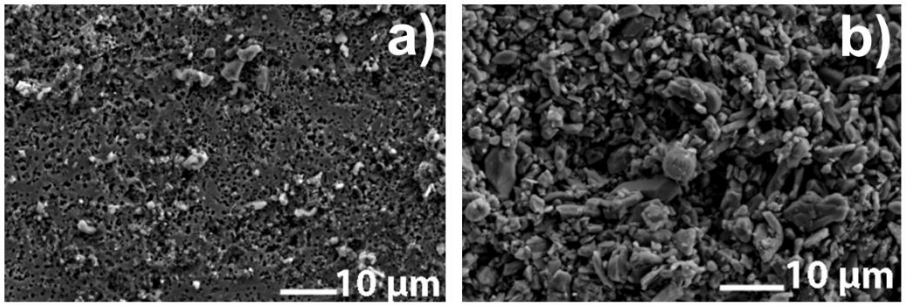

Figure 3.21*: Blue glass from Cuenca cathedral. Micrographs of the surface of this glass (a) grisaille, (b) areas with a thicker crust layer.*

Finally, the crust layer was confirmed as composed of calcium sulfate. In this sample, a uniform grisaille layer was not detected, as can be observed in figure 3.21.

X-ray mapping using XRF confirmed that the composition of the blue glass was different from that of the colourless and green glasses. The X-ray maps detected a significant amount of Si and a lower amount of Ca, a common trend in soda-lime glasses (fig. 3.23).

A similar trend observed in the other two glasses was followed by looking at the X-ray maps collected from the grisaille in the blue glass (fig. 3.24) i.e., the use of the lead silica

glass as the glass phase, adapted to the composition of the glass, and the use of iron oxide as pigment.

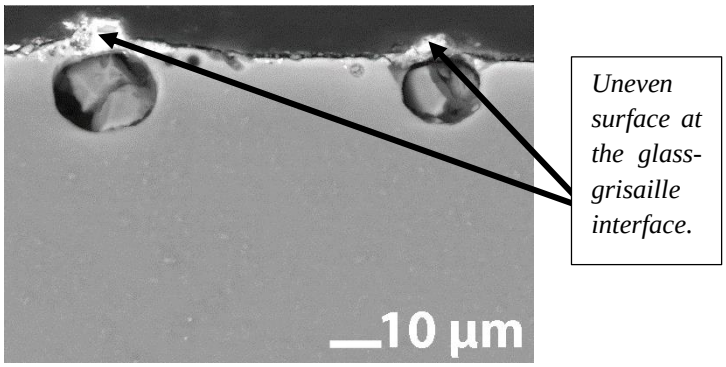

***Figure 3.22**: Blue glass from Cuenca cathedral. Detail of the interaction between grisaille and glass.*

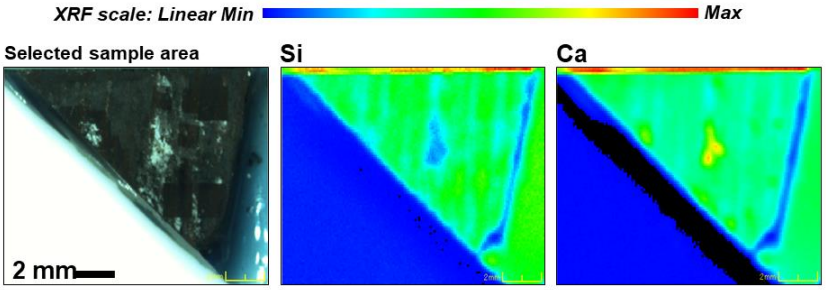

*Figure 3.23**:** Blue glass from Cuenca cathedral. XRF elemental map distribution of the glass forming elements.*

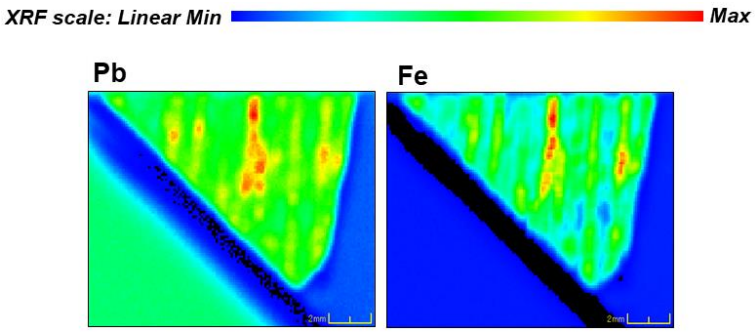

*Figure 3.24**:** Blue glass from Cuenca cathedral. XRF elemental map distribution of the grisaille layer.*

Finally, X-ray mapping presented in figure 3.25 also identified S and a higher

concentration of both Ca and P in areas that were covered with the crust. These elements were not evenly distributed and there was an indication that the crust was in an initial formation and very thin. The X-ray mapping in line with EDS analysis confirmed that the crust was composed of either gypsum ($CaSO_4 \cdot 2H_2O$) or anhydrite ($CaSO_4$). Also the presence of P in the mapping in figure 3.25 showed the formation of low amounts of phosphate-based compounds in the crust.

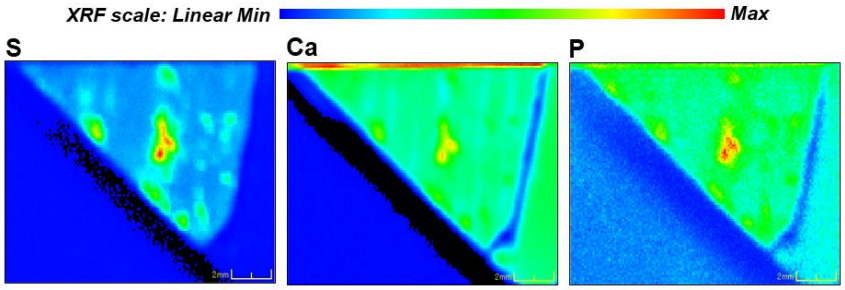

Figure 3.25: Blue glass from Cuenca cathedral. XRF elemental map distribution of the crust forming compounds.

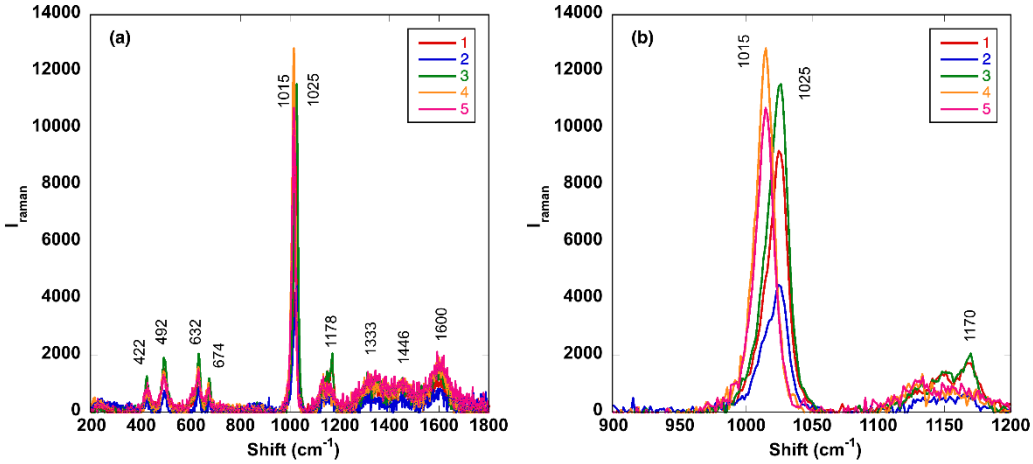

Figure 3.26: *Blue Cuenca glass. Raman spectra collected in 5 positions on the blue glass surface with a thick crust layer*

Figure 3.26 shows the spectra measured in five positions of the sample surface with a thick crust layer. The detail presented in Figure 3.26.b clearly indicates the presence of the two calcium sulfate compounds: anhydrite and gypsum. Details of the differences is presented in figure 3.27 where one type of spectra is presented and in figure 3.28, where the spectra of the other type, measured on positions 4 and 5, are presented. Clearly, it is observed that

the main difference is that the big peak associated with the symmetric stretch vibration mode of the SO_4 tetrahedra shifts from 1015 to 1025 cm^{-1} and that there is an additional peak at 1168 cm^{-1}.An analysis of the Rama spectra data base suggest that the compound detected in positions 1 and 3 could be anhydrite, while in the case of positions 4 and 5 this compound is gypsum. The rest of the spectra is similar to those measured in the green sample, in positions 2 and 5, where the calcium sulfate compound was observed, and that from this analysis can be associated to gypsum.

.

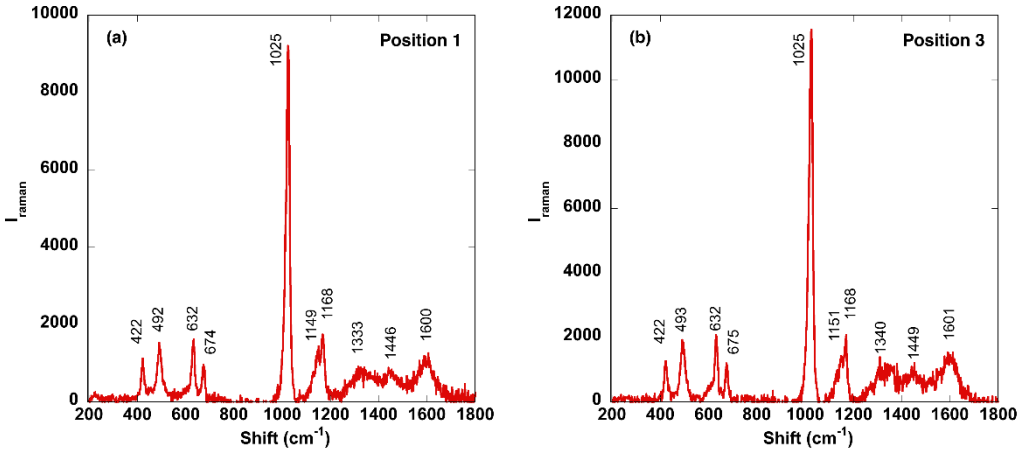

Figure 3.27: *Blue Cuenca glass. Calcium sulfate spectra recorded in positions 1 (a) and 3 (b).*

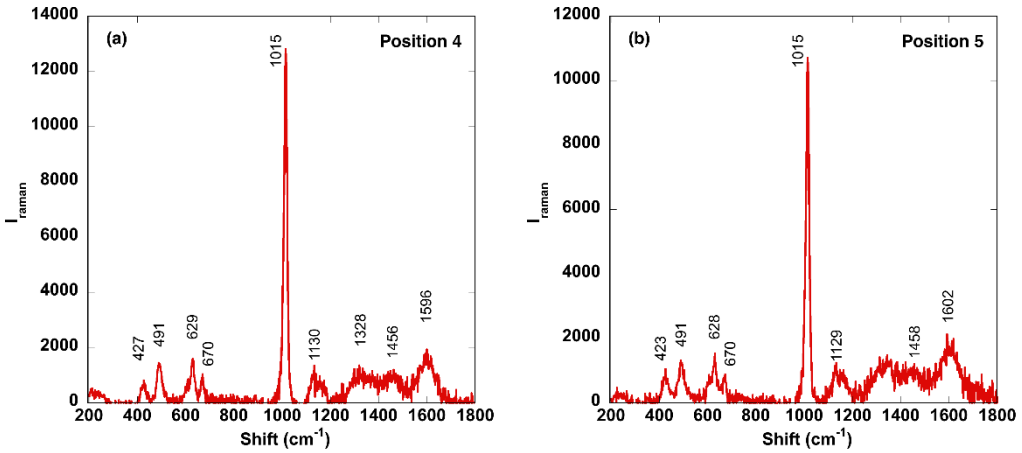

Figure 3.28: *Blue Cuenca glass. Calcium sulfate spectra recorded in positions 4 (a) and 5 (b).*

As a resume, it can be deduced that in the colourless glass, the crust is mainly composed by apatite and gypsum, in the green one by calcite and gypsum and in the bleu one by anhydrite and gypsum.

3.2.2. Description of the samples from the Chartres Cathedral (France)

Initial experiments were performed on a red coloured glass sample provided by the Maison-Lorin glass restoration workshop in Chartres, France. This glass piece measuring roughly 8 cm by 5.7 cm, is from Cathedral Notre-Dame, in Chartres (France) and is dated from the 13th century. The piece was photographed under normal reflected and transmitted light to observe the surface morphology and to determine the basic conservation status of the piece (fig. 3.29). The internal surface was covered with a very large deposit of a white limescale-type corrosion product as the one shown in figure 3.30. This white corrosion product was spread all over the glass surface. In addition, the inner face had an iridescence trace of mastic along the edges. The external face exhibited corrosion in the form of pitting and grooves spread out all over the glass face (top right photo in figure 3.29).

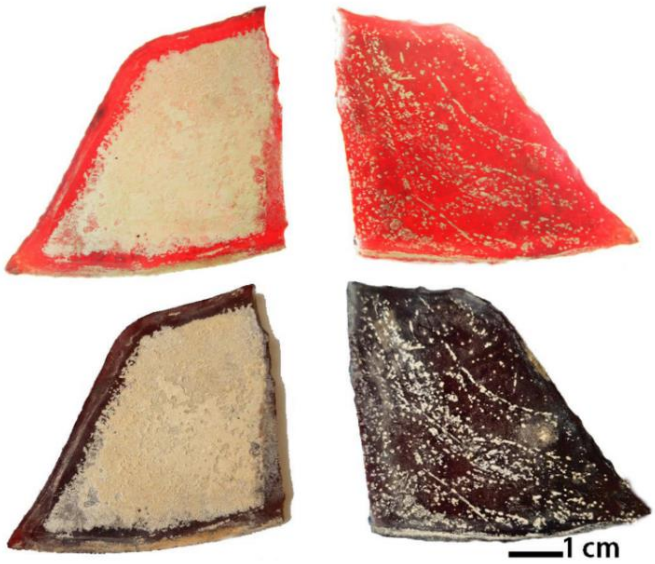

Figure 3.29: *Red glass from Chartres cathedral. Photograph of the glass taken under transmitted (top) and reflected (bottom) light. The internal face is on the left and the external one is on the right.*

Analyses by EDS, presented in table 3.10, on the red coloured glass from Chartres Cathedral detected that the main oxides in the glass composition are SiO_2 (60.7% wt), CaO (18.7% wt) and K_2O (10.0% wt). The presence of such a significant amount of K_2O indicated that this red glass piece is a potash-lime silica glass. Similarly, as was the case with the Cuenca colourless glass, the red Chartres glass showed high concentrations of the network forming Al_2O_3 and the network stabilizer MgO. EDS analysis showed that this glass had no grisaille layer on its surface as evidenced in table 3.10 by lack of elements that constitute the composition of grisaille i.e. Pb and Fe.

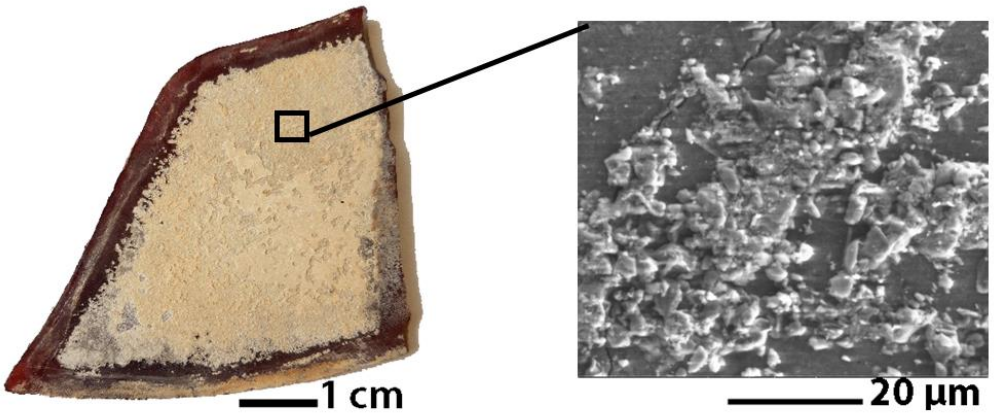

Figure 3.30: *Red glass from Chartres cathedral. On the right is a SEM micrograph of a region covered by white crust on the internal face of this red glass.*

The corresponding EDS analyses showed that the composition of the white crust included a significant amount of Ca and S (tab. 3.11). The presence of these two elements was an indication that the white crust was composed of sulfate compounds, either gypsum ($CaSO_4 \cdot 2H_2O$) or anhydrite ($CaSO_4$). The amount of P detected was too low to infer any presence of phosphate compounds in the composition of the crust.

% at	**O**	**Si**	**Ca**	**Na**	**K**	**Al**	**Mg**	**P**	**Fe**	**Pb**
	58.6	*23.4*	*7.7*	*1.0*	*4.9*	*1.1*	*2.0*	*1.1*	-	-
% wt	**SiO_2**	**CaO**	**Na_2O**	**K_2O**	**Al_2O_3**	**MgO**				
	60.7	*18.7*	*1.3*	*10.0*	*2.4*	*3.5*				

Table 3.10: *Red glass from Chartres cathedral. Elemental composition (%at) determined by EDS on the glass and % wt of the main oxides.*

	O	Si	Ca	Na	K	Al	Mg	P	Fe	Pb	S
Crust	*54.9*	*13.7*	*6.8*	*0.6*	*1.3*	*0.9*	*0.4*	*0.7*	*-*	*-*	*6.3*

Table 3.11: *Red glass from Chartres cathedral. Elemental composition (% at) as determined by EDS of the white surface crust on this glass.*

Studies to make comparisons between the use of conventional (chemical and mechanical) methods with laser cleaning techniques for restoration were performed on a glass sample also provided by the Maison-Lorin glass restoration workshop in Chartres, France. The glass sample, that appears colorless but with a faint greenish tint, measures about 8.5 cm by 6 cm, is from Cathedral Notre-Dame, in Chartres (France). The glass is dated from the 13th century. The glass sample seen in figure 3.31 was photographed under normal reflected light to observe the surface morphology and to assess its conservation status. As seen in figure 3.31, one of the glass face, which has spiral and mesh-like patterns made with brown grisaille is covered by a gypsum-like crust, limestone-like plaque deposit, with traces of rust, and mastic residues on the edge that was probably under the lead. The other face shows extensive pitting, continuous craters, significant residues of weathering products in the craters, black halo corresponding to the trace of rust on the opposite face, greasy-looking deposits and mastic residue on the edges.

Figure 3.31: *Stained glass from Chartres cathedral, France.*

CHAPTER 4: LASER CLEANING PROTOCOLS USING A HIGH FREQUENCY LASER SYSTEM

Lasers, that are usually used in Cultural Heritage, work with low frequency values, of the order of 5 to 25 Hz. By contrast, short pulse lasers, such as the 800 picosecond IR laser, used in this study, can work with high frequencies. In this case, laser has the possibility of working with frequencies between 200 and 800 kHz. This laser property opens up the possibility for designing fast cleaning protocols. But also, with these frequency values and supposing that the time between consecutive pulses is between 1.25 and 5 μs, the sample has no time to cool down between two pulses and in this scenario, heat accumulation is important, a fact that can produce high temperature gradients on the sample surface. This requires to develop new cleaning protocols to usual laser scanning ones. In this chapter, we have explored the possibilities that new protocols offer based on the burst configuration.

4.1. Single burst configurations

In order to separate the contributions of the temporal and spatial overlap with this system, the burst mode configuration was selected. Treatments were applied in areas of 2 × 2 mm^2 and with a distance between spots of 200 μm in order to study the effect of the temporal overlap in each position. The laser treatment was initially applied directly on the uncoated glass surface, in order to define a damage threshold. A high power and low frequency values were selected, resulting in a pulse energy value of 24 μJ (fluence 0.49 J/cm^2, irradiance 0.61 GW/cm^2). Different experiments were performed increasing the number of pulses in each position following this sequence; 200, 1000, 2000, 5000 and 10000. In the case of the colourless, blue and red glasses, no interaction with the glass surface could be observed, even if the number of pulses in each position increased up to 10000. As was expected, considering the optical behaviour observed in table 3.2 and figure 3.4, the green glass was an exception. This glass exhibited absorption values close to 68% for this wavelength and, in consequence, an important level of heat accumulation on the glass sample was expected.

The different phenomenology observed in the green glass was reflected in the generation of a considerable degree of damage when the number of pulses applied in each position reached a value of 5000 pulses (fig. 4.1.a, b and c). Laser treatment was performed on an

unidirectional configuration starting the scanning in each line at the bottom part in figure 4.1.a, and moving the scanning line from the left to the right. As it can be observed in figure 4.1.c, the cavities generated by the laser reach a depth of 80 μm. Images clearly show that the level of damage increases when the laser treatment is evolving. The average glass temperature increase during the laser treatment was recorded using the thermocamera. Figure 4.1.d shows this evolution in case of red and green glasses for one series of 200 pulses and after having repeated the laser treatment 5 times. It was recorded that the time required to treat this area with these processing parameters is approximately 0.42 s and figure shows that the time required to cool down the sample is 20-25 s.

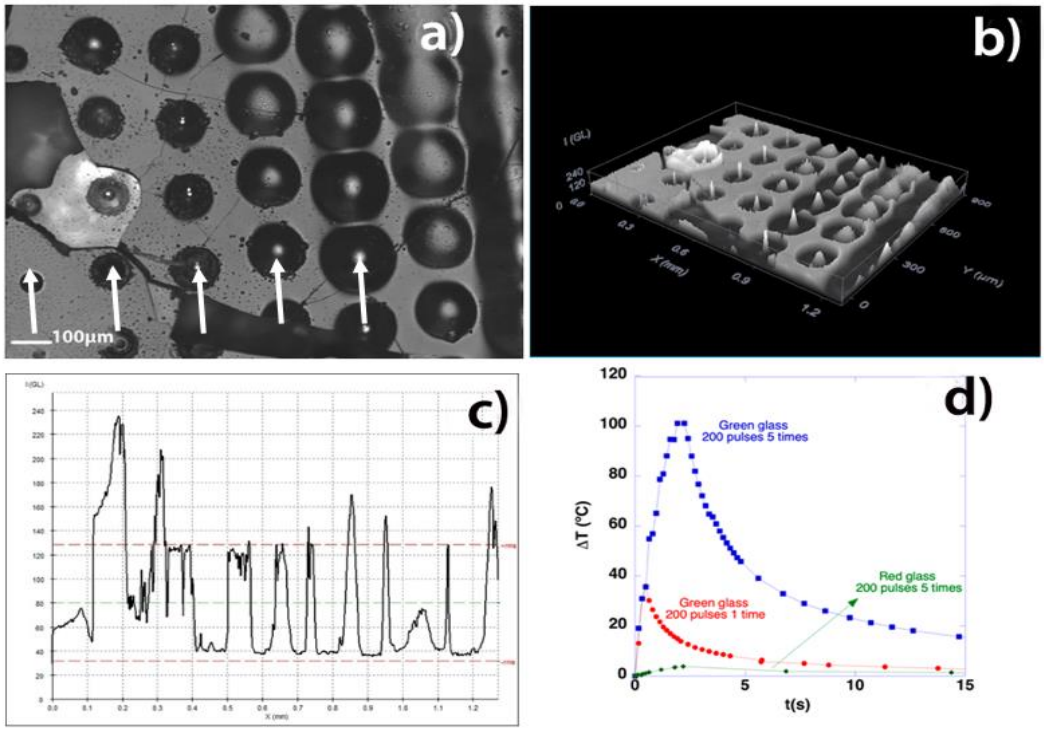

Figure 4.1: *Modern glasses from Verrière de Saint-Just factory. (a) SEM micrograph of the surface of the green glass after direct laser irradiation with 5000 pulses in each position. The distance between two positions is 200 μm. The laser scans in the vertical direction of the image using an unidirectional configuration, as it is shown with the arrows, starting on its left lower corner and showing that the damage level increases while the laser treatment evolves. (b, c) Isometric display and profilometry of the treated area. (d) Temperature increase recorded with a thermal camera for approximately 30 s on the glass surface during several laser treatments (series of 200 pulses in each position) performed on the uncoated green and red glasses*

The curve measured in the green glass sample during the treatment in which 5 series of 200 pulses were applied clearly showy the heat accumulation effect, observing a linear temperature increase evolution during the laser treatment.

Table 4.1 shows the maximum temperature increment measured during these experiments in the red and green glasses. Measured values reach $\Delta T = 3.9ºC$ for the red glass after 5 series of 200 pulses in each position. By contrast, values of 35.9ºC (200 pulses) and 100.9ºC (5 × 200 pulses) were reached when the laser was applied directly on the surface of the green glass with similar irradiation conditions. No damage was observed when the uncoated surface of the green glass was irradiated 5 times with 200 pulses in each position. This fact indicates that damage is not directly related with the level of energy per pulse that is applied in each position. By contrast, due to heat accumulation, the temperature of the glass increases while the laser treatment evolves, increasing also the level of thermomechanical stress that can induce crack generation and glass failure (de Cruz *et al.*, 2014; Lapczyna *et al.,* 1999).

	Green glass		**Red glass**	
	200 pulses once	200 pulses 5 times	200 pulses once	200 pulses 5 times
Without Ink	35.9ºC	100.9ºC	1.1ºC	3.9ºC
With Ink	81.9ºC	---	9.3ºC	21.0ºC

Table 4.1: *Modern glasses from Verrière de Saint-Just factory. Maximum temperature increments reached on the surface of the green and red contemporary glasses after several laser treatments in which successive burst laser treatments with 200 pulses in each position have been applied.*

Similar studies were performed during cleaning protocols, covering selected glass surface areas with blue permanent ink that provided strong adhesion properties to the glass. The following experiments were performed with the objective of removing this ink from the glass surface, as well as to observe the after-cleaning effect on the substrate using the same irradiance levels. It is important to mention that the ink coating layer was not uniform, with thickness values ranging between 450 nm and 1.6 µm. Irradiation experiments were initially performed on the colourless, blue and red glasses. Evidence of laser interaction with the ink coating was observed after 200 pulses, when the thinnest regions of the ink were removed from the glass surfaces. After this laser treatment, the sample surface did not present any apparent damage, demonstrating that these laser emission parameters do not cause critical photo-thermal stress in the irradiated glass. In contrast, when the number

of pulses in each position increases to 500 (fig. 4.2 for the blue glass), the cleaning process generates a large number of visible defects on the glass. These are observed even if the number of applied pulses is one order of magnitude lower than those applied to the uncoated glasses without affecting their surface. A closer look at the detail of the marks observed in the coating suggests that pulsed laser irradiation has induced melting of the ink. Moreover, it seems that significant heat transfer takes place from the coating to the glass underneath, increasing the temperature at the glass surface. Consequently, the associated thermo-mechanical stress leads to the observed micro-crack formation on the glass substrate.

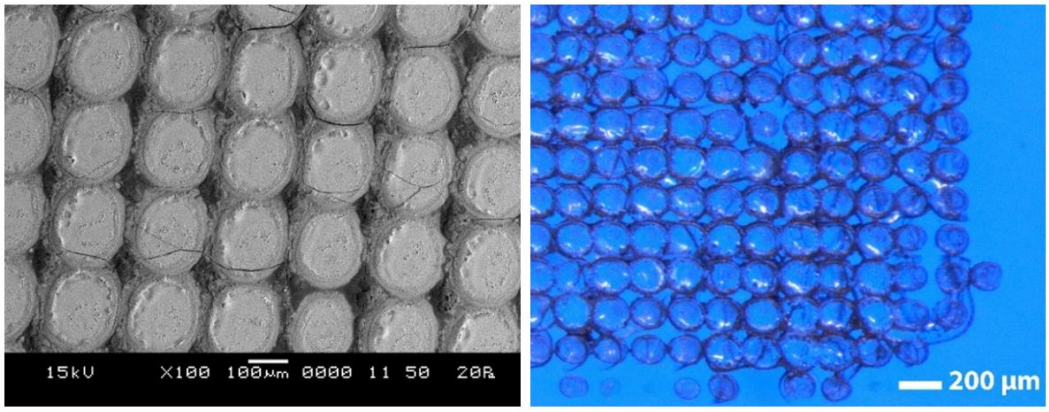

Figure 4.2: *Blue glass from Verrière de Saint-Just factory. SEM micrograph (left) and photograph (right) of the ink-coated contemporary glass sample after laser irradiation with 500 pulses in each position.*

These experiments show that the damage in the glass is not caused by the direct laser-glass interaction. Cracks are generated by heat accumulation in the coating, which generates a significant local temperature gradient on the glass surface and induces thermo-mechanical stresses above the fracture limit of the material. In consequence, the laser parameters have to be defined in order to control this heat accumulation.

As these experiments were initially performed with pulse frequency values close to the lowest ones allowed in this system, the option of reducing the frequency is not available. An alternative approach has been explored. Additional experiments were performed maintaining series of 200 pulses and repeating these series several times. In this configuration, the laser covers an area applying 200 pulses in each position during 0.67 ms and subsequently moves to the adjacent position. Once it has covered the desired area

(in this case 0.42 s for a single series covering an area of 2 mm × 2 mm), the process is repeated again for the desired number of times. Figure 4.3 shows how average temperature has increased in the sample surface of the red and green glasses after several of these treatments, where the laser protocol has been repeated once or five times.

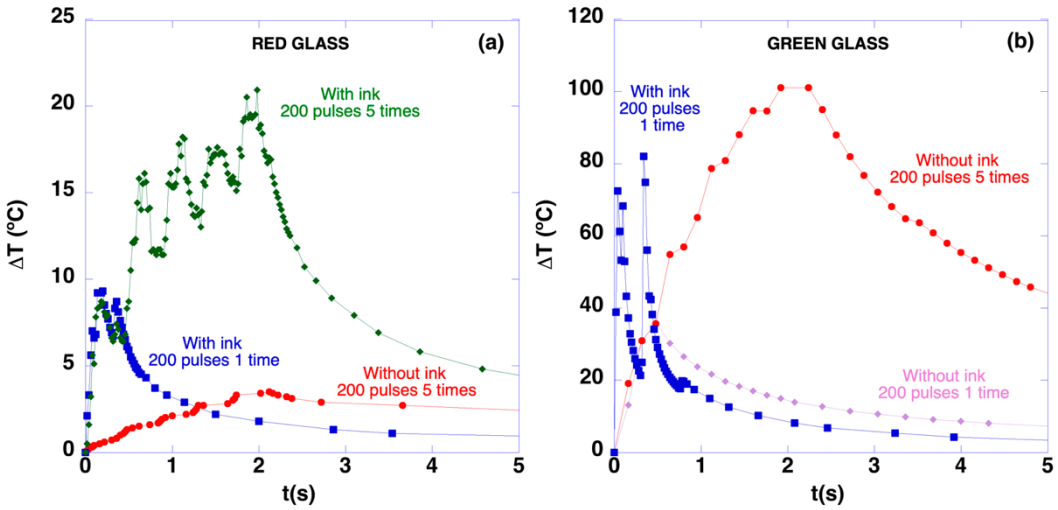

Figure 4.3: *Modern glasses from Verrière de Saint-Just factory. Comparison of the average maximum temperature increment reached in the glass measured with a thermal camera during laser cleaning processes in the (a) red and (b) green contemporary glasses with and without the ink coating.*

The increment in the temperature (tab. 4.1) is clearly higher when the laser treatment is applied to remove the ink layer than when the same laser treatment is performed directly over the non-coated glass surface. The evolution of an ink-coated colourless glass surface after irradiation with several series of 200 laser pulses is presented in figure 4.4(a) and (b) shows the aspect after the first series. The ink starts to melt mainly in the centre of the spot, due to the Gaussian energy distribution within the laser beam cross-section, but it is not removed from the glass surface. The size of the area affected by the laser spot depends on the thickness of the original coating. In the thinnest regions (left column in figure 4.4.a) the diameter of these affected areas is smaller than 50 µm (left column in figure 4.4.a); in the thickest regions, the diameter of the spot left by the laser increases up to approximately 200 µm. After cleaning the ink with alcohol, the glass surface did not exhibit any visible damage.

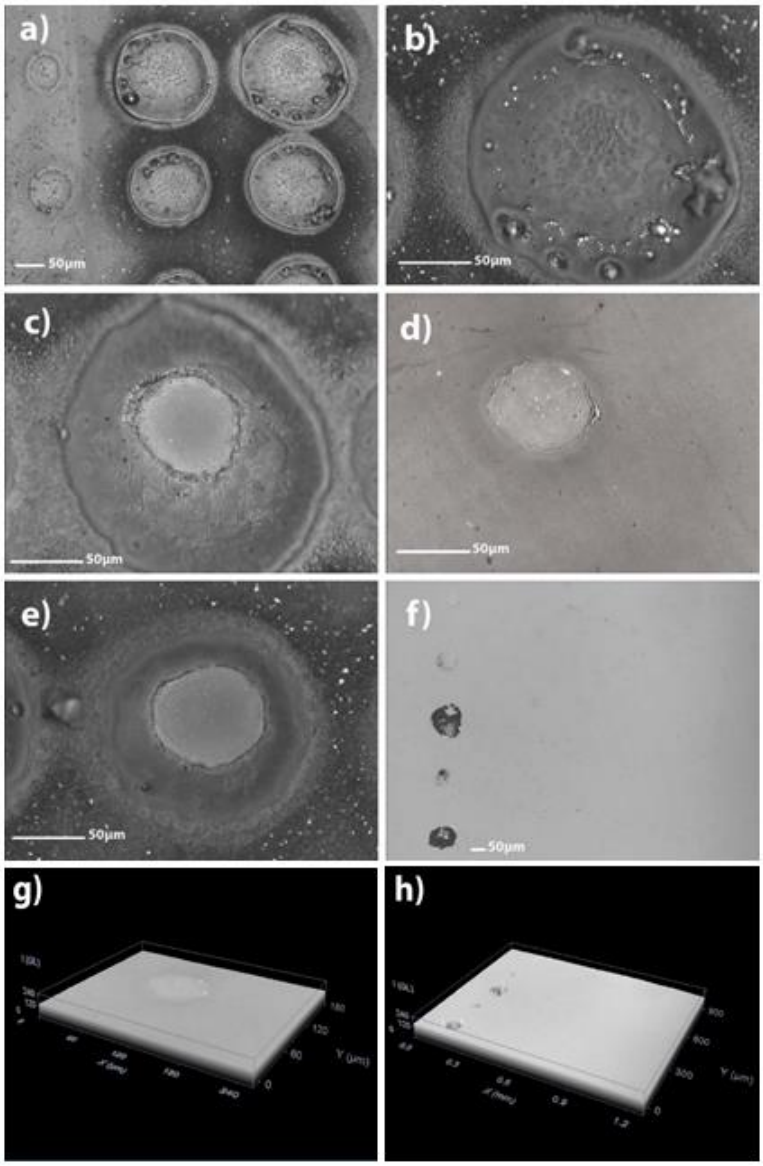

Figure 4.4: *Colourless glass from Verrière de Saint-Just factory. Optical micrographs of the surface of the ink-coated glass after irradiation with one (a and b), five (c and d) and 10 (e and f) series of 200 pulses. (d) and (f) show the aspect of the glass surface after conventionally removing the remaining ink on the glass surface, once the laser treatment was completed. Several defects generated during the laser treatment are thus revealed. Figures g and h show isometric aspects of (d) and (f).*

When the number of series increases up to 5, equivalent to a total of 1000 pulses (fig. 4.4.c), it is possible to eliminate the ink layer over the glass surface in the centre of each

spot, where the energy is maximum. This area is surrounded by a region that has been affected by temperature increases in the ink layer. There is some evidence of damage of the glass surface, however, mainly observed in the centre of the spot after having removed the rest of ink over the glass surface (fig 4.4.d). This level of damage is not the same in all the spots, and apparently depends on the uniformity of the ink layer thickness. This reflects the difficulty of working with a coating thickness that is not uniform. This situation is common in historical stained-glasses, where non-uniform grisaille and crust layers are usually found.

When the number of series increases to 10, removal of the coating is observed more easily at the centre of the spot (fig. 4.4.e). As in previous cases, some defects are observed on the glass surface after cleaning (fig. 4.4.f), mainly located in sections where the coating is thicker. Topographies of these regions with defects are presented in figure 4.4.g and h. Comparing the levels of damage presented in figure 4.2 (500 pulses in each position) and figure 4.4 (10 series of 200 pulses), it is observed that it is possible to apply 2000 pulses on top of the coating generating a lower number of cracks on the glass, as long as a sufficient time lapse between burst series is applied. Subsequently, it is important to have an additional reduction in the heat generated during the laser treatment. This reduction is achieved by increasing the time lapse between two series of pulse bursts up to several seconds. From the analysis of the dependence presented in figure 4.1.d, a time lapse of approximately 26 s is needed to reduce ΔT generated in one series to values lower than 1ºC.

Figure 4.5 shows representative optical micrographs of the marks generated by the laser indifferent sections of the ink-coated red glass sample with a time lapse of 30 s between two series. As in previous experiments, the laser covers an area of 2 mm x 2 mm, marking a point every 200 µm and applying 200 pulses in each position. Figure 4.5.a and b correspond to a situation in which five series of 200 dots were applied. The time lapse between two series allows a more effective cooling of the glass between the laser treatments and reduces the heat accumulation level. Obviously, with this laser protocol, the coating thickness removed in each series is reduced but the laser treatments are safer for the glass integrity. Figure 4.5.b shows that this initial treatment was not sufficient to remove completely the coating in some regions, though selective removal was observed as in the previous experiments.

Figure 4.5.c and d shows also the aspect of the surface after applying 10 series of 200 pulses. The coating on the surface of the red glass (centre of the spot) was removed with no observable damage to the substrate. This is also clearly observed in the inset of figure 4.5.d. After completely removing the ink layer, no substrate alteration was observed on the glass. In this case, the cleaning threshold was achieved by using a given set of minimum number of pulses per treated area, combined with short intervals between each exposure.

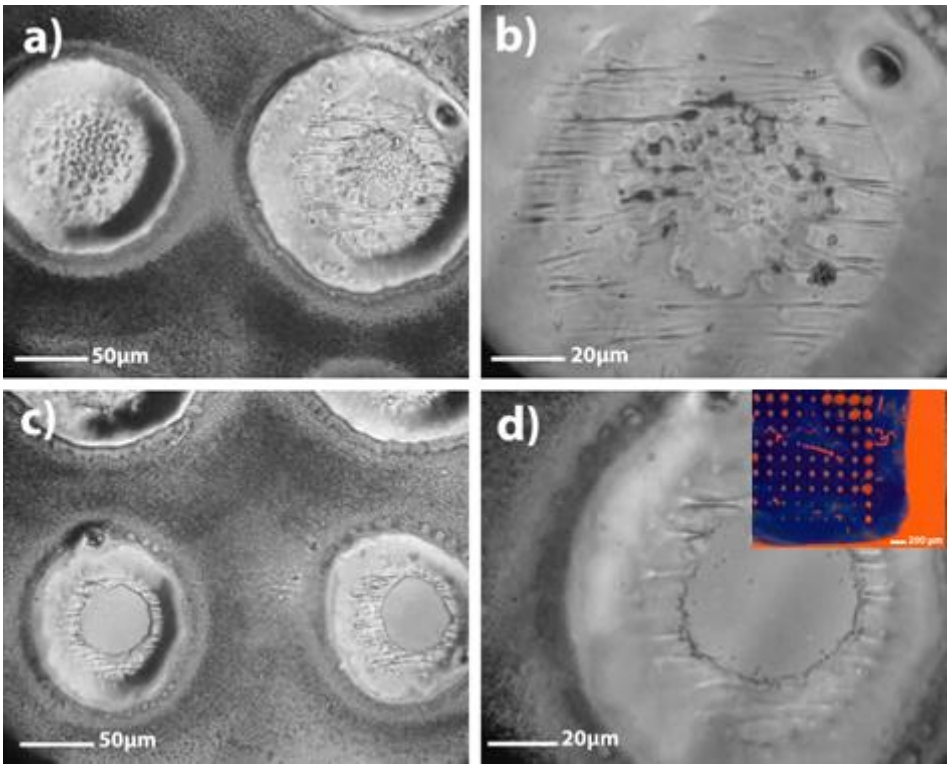

Figure 4.5: *Red glass from Verrière de Saint-Just factory. Optical micrographs of this glass surface irradiated with five (a and b) and 10 (c and d) series of 200 laser pulses. A 30 s time lapse between two consecutive series of pulses was applied. The inset corresponds to a photograph of the glass surface after the laser treatment.*

This laser protocol has also been applied to the ink-coated green glass surfaces. Figure 4.6 shows that the coating can be removed from the sample surface also in this glass, applying 10 series of 200 pulses. Comparing figure 4.6 with figure 4.2 it can be deduced that, maintaining the number of pulses at 200 and irradiating 10 times with the corresponding time-lapse intervals resulted in an acceptable removal of the surface coating with no damage to the substrate.

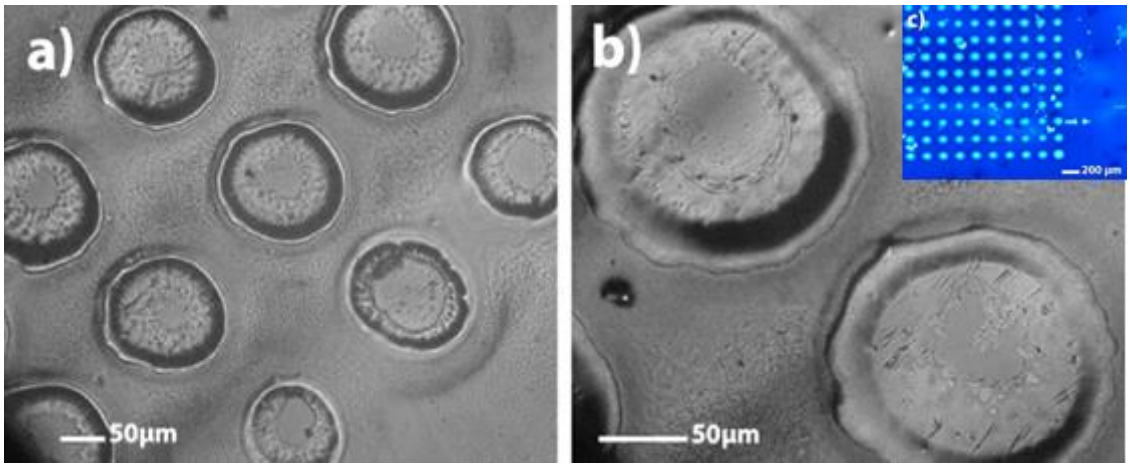

Figure 4.6: *Green glass from Verrière de Saint-Just factory. Optical micrographs (a and b) of this glass surface irradiated with ten series of 200 pulses and a time lapse of 30 s between two consecutive series of pulses. The inset corresponds to a photograph of the glass surface after the laser treatment.*

4.2. 2D configurations

A protocol was developed to uniformly clean a given area using a burst mode that has been explained in the previous section. Initially, the possibility of reducing the distance between dots was considered. This was not the best option in this case because the heat accumulation generated in one position can be affected by the temperature increase generated in the previous positions. For this reason, a new protocol was explored.

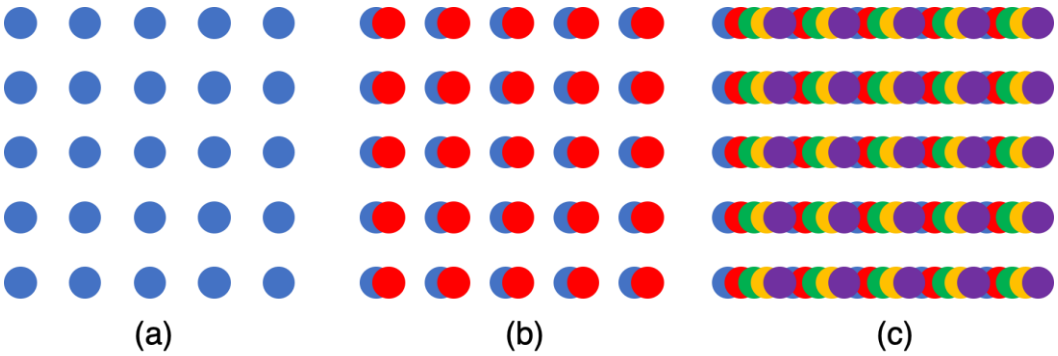

Figure 4.7: *Scheme of the cleaning protocol to clean several lines. (a) Standard burst configuration. (b) The same configuration is repeated shifted in the horizontal direction a percentage of the radius of the mark created for the initial treatment. (c) The process is repeated several times until the horizontal lines are cleaned.*

The proposed cleaning protocol described in the previous section generates a square lattice of cleaned spots, as it can be seen in figure 4.7.a. As a first step, the process is repeated moving the lattice of positions in one direction. This is shown in figure 4.7.b where this displacement has been performed in the horizontal direction. The maximum distance that can be displaced is a fraction of the radius, approximately no more than $0.9r$. If this process is repeated the number of times required to overlap again with the initial position, a set of horizontal parallel lines will be cleaned (figure 4.7.c).

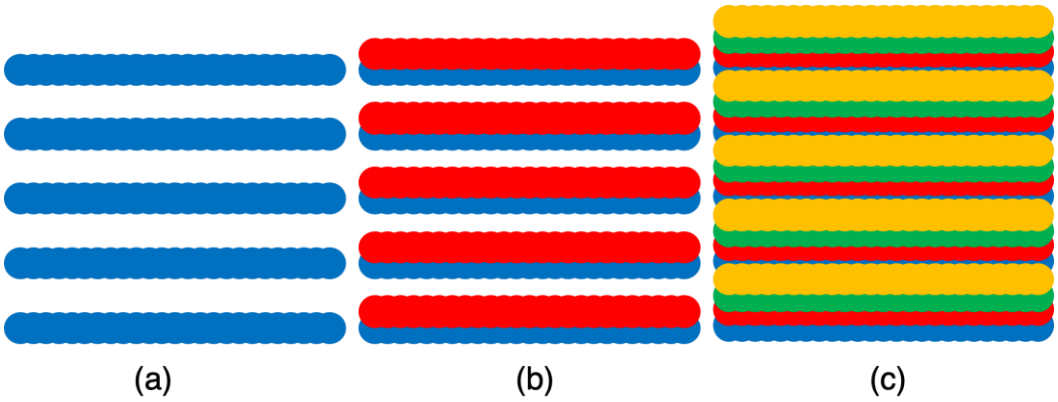

Figure 4.8: *Scheme of the cleaning protocol to clean an area. (a) Parallel lines cleaned with the protocol described in figure 4.7. (b) The same protocol is repeated shifted in the vertical direction a percentage of the width of the mark created for the initial treatment. (c) The process is repeated several times until the complete area is cleaned.*

In order to clean the complete area, the protocol described in figure 4.8 can be used. Once the previous lines have been cleaned (fig. 4.8.a), the process is repeated moving all the positions lattices a fraction of the line width typically of the order of 0.45 times the width of the line (figure 4.8.b) and this is repeated until there is a complete cleaning of the surface (figure 4.8.c).

In the previous sections, it was observed that it was possible to eliminate the permanent ink without deteriorating the glass using series of 200 pulses of 24 μJ at 300 kHz, using a lapse time of 30 s between two consecutive series. These conditions have been applied to clean a surface in some contemporary glasses. As can be observed in figure 4.9.a, when the burst treatment was applied, the ink was removed in a circular region at the centre of the incident position in a region of approximately 50-60 μm in diameter. Afterward, the process was repeated moving the positions by 25 μm in the horizontal direction. This distance was selected because it is slightly smaller than the radius of the cleaned regions

in the first treatment. This process was repeated six times more, moving every time the positions by 25 μm. After eight treatments, lines of approximately 100 μm thick were uniformly cleaned, as can be observed in figure 4.9.b. To cover the desired area, the process was repeated moving the position matrix by 50 μm in the vertical direction, using a similar criterion as the one selected for the horizontal treatments. All the processes were repeated moving the positions by 100, and 150 μm. A waiting time of 10 s was applied after each one of the laser steps that had been developed. After all the processes were completed, there was a full area uniformly cleaned without deteriorating the glass surface, as can be observed in figure 4.9.c.

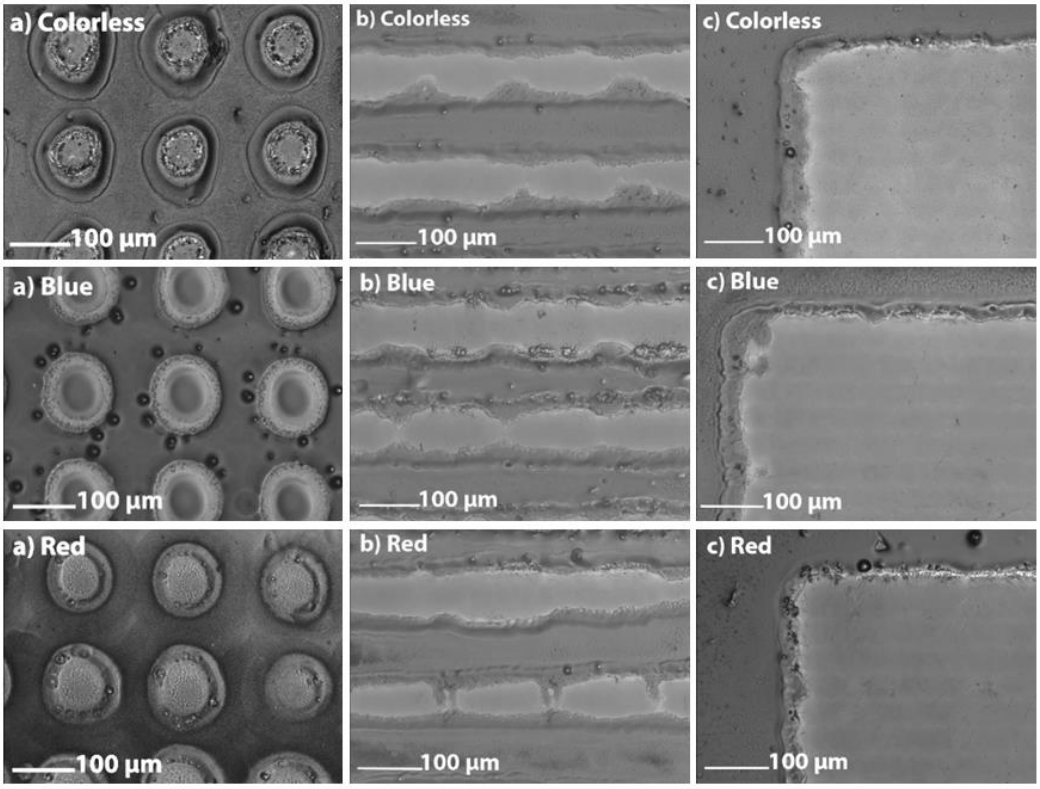

Figure 4.9. *Modern glasses from Verrière de Saint-Just factory. Optical microscope images of the colourless, blue and red glass sample surfaces after the three steps of the cleaning protocol: (a) Single treatment with 200 pulses; (b) after the eight treatments that were done horizontally; and (c) after the treatments that were done vertically.*

The uniformly cleaned areas were observed under a confocal microscope, as can be seen in figure 4.10.a and b, approximately 1.5 μm of the ink layer was removed revealing a cleaned glass surface.

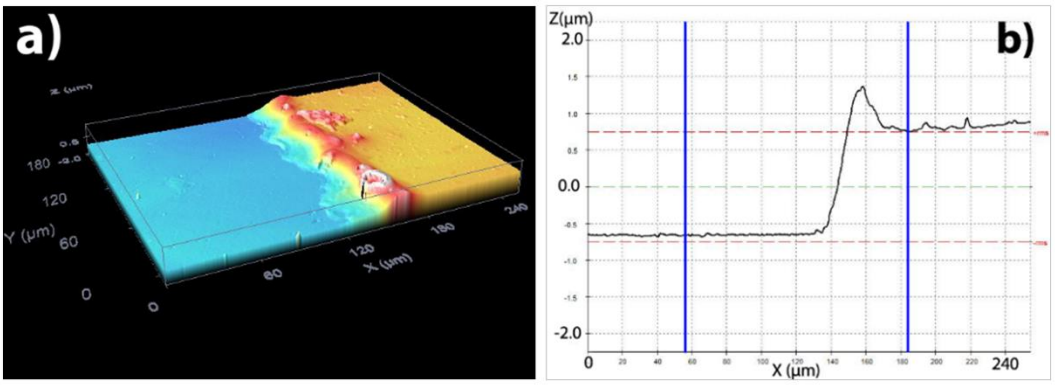

Figure 4.10: *Colourless glass from Verrière de Saint-Just factory. (a) Confocal isometric display of the glass after all the treatments were done (Figure 4.9.c). (b) Profile showing the amount of coating removed from this glass after the treatment was completed (approximately 1.5 µm of coating removed).*

One of the problems associated with this cleaning protocol is the excessive number of waiting times that the process requires. An option to avoid these problems is to increase the size of the area that is being treated. This is a good option if the time required to complete a single series is longer than 30 s. Taking this into consideration, the laser will return to the initial position to start the following step after this area of the sample has cooled after the previous treatment.

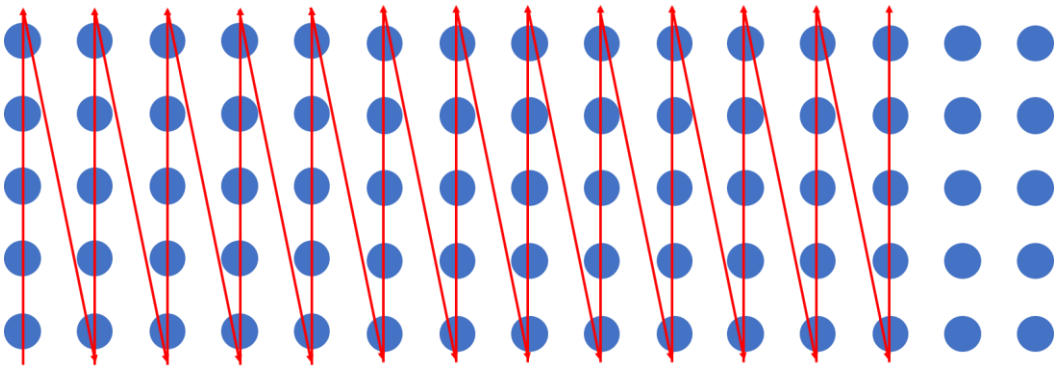

Figure 4.11: *A configuration where the laser cleaning is performed on a rectangular shaped area with long length/width ratios with the scanning direction moving towards the width of the glass sample. The left side of the sample has enough time to cool down (above 30 s in this case) before the laser covers the entire length towards the right side of the glass.*

CHAPTER 5: CLEANING PROTOCOLS WITH fs PULSED LASERS

5.1. Influence of laser effective frequency

Following the ideas deduced from the previous experiments, additional studies were performed with a femtosecond IR laser system using the beam scanning protocol. In this case, using the PPD option, lower pulse repetition frequencies are available. In consequence, it is possible to control heat accumulation by reducing the effective pulse repetition frequency. Weber *et al*. (Weber *et al.*, 2014) calculated the maximum temperature reached during laser treatment and determined that this temperature increases with the pulse laser frequency and it is particularly dependent on the material's properties. Using the IR fs laser, initial experiments were performed on the contemporary colourless glass sample by selecting the beam scanning configuration, high power (40 W) and a basic frequency value of 200 kHz, giving a pulse energy value of 200 µJ (2.55 J/cm^2, 10^4GW/cm^2, 5000 times higher than the value reached with the 800 ps laser). Using the Pulse Peak Divider option, it was possible to select the effective frequency, and, in consequence, the time between two consecutive pulses, maintaining the pulse energy value constant. As it can be observed in table 5.1, the effective frequency and the scanning laser speed values were initially selected maintaining a distance of 10 µm (overlapping of a 90% of the beam radius) between spots. The same value was selected for the distance between two scanning lines in order to maintain similar overlapping in both scan directions. Some experiments were repeated twice, rotating the laser scanning direction in the second treatment by 90º.

The first treatment (T1) was applied directly on the colourless glass and it was observed that even with the higher pulse repetition frequency selected in these experiments (40 kHz), the energy absorption was low during the laser treatment and no damage was observed on the glass surface, even if the laser treatment was repeated twice.

By contrast, when a laser treatment with the same laser parameters was applied in a region that was covered with ink (T2), it was observed that heat accumulated in the ink induced thermal stresses on the glass substrate, leading to crack generation, as can be observed in figure 5.1(a). In order to reduce heat accumulation, the same cleaning experiment was performed reducing the effective frequency to 20 kHz. The scanning speed was also reduced to 200 mm/s to maintain the overlapping percentage and the spatial energy

Treatment	Frequency (kHz)	Laser speed (mm/s)	Distance between lines (µm)	No. of times	Observations
T1	40	400	10	2	Plain glass with no ink. No effect.
T2	40	400	10	2	Ink removed. Cracks observed on the substrate.
T3	20	200	10	1	Ink removed. No cracks.
T4	20	200	10	2	Ink removed. No cracks.

Table 5.1: *Colourless glass from Verrière de Saint-Just factory. Cleaning parameters applied on the glass using the fs IR laser. In all cases, overlap between consecutive pulses or lines is 90% of the beam diameter.*

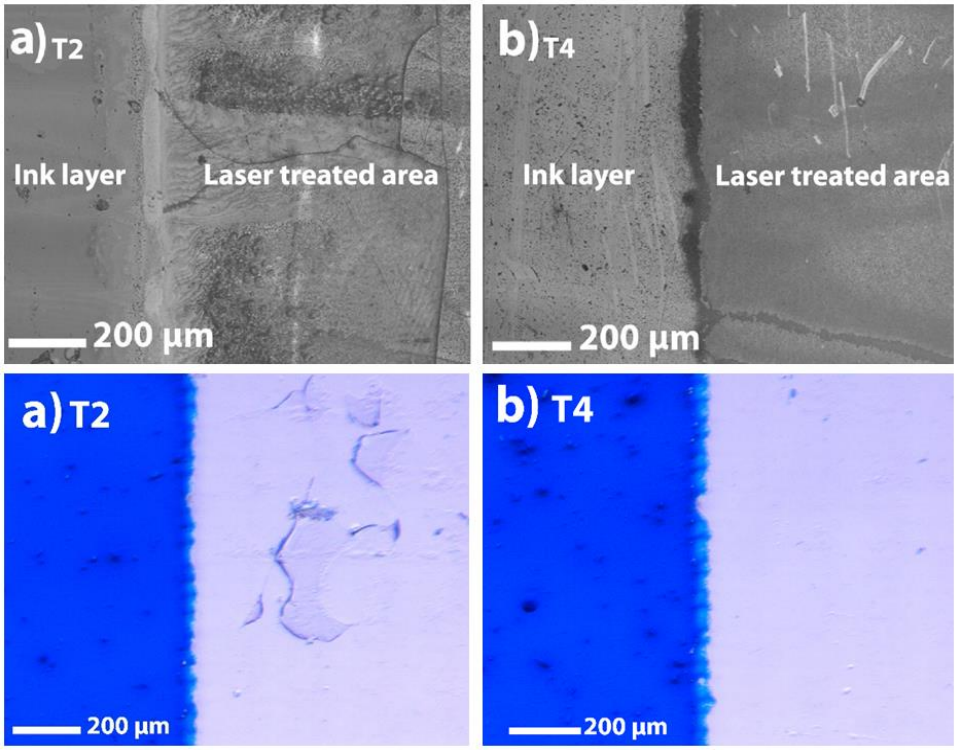

Figure 5.1: *Colourless glass from Verrière de Saint-Just factory. Optical micrographs (top) and photographs (bottom) of the glass surface after two different laser cleaning protocols were carried out (a) at 40 kHz as described in treatment T2 and (b) at 20 kHz as described in treatment T4 with parameters detailed in Table 5.1.*

distribution. This approach increases the time between two consecutive pulses, reducing the maximum temperature reached on the coating that has to be eliminated. As can be observed in table 5.1 (treatments T3 and T4) and in figure 5.1(b), ink was removed from the glass surface without generating any defect on the glass surface.

Experiments performed on contemporary stained-glass clearly indicated that in the development of safe laser cleaning procedures, an essential limiting factor is the maximum average temperature that can be reached on the glass surface while the coating is being removed. In particular, when glass is highly transparent to the laser irradiation employed, defects in the glass are caused not by direct laser-glass interaction, but by the thermal stresses associated with the heat accumulated within the absorbing deposits or contaminants on its surface.

5.2. Optical damage using the fs UV laser

In the previous section, it has been demonstrated that safe cleaning conditions with a nIR laser can be reached when the effective laser frequency is reduced to values lower than 20 kHz. As it can be showed in chapter 3, in historical stained-glass samples, it is highly likely that the material to be removed from the surface of the glass is a patina of gypsum, anhydrite or calcite compounds, with an external layer with carbon-like ones. This layer is often formed due to pollution and environmental contamination (Byrne, 2017; Comite *et al.*, 2020; Garcia-Vallès *et al.*, 2003; Schreiner, 1991). In this case, this laser wavelength is very effective for removing this external layer because this layer has a high absorption level. However, once this layer is removed exposing the clean white patina underneath, the effectiveness of the fs IR laser treatment is strongly reduced. For this reason, the possibility of using fs UV radiation was also explored.

Energy per pulse levels below the mechanical damage threshold on the contemporary glasses were selected to do these experiments. It was observed that, from a given level of energy, that can be called, optical damage threshold, there was a gradual lowering of transmittance values and browning of the colourless glass with the green glass showing faint darkening as the laser power was increased. Similar solarization effects were observed in glasses treated with UV radiation as was reported by Byrne (Byrne, 2017) and these effects were associated with photo-oxidation of some of the elements that are present in the glass composition. In consequence, when UV radiation is used, in addition to

mechanical damage processes, these chemical damage processes have also to be considered.

Initial treatments were performed using the burst mode. 500 pulses were applied in each position with a distance between adjacent positions of 100 µm. Two different levels of pulse energy were selected; the first one, 0.18 µJ/pulse, is just above the optical damage threshold in the colourless contemporary glass; and the second one has been selected increasing until 3.19 µJ/pulse. The second set of treatments have been performed using a beam scanning configuration with the same two levels of energy per pulse and using a laser scanning speed of 150 mm/s, an effective frequency of 10 kHz and a distance between scanning lines of 15 µm.

When this optical interaction generates a change in colour, the D^2-method (J. M. Liu, 1982) can be used to determine the energy threshold. In cases where no visible colour change is observable, transmittance tests can be used to investigate if a given level on energy can modify the optical behaviour of the material. Following this, the transmittance spectra were recorded before and after laser treatment in the four cases. Results are presented in figure 5.2 for the colourless and blue glasses and in figure 5.3 for the red and green glasses.

Figure 5.2 shows the evolution of the spectra in the colourless and blue glasses. The transmittance value changes were more pronounced in the colourless glass. In the first case (fig. 5.2a), when the two treatments (beam scanning and burst mode configurations) were applied with the lower level of energy per pulse (0.18 µJ/pulse), a reduction in the transmittance values at wavelengths higher than 440 nm was observed. Secondly, when the energy was increased, in this case to 3.19 µJ/pulse, the transmittance level within this UV region started to decrease significantly. This reduction in transmittance values was evident with the browning of the colourless glass, that becomes stronger, as it can be observed in figure 5.3.

Treatments on the blue glass resulted in a slight increase on the transmittance values which was observed in the shoulder that appeared in the range between 440 and 560 nm (fig. 5.2b). This increase was indepedent of the level of the energy per pulse, at least in the range of analysed energies, indicating that the damage threshold was lower than 0.18 µJ/pulse in this sample. Changes induced by the UV laser were higher in the beam scanning configuration.

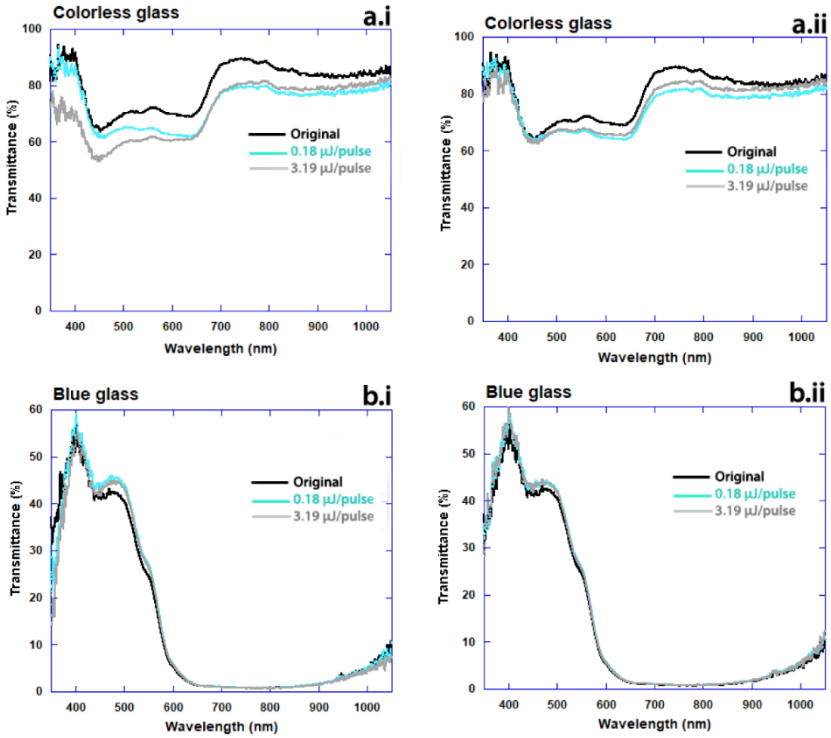

Figure 5.2: *Modern glasses from Verrière de Saint-Just factory. Transmittance spectra obtained before and after performing laser treatments directly on the colourless and blue glass surfaces respectively (a and b). The spectra on the left represent treatment done using the laser beam scan configuration and, on the right, using the burst mode.*

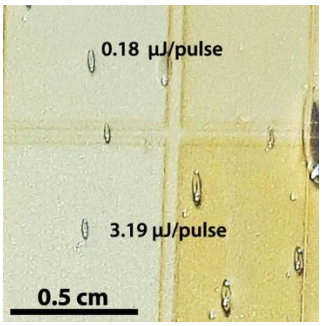

Figure 5.3: *Colourless glass from Verrière de Saint-Just factory. The aspect of this glass surface showing the optical damage after treatments with the fs UV laser at 0.18 µJ/pulse and 3.19 µJ/pulse using the beam scanning (right) and the burst mode (left) configurations.*

In comparison with the other glasses, the main differences in the treatments on the red glass were associated with a reduction on the transmittance values at wavelength values

above 650 nm. The reduction in the transmittance values in the red glass increases when the energy per pulse increases (fig. 5.4c).

In the green glass, the main changes were observed in the reduction on the transmittance values in the peak at 530 nm. This reduction seen at the highest energy level in both configurations (fig. 5.4d), indicated that the optical damage threshold for this glass was between 0.18 µJ/pulse and 3.19 µJ/pulse, unlike the other glasses which all had the optical damage threshold below 0.18 µJ/pulse.

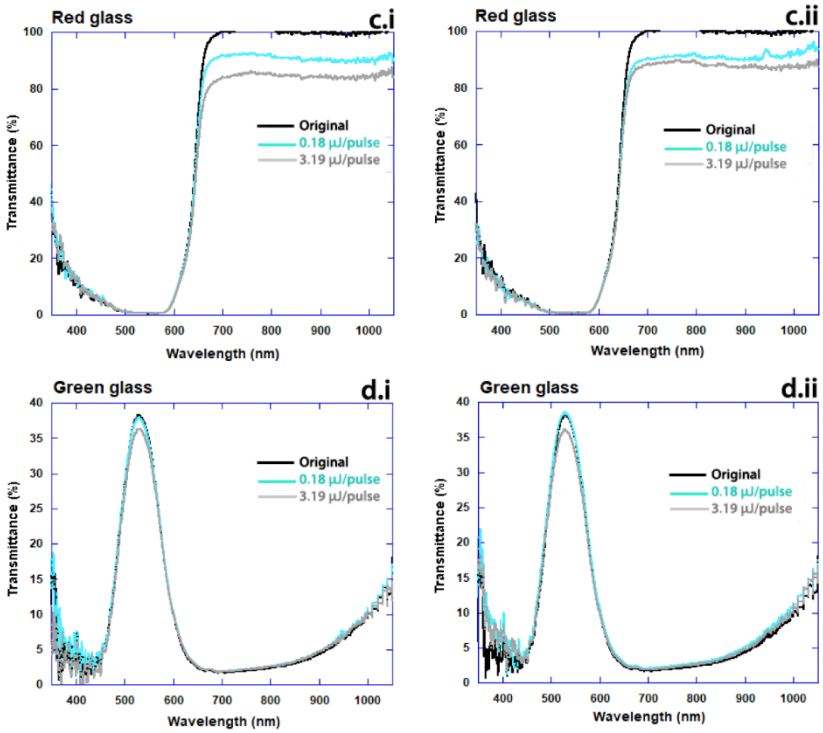

Figure 5.4: *Modern glasses from Verrière de Saint-Just factory. Transmittance spectra obtained before and after performing laser treatments directly on the red and green glass surfaces respectively (c and d). The spectra on the left represent treatment done using the laser beam scan configuration and, on the right, using the burst mode.*

These treatments with the contemporary glasses implied that when using fs UV radiation, safe cleaning protocols would be realized by combining low frequency values that avoid heat accumulation, with pulse energy values lower than the optical damage threshold.

5.3. Application of the cleaning protocol using the n-IR fs laser in samples from the Cuenca Cathedral, Spain.

Following the same criteria used to define the laser cleaning protocol on contemporary glasses, with a beam scanning configuration, new experiments using the n-IR fs laser were applied on the colourless historical stained-glass sample from the Cuenca Cathedral, Spain. The glass exhibits a patina of white crust spread over the full area and also remnants of putty is present in the border of the piece. These experiments have been performed on areas covered by putty. Changes induced by laser cleaning in three regions are presented in figure 5.5. Cleaned areas have been marked with a square. Laser parameters used in each of the treatments are presented in table 5.2.

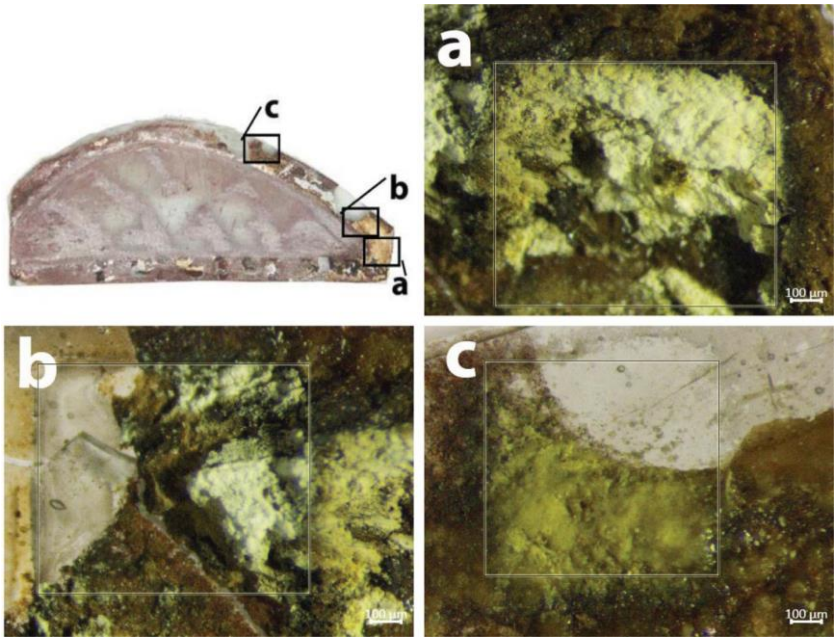

Figure 5.5: *Colourless glass from Cuenca cathedral. Optical micrographs of the historic glass surface after cleaning using a fs IR laser. The treated areas are marked with a square. Note the colour change from dark-brown (untreated surface) to whitish-brown (treated surface).*

Initial experiments were carried out on this sample in order to check possible damage on the glass when irradiation takes place directly on its surface. With the maximum level of irradiance that can be reached with this nIR fs laser, $10^4 GW/cm^2$, no damage was detected.

Same levels of energy per pulse were applied in the regions covered with putty. In positions *a* and *b*, the importance of heat accumulation was also checked. Treatment in region *a* was the same as that of T4 in the contemporary glass (fig. 5.1), maintaining the effective pulse frequency at 20 kHz and keeping a distance between laser pulse positions at 10 µm in both scan directions. As is observed in figure 5.5.a, this treatment was able to eliminate the upper brown layer of the putty. Below this upper layer, a white layer was revealed and the efficiency of the IR radiation for removing this material decreased. In region *b*, the frequency was increased to 40 kHz, reaching the conditions similar to those of treatment T2 that induced cracks in the contemporary glass (fig. 5.1), and also a crack was observed in the historical glass. On the top left part of the cleaned area in figure 5.5.b, a white crust layer was present on top of the glass. Laser treatment could eliminate completely this layer without inducing thermal damage on the glass. By contrast, when laser treatment was applied in a region containing putty (right part of the image) a crack was generated.

In region *c*, the applied laser treatment was less intense, the frequency was reduced to 10 kHz and the laser scanning speed was increased up to 300 mm/s, increasing also the distance between pulse spots up to 30 µm (overlapping of a 70% of the beam diameter). The process was repeated 20 times and no damage was observed on the sample. When the laser irradiation reached the glass surface directly (upper right corner of the treated area), the crust layer was removed without deteriorating the glass. The putty layer started to be affected by the laser. In consequence, the laser treatment could be repeated several times without affecting the glass surface while eliminating the putty. The main limitation is that when inner layers of putty or crust appear, the efficiency of the cleaning process reduces because the absorption of the laser radiation becomes lower.

Treated Region	Frequency (kHz)	Laser speed (mm/s)	Distance between lines (µm)	No. of times	Observations
a	20	200	10	2	Cleaning achieved.
b	40	400	10	1	Cleaning achieved. Micro-cracks generated.
c	10	300	30	20	Cleaning achieved.

Table 5.2: *Colourless glass from Cuenca cathedral. Cleaning parameters applied on the historical glass using the fs IR laser. In regions a and b the overlap between consecutive pulses or lines is 90% of the beam diameter, while this is reduced to 70% in region c.*

5.4. Application of the cleaning protocol using the fs UV laser in samples from Cuenca Cathedral (Spain) and Chartres Cathedral (France)

Final laser cleaning protocols to remove the white crust covering the surfaces of historic glasses were used working with the fs UV laser. As frequencies lower than 20 kHz were available, the beam scanning protocol was selected, as was the case when the nIR laser was used to eliminate the putty in this glass. Laser cleaning protocols were defined maintaining the effective frequency at 10 kHz in order to maintain heat accumulation within safe levels. The oscillator frequency was set at 200 kHz and a PPD value of 20 was selected. Laser scanning speed was fixed at 150 mm/s, that gave a distance of 15 μm between pulses. The distance between lines was also fixed to 15 μm. This is the minimum distance that assures a homogeneous treatment with the beam size of this laser at the focal distance. The effectiveness of the treatments was checked combining the energy of each pulse and the number of times that the cleaning process was repeated. Laser scanning direction was rotated 90º every time.

Colourless glass from Cuenca Cathedral

Initial laser treatments were applied in areas of 6 × 6 mm^2 targeting the white coloured crust covering both the glass and the brown grisaille layer. The objective of these initial treatments was to check the performance of the selected laser parameters and to make a prior assessment of any damages that may be induced on the glass and the paint layer. The laser irradiation was applied gradually increasing the energy per pulse while carefully monitoring any colour or physical changes on the surface of the glass. At each power level, the laser irradiation was applied a number of times i.e. from 1 time to about 10 times or until crust removal was detected. The laser parameters applied for these initial treatments are listed in table 5.3.

The white crust started to be removed when the energy per pulse reached about 0.8 μJ/pulse with 10 series of laser irradiation (fig. 5.5). With this level of energy per pulse the crust started being ejected from the surface with each series of irradiation. The process was repeated to a maximum of 10 times and it was observed that the crust was being removed at a slow rate and would require either a higher laser power or an increase in number of irradiation series. As can be observed in figure 5.5, the underlying brown paint could be seen and had not been affected by the laser irradiation. At this juncture, there was

no complete cleaning as small remnants of the white crust could still be seen on the glass and paint surface.

Cuenca colourless glass	**1st treatment**	**2nd treatment**	**3rd treatment (putty)**
Power (W)	0.16	0.22	1.29
Energy per pulse (µJ)	0.8	1.12	6.47
Fluence (J/cm²)	0.11	0.16	0.91
Irradiance (GW/cm²)	475.53	665.75	3833.99
No. of series	1 to 10	1 to 5	1 to 10

Table 5.3: *Cuenca colourless glass. Initial cleaning parameters performed using the fs UV laser.*

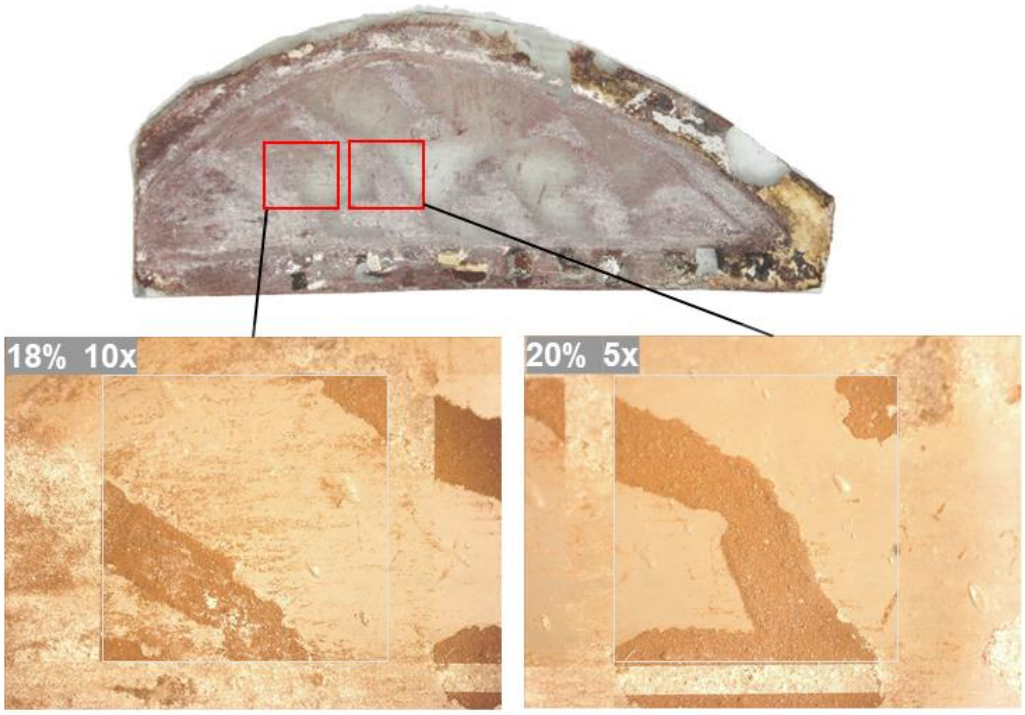

Figure 5.6: *Colourless glass from Cuenca cathedral. Optical micrographs of the historic glass surface after cleaning using 10 series with 0.8 µJ/pulse and 5 series with 1.12 µJ/pulse, respectively. The treated areas are marked with a square.*

By increasing the energy per pulse until 1.12 µJ/pulse the crust layer could be removed slowly after each series. 5 laser irradiation series were enough at this power level (1.12 µJ/pulse) to remove all the crust form the surface without inducing any damage to the glass substrate and to the paint layer (fig. 5.6). Some details can also be observed in figure 5.7. Photographs of figure 5.7.a and 5.7.b show the same region in the side with the grisaille.

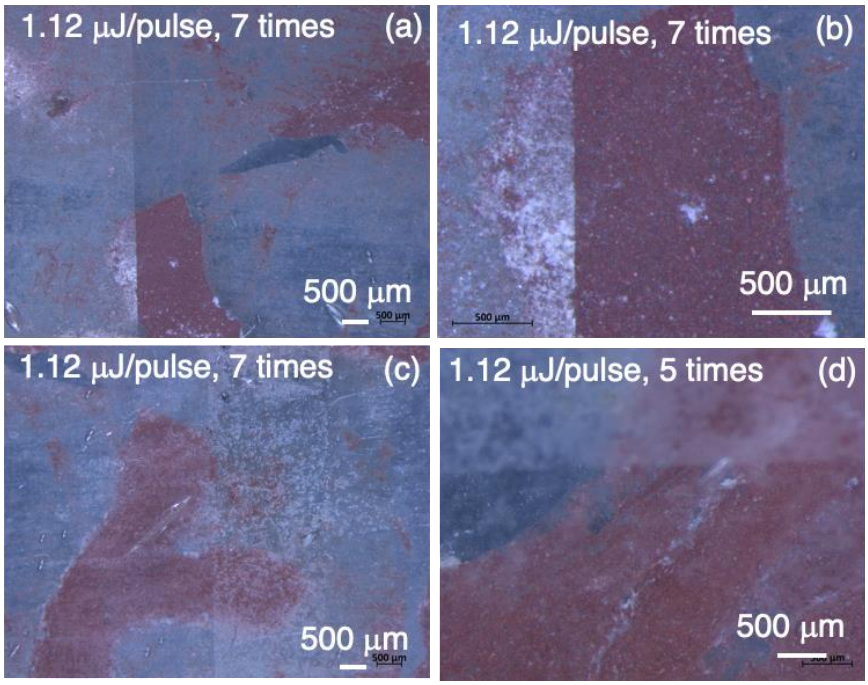

Figure 5.7: *Colourless glass from Cuenca cathedral. Optical micrographs of the historic glass surface after cleaning using different number of series with 1.12 µJ/pulse. (a) and (b) correspond to the side with grisaille and (c) and (d) to the opposite side.*

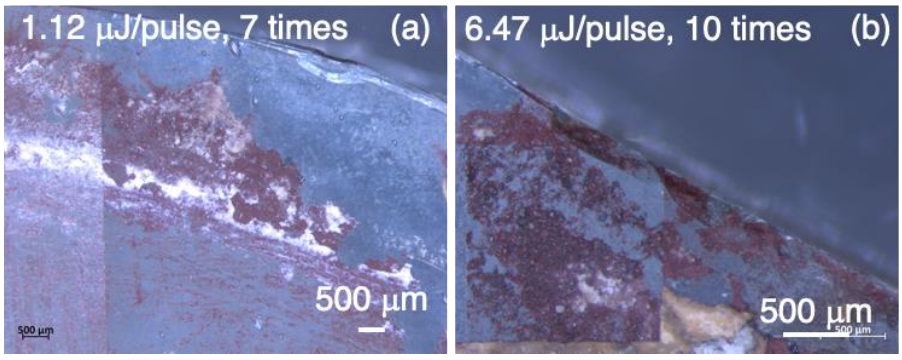

Figure 5.8: *Colourless glass from Cuenca cathedral. Optical micrographs of the historic glass surface after cleaning and area with putty using (a) 7 series with 1.12 µJ/pulse and (b)10 series with 6.47 µJ/pulse*

Clearly, these images show that the selected laser parameters do not affect the grisaille, even in the region of the glass where a thin layer of grisaille was deposited. Treatments in

the opposite side are presented in figures 5.7.c and 5.7.d, showing that these conditions are also effective in this side.

When similar laser cleaning parameters are applied in the region with putty, it is observed that 7 series with 1.12 µJ/pulse are not enough to completely eliminate all the putty (fig. 5.8.a). Increasing the energy per pulse to 6.47 µJ/pulse completely eliminated the putty but this level of energy modifies the grisaille that was under the putty material (fig. 5.8.b). In consequence, to clean the putty without affecting the grisaille, it was needed to return to low levels of energy per pulse, but it was still necessary to increase the number of times the process had to be repeated.

Following this first treatment, other areas of the glass were selected to be laser cleaned using 1.12 µJ/pulse as it has already been established that this power level was safe for both the glass substrate and the grisaille. The laser parameters applied in this case are presented in table 5.4. The laser treatment started similarly targeted those areas that had the crust covering the glass surface and the paint (fig. 5.9).

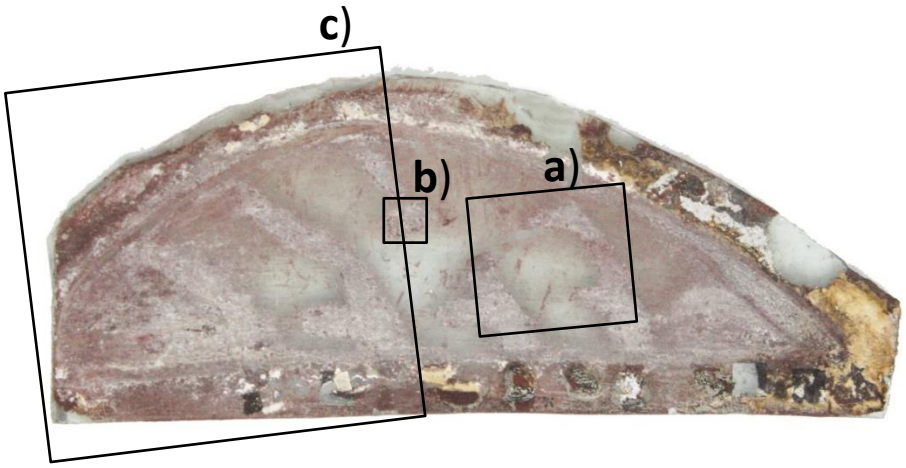

Figure 5.9: *Colourless glass from Cuenca cathedral. Areas selected for cleaning with the fs UV laser. The treatment begun with the area on the right (a) and then that in the middle (b) and lastly that on the left (c).*

Initially, laser irradiation was applied on area *a* (10mm x 10mm) in series maintaining the energy per pulse at 1.12 µJ/pulse. As it was observed in earlier laser treatments, the effectiveness of the crust removal increased as the number of irradiation series were increased. In the case of area *a*, the number of series requires to effectively remove the crust was 7. The aspect of the glass and paint layer before and after laser treatment can be

seen in the SEM micrograph presented in figure 5.10, that shows the limit of this region that was treated with laser (right part of the image). Figure 5.11.a shows a detail of the glass surface after the laser cleaning treatment. No damage was observed on the glass substrate and the pigment layer was not affected, even in this is a region with a thin grisaille layer. Figure 5.10 shows that the glass surface before cleaning exhibited a striped structure with vertical lines. This structure was created in previous laser treatments carried out on this glass piece with lower energy values. Figure 5.11.b shows that the crust layer in this region appeared as structures with a laminar aspect.

Cuenca colourless glass	***a***	***b***	***c***
Power (W)	0.22	0.22	9.33
Energy per pulse (µJ)	1.12	1.12	46.65
Fluence (J/cm^2)	0.16	0.16	6.60
Irradiance (GW/cm^2)	665.75	665.75	27729.5
No. of series	1 to 7	1 to 5	1

Table 5.4: *Cuenca colourless glass. Cleaning parameters applied on the three different areas of this glass using the fs UV laser. See figure 5.9 for the three treated areas.*

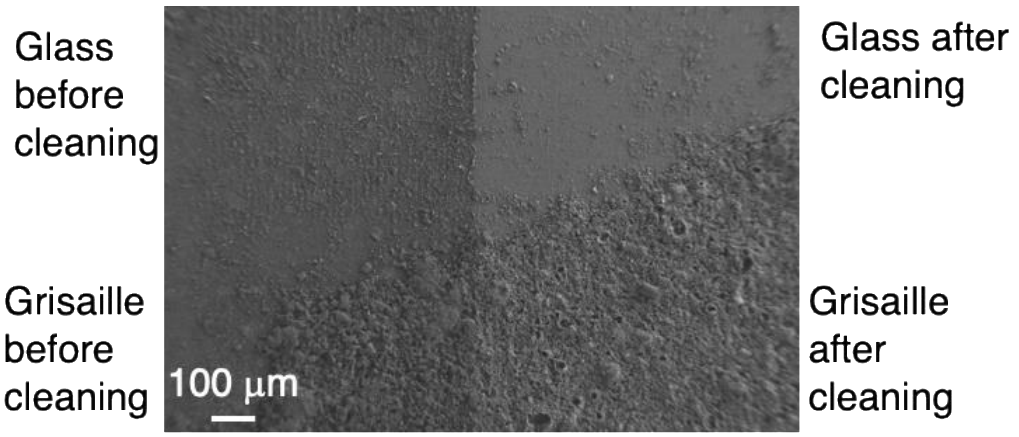

Figure 5.10: *Colourless glass from Cuenca cathedral. SEM micrograph showing the border between cleaned and non-cleaned regions.*

When the laser is applied on top of the grisaille, the surface maintains its topography, as it can be observed in figure 5.12. No big differences have been observed between the sample surface before and after laser treatment. In some particles, like those presented in figure 5.13, laser induced periodic structures (LIPS) have been generated. These are common nanostructures observed in a great variety of materials when they are processed with

pulsed lasers. They are more evident when ultra-short pulse lasers are used because the amount of molten material is very low. In our case, the period is close to 230 nm, a 67% of the laser wavelength.

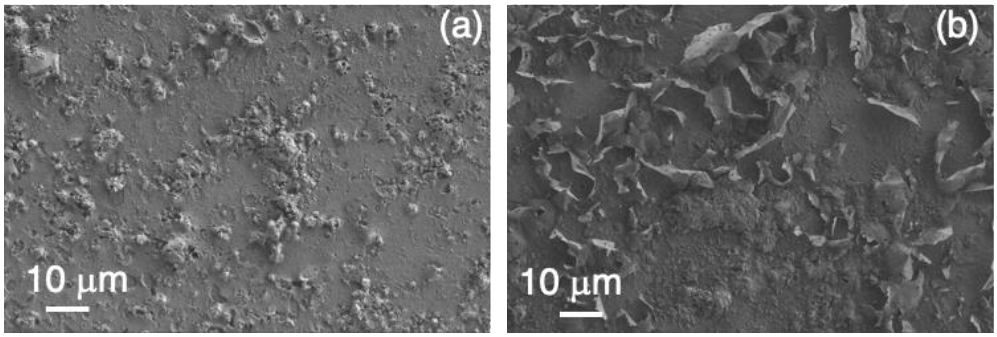

Figure 5.11: *Colourless glass from Cuenca cathedral. SEM micrograph of treatment from area* ***a****. (a) Glass surface with a thin grisaille layer after cleaning. (b) Similar surface before cleaning.*

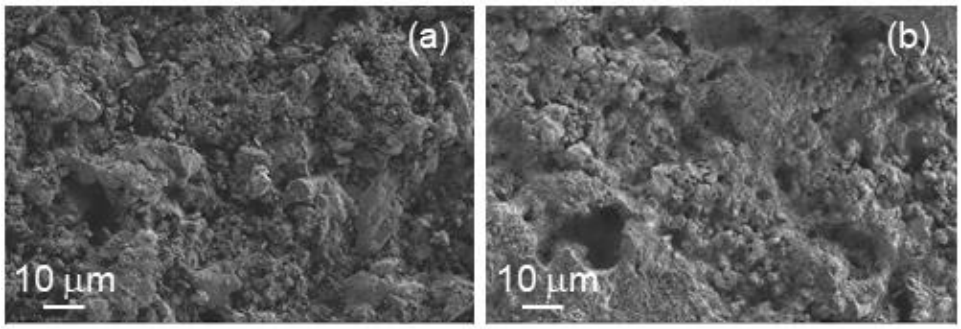

Figure 5.12: *Colourless glass from Cuenca cathedral. FESEM micrographs of the surface from area* ***a****. (a) Grisaille surface before cleaning. (b) Grisaille surface after cleaning.*

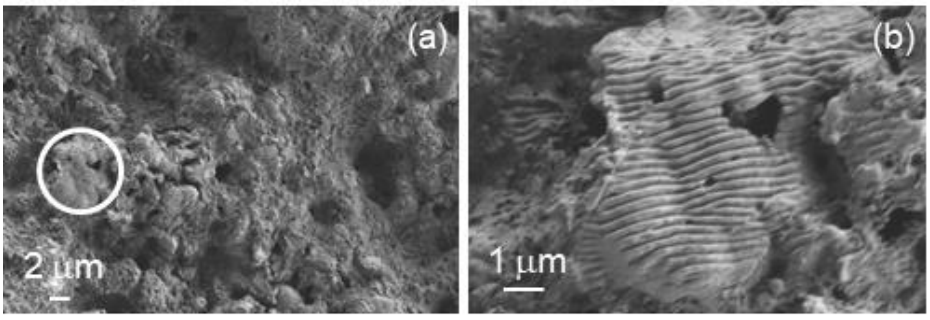

Figure 5.13: *Colourless glass from Cuenca cathedral. FESEM micrographs showing the periodic nanostructures that are generated on some particles of the grisaille after laser cleaning. Particle presented in (b) corresponds to the particle in the circle in (a).*

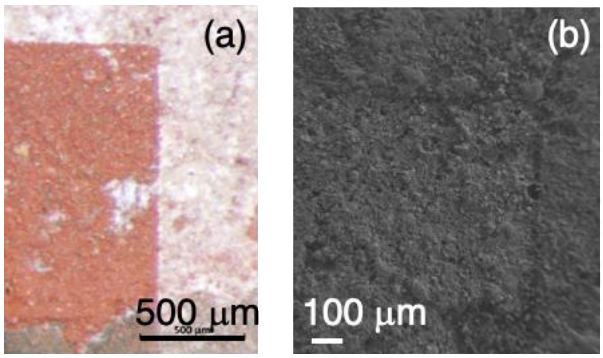

Figure 5.14: *(a) Colourless glass from Cuenca cathedral. (a) Optical micrograph of area b after laser cleaning with 5 series using 1.12 µJ/pulse. (b) FESEM micrograph showing the aspect of the surface before and after laser irradiation.*

A similar laser cleaning treatment was also applied on area *b*. In this case, only 5 series were applied. Figure 5.14 shows that these cleaning conditions were enough to have an efficiently cleaned section maintaining the integrity of the original sample in most of the area, but they were not enough to clean completely all the area. Both images show that the unwanted white crust was efficiently removed without inducing any melting or change of colour in the underlying paint layer. SEM micrographs presented in figure 5.15 shows the aspect of the paint layer in area *b* before laser irradiation, a region that is denser than in the region presented in figure 5.12.a, and the resultant aspect after laser cleaning with no damage on the pigment.

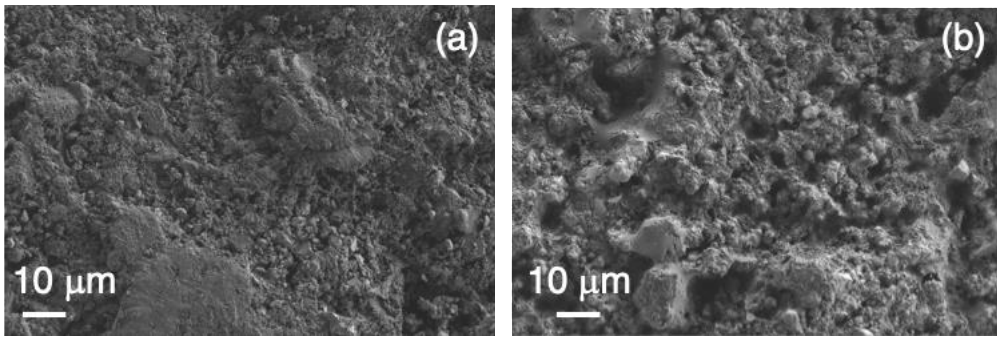

Figure 5.15: *Colourless glass from Cuenca cathedral. SEM micrograph of treatment from area* ***b****. (a) Pigment covered with the unwanted crust before laser irradiation. (b) Grisaille layer after laser irradiation showing the removal of the unwanted crust.*

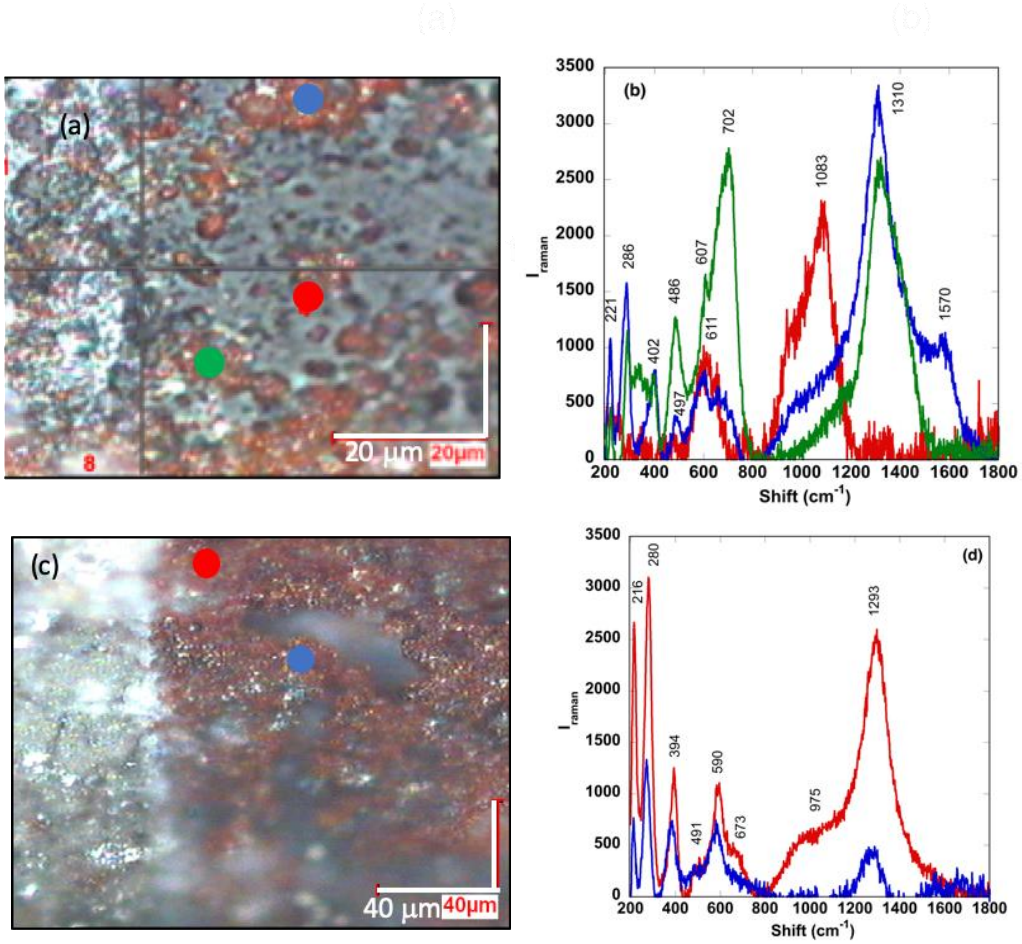

Figure 5.16: *Raman spectra in two cleaned regions of the colourless glass from Cuenca cathedral. (a) and (c) show the positions where the spectra were recorded. Circles show the exact position for each spectrum. (b) and (d) show the spectra.*

EDS analysis performed in the cleaned region shows a great reduction of the characteristic elements of the different compound that are present in the crust, mainly S and P. This has been confirmed with Raman analysis. Figure 5.16 shows the spectra measured in two regions that were cleaned with laser. It is important to mark the differences between these spectra and those recorded in regions that were not cleaned and that were presented in figure 3.9. The first difference is that the Raman intensity is very low in these spectra in comparison with those measured in similar regions before cleaning. And the second one is that they are completely different showing that the crust has been completely removed. Images in figures 5.16.a and 5.16.c show the areas that were analysed and the particular points are marked with circles of the same colours with the corresponding colours used in

the spectra (fig. 5.16.b and 5.16.d). In the first region, red point has been measured on a region without grisaille, while blue and green spectra were recorded in the region with grisaille. The spectra on the glass (red point in fig. 5.16.a and red spectrum in fig. 5.16.b) exhibits a characteristic peak at 1083 cm^{-1} and a second one at 611 cm^{-1}. In the other four positions, on top of the grisaille, the trends are different, showing a big peak in the region 1290-1310 cm^{-1} and some other peaks in the region 200-600 cm^{-1}. Optical photography, SEM and Raman confirm that the developed laser cleaning protocol is effective to eliminate the crust layer without affecting neither the glass nor the grisaille.

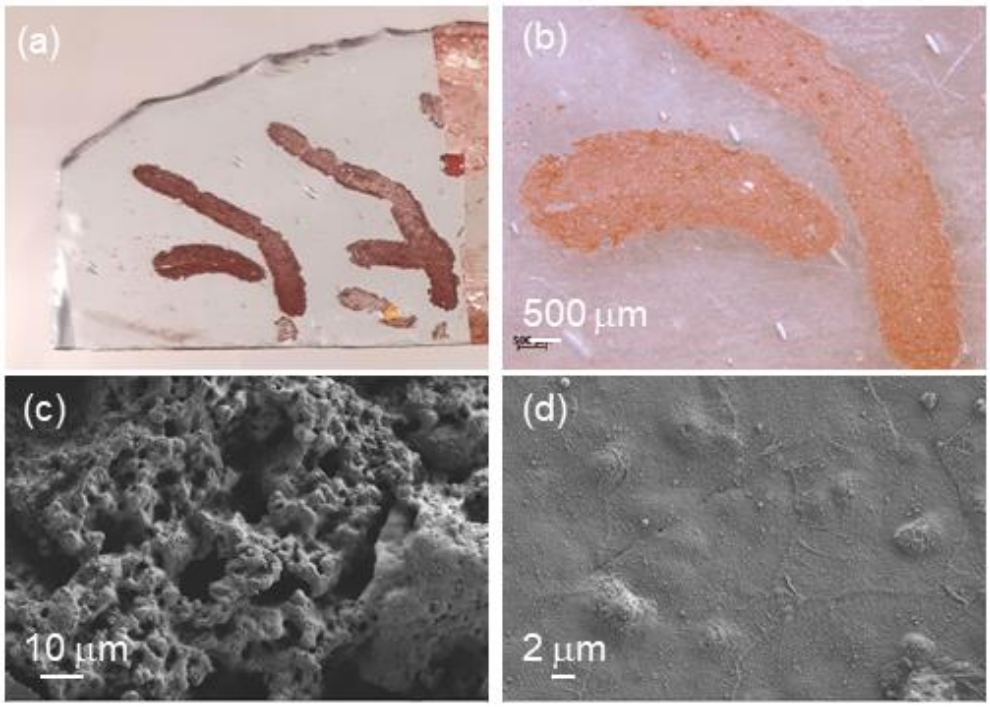

Figure 5.17: *Colourless glass from Cuenca cathedral. (a & b): Optical micrographs of the area that was irradiated with an energy level of 46.6 μJ/pulse in a single series. Note the colour change of the pigment in image a. SEM micrograph (c) show a FESEM image of the grisaille layer after the irradiation, while (d) shows the aspect of the glass surface after the laser treatment with these conditions.*

Due to some error with the laser control software, a region was processed with high energy per pulse values, in particular with an energy level of 46.6 μJ/pulse. This treatment deteriorated the sample surface, but it showed some interesting particularities in the response of this historical glass to UV laser radiation. As it can be observed in figure 5.17, the glass substrate did not show any damage due to photo-oxidation as had previously been

observed when a colourless contemporary glass was irradiated using the fs UV (fig 5.3). The brown grisaille was however affected as evidenced by the change in the colour contrast in figure 5.17.a. The treated area was observed under scanning electron microscopy and it was evident that under this laser level of energy even with a single irradiation series, it was possible to start melting the pigment layer as well as inducing some colour alteration of this layer (fig 5.17.c). The glass substrate, as seen in figure 5.17.d did not reveal any damage in the form of micro-cracks or colour change. However, there was slight indication of surface melting and polishing due to laser treatment. Also, the laser treatment has completely eliminated the putty and the thin grisaille layer that covered the glass. This error expose that it is important that the laser system has a double-checking protocol that forces the restorer to double check the emission parameters before the treatment is performed.

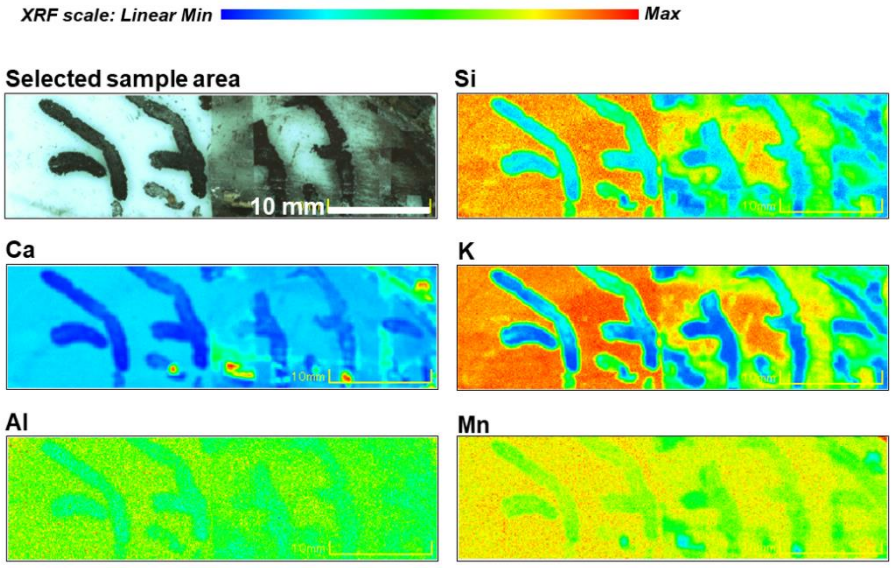

Figure 5.18: Colourless glass from Cuenca cathedral. XRF elemental maps of a section of this glass. The left half section of this glass had previously been irradiated with laser as part of the cleaning process.

A study to determine the elements present in the different regions of the colourless glass was also performed by XRF mapping. XRF mappings were obtained from an area of the glass sample with dimensions 42 x 15 mm (fig. 5.18). The X-ray mappings obtained are presented in figure 5.18, 5.19 and 5.20. In this case, the left half region had the crust already removed from glass and the grisaille surface.

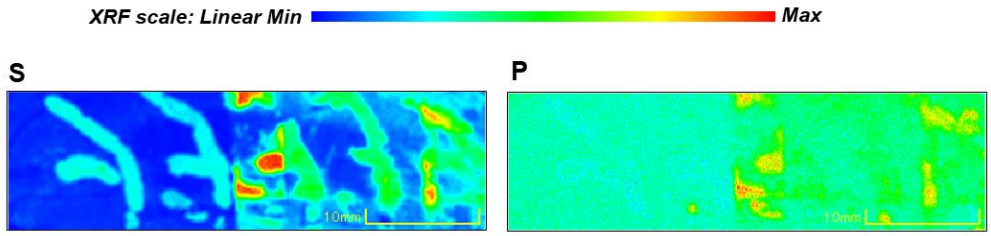

Figure 5.19: Colourless glass from Cuenca cathedral. XRF elemental maps showing the distribution of S and P in areas with crust on the surface. The left half side of the sample had been laser cleaned

Analysing the map of Si and K, clearly it is observed that the cleaning protocol is effective in removing the crust layer and the glass surface can be reached during the measurement. Obviously, the amount of these two elements is higher in the overcleaned area, but also an increase can be detected in the other two regions that have been cleaned with the correct cleaning conditions. Ca shows a different behaviour (fig. 5.18). Its presence is higher in the non-treated areas, indicating the presence of Ca compounds in the crust layer. The same trends are observed in the distribution of the other two elements that are expected in the crust layer, S and P (Figure 5.19). As it was deduced from Raman measurements in this glass before laser cleaning, the more probable compounds are gypsum ($CaSO_4 \cdot 2H_2O$) and apatite (Calcium phosphate). Figure 5.18 also shows the other two elements that are present in the glass composition, Al and Mn. Both elements are uniformly distributed in the glass sample and a light increase can be detected in the areas that have been cleaned.

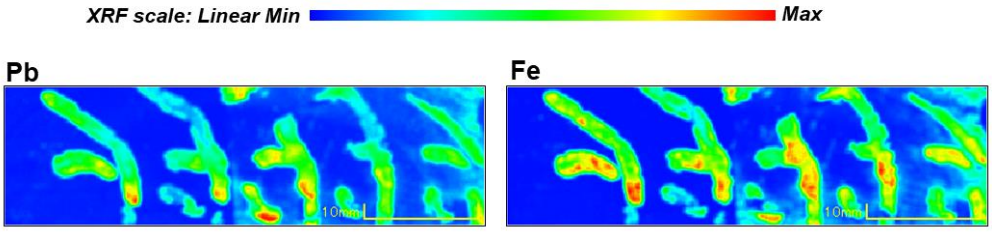

Figure 5.20: Colourless glass from Cuenca cathedral. XRF elemental maps showing distribution of Pb and Fe in areas covered by grisaille.

The detection of the elements Pb and Fe as presented in figure 5.20 was important in the identification of areas covered by grisaille. These elements (Pb and Fe) were confined to the flowery patterns that had been painted using a grisaille that appeared to have a matrix of lead silica glass phase and iron oxide (Fe_2O_3) as the pigment. The composition of this

matrix largely formed by oxide particles had been identified by EDS analysis of the regions covered by grisaille on this glass (tab. 3.4).

Blue glass from Cuenca Cathedral

The blue glass from Cuenca Cathedral had a white crust covering the surface in a striated manner, and this glass also had a brown grisaille applied in no particular pattern. As was the case with the colourless Cuenca glass, an initial treatment was performed with the same set of laser parameters to make a prior assessment of any damages that may be induced on the glass and the grisaille layer. The distance between lines was kept at 15 μm, a laser speed of 150 mm/s and a frequency of 10 kHz.

The laser treatment was applied in six selected areas of 1 × 1 mm^2 targeting the white coloured crust covering both the glass and the brown grisaille layer (fig. 5.21). The laser power was increased gradually while carefully observing the crust removal or any changes on the surface due to the laser irradiation. The laser parameters applied here are listed in table 5.5. For this initial treatment, only one series of laser irradiation was applied in each square box. As can be observed in figure 5.21, in some areas the crust was thicker and using a higher laser power with a single series was not sufficient enough to removal all the crust. In some areas, low levels of energy per pulse (0.18 μJ/pulse), were sufficient to make some significant removal of the white crust. It was also observed that, energy per pulse of about 2 μJ/pulse could be applied to remove the crust on this blue glass without inducing any damage to the underlying grisaille or to the glass substrate (2.02 μJ/pulse square in fig.5.21).

Cuenca blue glass				
Power (mW)	36	97	224	405
Energy per pulse (μJ)	0.18	0.49	1.12	2.02
Fluence (J/cm²)	0.025	0.069	0.16	0.29
Irradiance (GW/cm²)	106.99	288.29	665.75	1203.69
No. of series	1	1	1	1

Table 5.5: *Cuenca blue glass. Initial cleaning parameters applied on the squares marked in figure 5.21 of this glass using the fs UV laser.*

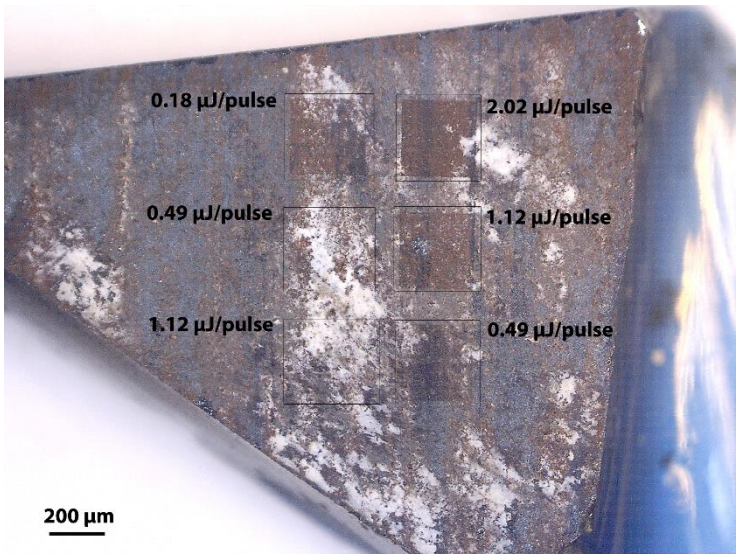

Figure 5.21: *Blue glass from Cuenca cathedral. Optical micrograph of the 1 x 1 mm^2 squares where initial treatments were carried out with different laser power percentages.*

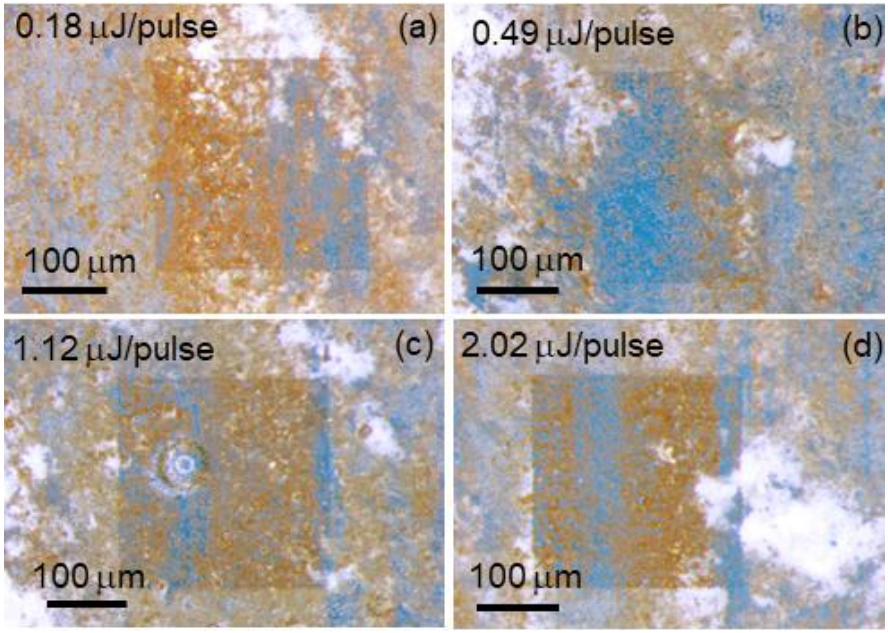

Figure 5.22: *Blue glass from Cuenca cathedral. Optical micrographs of the glass surface after cleaning using a single series each with (a) 0.18 µJ/pulse (b) 0.49 µJ/pulse (c) 1.12 µJ/pulse and (d) 2.02 µJ/pulse.*

Cuenca blue glass	***a***	***b***	***c***
Power (mW)	405	405	405
Energy per pulse (µJ)	2.02	2.02	2.02
Fluence (J/cm^2)	0.29	0.29	0.29
Irradiance (GW/cm^2)	1203.69	1203.69	1203.69
No. of series	5	10	15

Table 5.6: *Cuenca blue glass. Cleaning parameters applied on the three areas in figure 5.21 of this glass using the fs UV laser.*

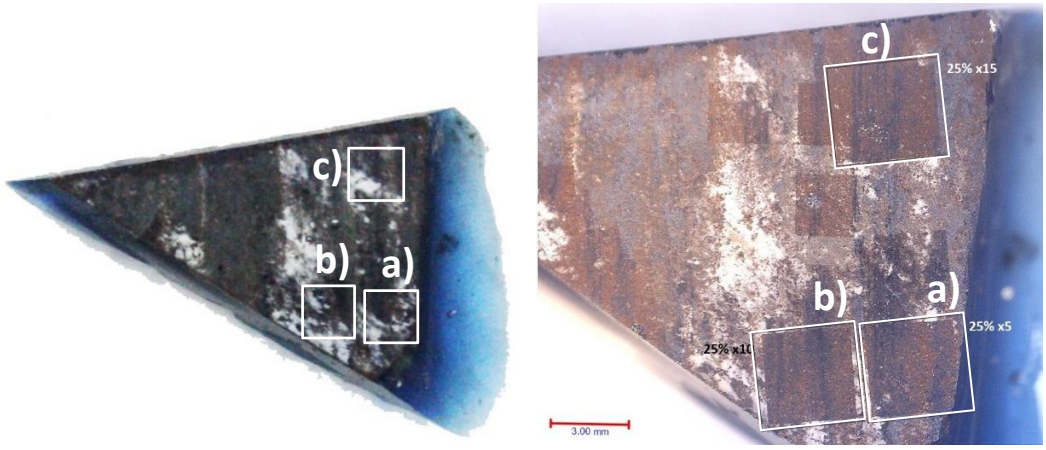

Figure 5.23: *Blue glass from Cuenca cathedral. Left: The areas selected for the laser treatment. Right: The selected areas after laser irradiation 2.02 µJ/pulse applied a) 5 times, b) 10 times and c) 15 times.*

Optical micrographs in figure 5.22 show four regions with a grisaille layer after a single laser irradiation in each increasing the energy per pulse from as low as 0.18 µJ/pulse up to 2.02 µJ/pulse. In all the cases and with the laser conditions applied, it is observed that the crust could be removed without affecting the underlying grisaille. Even when a higher value of energy per pulse is reached (fig. 5.22.d), the grisaille layer is unaffected and thus by increasing the number of irradiation series at this juncture the crust could gradually be eliminated as will be discussed in the following paragraphs.

Following this observation on the effectiveness of safely applying a higher power, the subsequent laser treatments were performed with an energy per pulse of 2.02 μJ/pulse. A similar protocol as that applied on the colourless glass i.e. increasing the number of laser irradiation series per treated area was adopted for this glass as well. A number of areas were selected for the laser treatment, see figure 5.23. Table 5.6 list the parameters applied on the three selected areas in figure 5.23.

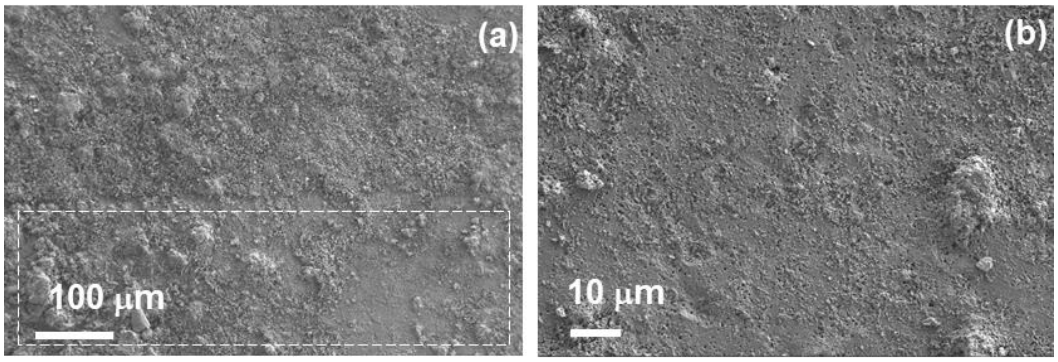

*Figure 5.24: Blue glass from Cuenca cathedral. (a) SEM micrograph of the pigment layer in area **a** in figure 5.23 showing the border before laser irradiation (top) and after 5 series of laser treatment (marked with dotted lines). (b) A close-up from area **a** showing the surface aspect of the pigment and glass substrate after removal of the unwanted crust.*

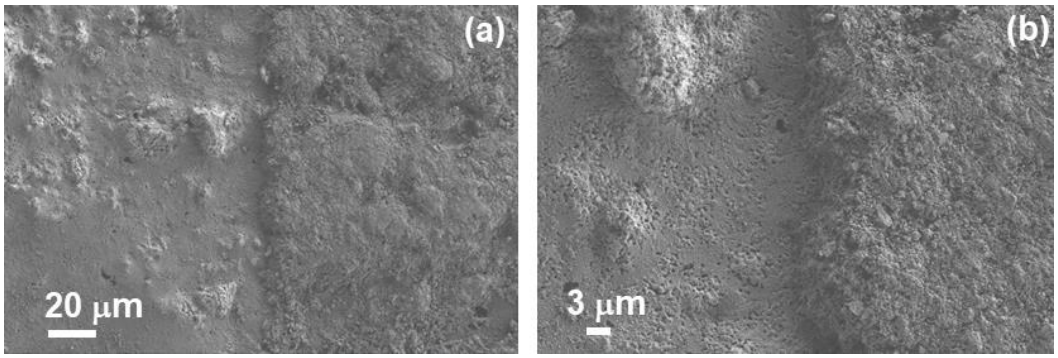

*Figure 5.25: Blue glass from Cuenca cathedral. (a) The left side is a surface with pigment after 10 series of laser irradiation on area **b** in figure 5.23, the right side is a non-treated pigment layer covered by the white crust. This crust is the untreated interface between **b** and **c** in figure 5.23. (b) A close-up of the micrograph on the left.*

The laser removal of the white surface crust from the surface of the grisaille and from sections with exposed glass substrate proved to be effective with energy per pulse of 2.02 μJ/pulse. By increasing the number of laser irradiation series up to 5 times, the crust could

be eliminated without causing any damage to the glass or to the pigment as can be seen in FESEM images presented in figure 5.24. The laser irradiated section is marked in dotted lines in figure 5.24.a. There was no evidence of pigment melting or micro-cracks on the glass substrate indicating that the set laser conditions and the applied protocol was sufficiently safe for the removal of the unwanted surface crust. Subsequently, for laser cleaning of section *b* in figure 5.23, the number of laser irradiation series were gradually increased up to 10 times maintaining the laser energy at 2.02 μJ/pulse. Similarly, no damage was induced on the pigment and the glass, though, as seen in figure 5.25 the effectiveness of crust removal was more pronounced in this case than when 5 series were applied. This laser cleaned part is one of the sections of the glass with the thickest layer of the unwanted crust.

In area *c* (fig. 5.23), the number of times the process was repeated was increased up to 15, maintaining all other laser conditions as in the previous treated areas. This area had most of the thinnest layer of the unwanted crust covering the pigment layer. As can be observed in figure 5.26, applying 15 laser irradiation steps successively it was possible to safely and effectively remove the unwanted white crust from the surface maintaining the integrity of the underlying pigment. Even at this significantly high number of laser irradiation series the areas with exposed glass substrate remained unaffected (fig. 5.26.b) proving the effectiveness of using low frequencies to avoid damage induced by temperature gradients associated with heat accumulation.

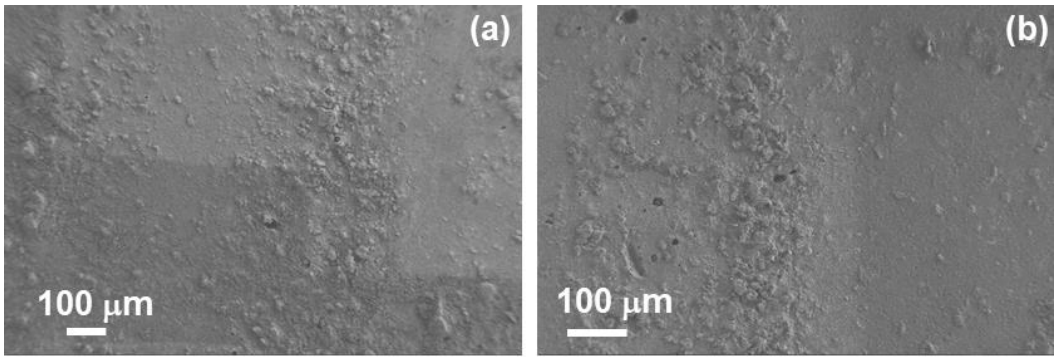

Figure 5.26: Blue glass from Cuenca cathedral. (a) SEM micrograph of area ***c*** *in figure 5.23 showing the laser irradiated regions that appear in a lighter contrast on the top right part of the first image (15 series of irradiation). (b) SEM micrograph showing the surface aspect of the grisaille layer (left side of image) and the glass substrate (right side of image) after the removal of the unwanted crust from area* ***c****.*

As it was previously observed with the colourless glass, in this blue glass there were differences between Raman spectra recorded on regions after laser cleaning with those recorded in regions that were not cleaned and that were presented in figures 3.26, 3.27 & 3.28. Before cleaning, spectra clearly show the presence of Ca sulfate compounds with large peaks at 1015 cm^{-1} and 1025 cm^{-1}. The spectra collected from laser cleaned regions indicated a higher reduction in intensity compared to those collected from the non-treated regions within the same section. The spectra from both the cleaned and non-cleaned regions were completely different a confirmation of complete crust removal. In the blue glass sample, after laser cleaning, regions were observed featuring a thin layer of grisaille covering the glass surface. Analysis were carried out on these areas that revealed a grisaille underlayer and also on areas without grisaille. Figures 5.27.a and 5.27.c show the images and particular points on top of grisaille that were analysed and their respective spectra (fig. 5.27.b and 5.27.d). Additional analysis was performed in areas that were without any grisaille layer, directly on the glass surface, and these images are presented in figures 5.28.a and 5.28.c with their corresponding spectra in figures 5.28.b and 5.28.d respectively.

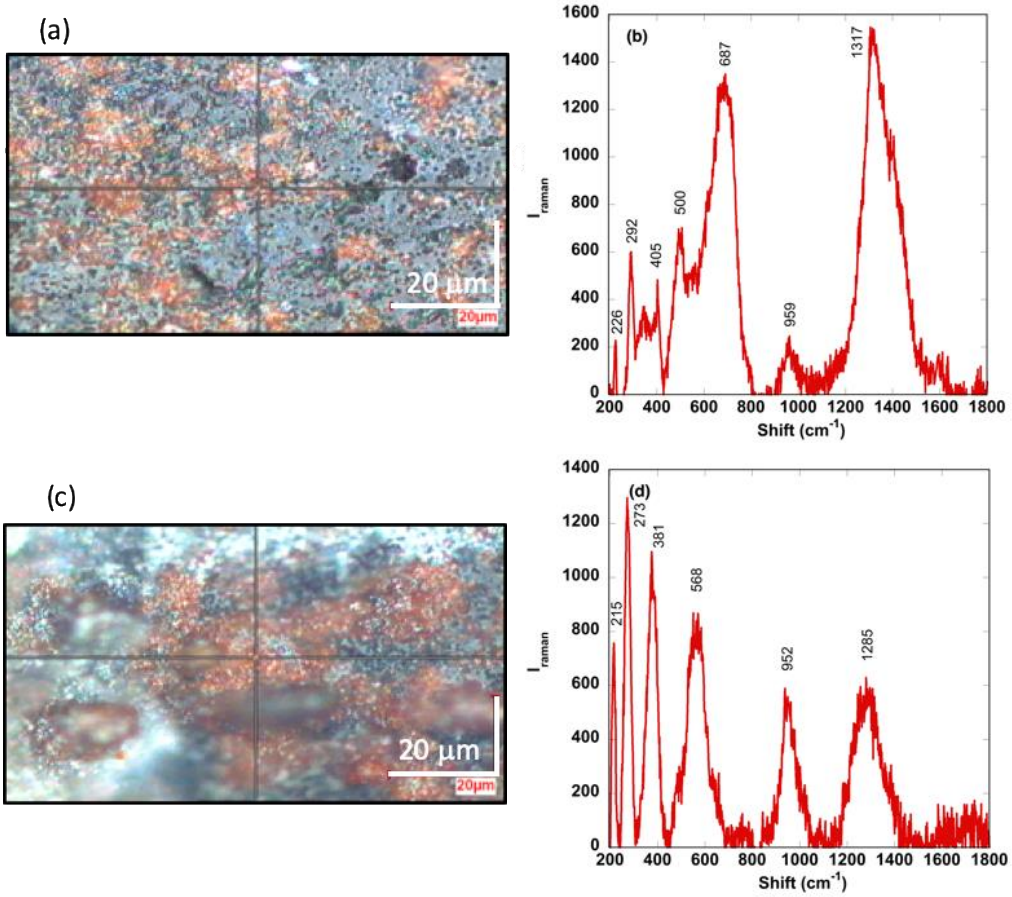

Figure 5.27: Blue glass from Cuenca cathedral. Raman spectra in two positions where grisaille is observed after laser cleaning. (a) and (d) show the position where spectra were recorded and (b) and (d) present the measured spectra.

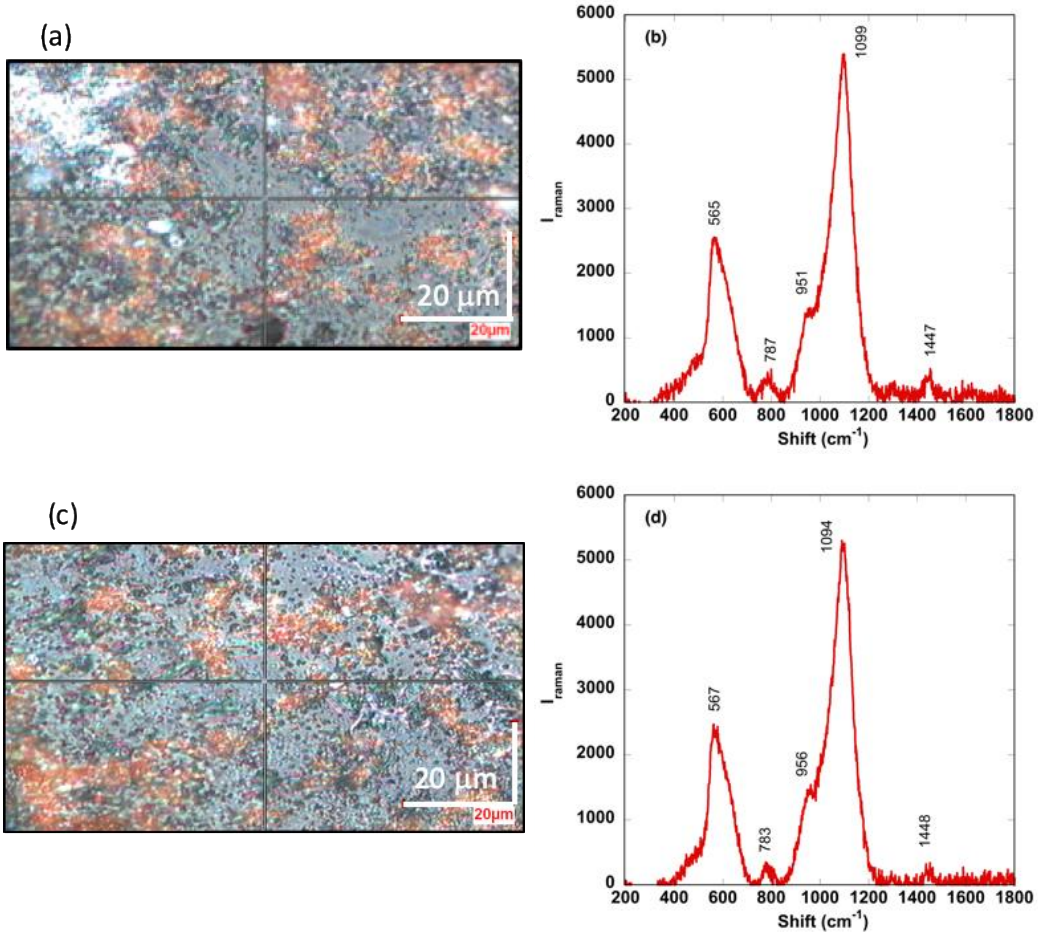

Figure 5.28: Blue glass from Cuenca cathedral. Raman spectra in two positions where glass is observed after laser cleaning. (a) and (d) show the position where spectra were recorded and (b) and (d) present the measured spectra.

Many of the peaks in figures 5.27.b and 5.27.d such as the peak seen at about 960 cm^{-1} were associated to Fe_2O_3 detected from the thin grisaille layer revealed after laser cleaning and subsequent removal of the crust. As can be observed in the spectra on the grisaille in figures 5.27.b and 5.27.d a larger peak appeared in the region 1285-1317 cm^{-1} and some other peaks in the region 210-690 cm^{-1}.

The spectra recorded from the glass without any grisaille layer (fig. 5.28.b and 5.28.d) exhibited a characteristic peak at about 1094 cm^{-1} observed in soda rich glasses and a second peak at 567 cm^{-1}. The shoulder observed at about 956 cm^{-1} close to the peak 1094

cm^{-1} in figures 5.28.b and 5.28.d was associated to the presence of some amount of Fe_2O_3 in the glass composition.

The results obtained from Raman analysis performed on the laser cleaned regions on this glass were in agreement with the EDS analysis carried out in similar cleaned regions, with the latter showing a great reduction of the characteristic elements constituting the different compounds of the crust, mainly S and P. Additionally, as was the case with the colourless glass, optical photography, SEM and Raman confirmed that the laser cleaning protocol developed is effective in removing the unwanted surface crust layer without affecting neither the glass nor the grisaille.

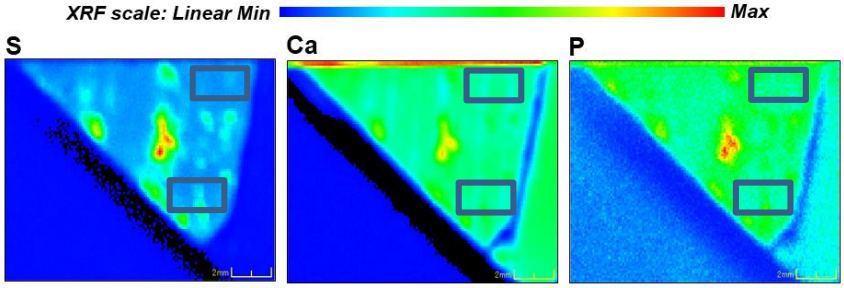

Figure 5.29: Blue glass from Cuenca cathedral. XRF elemental map distribution of the crust forming compounds in areas of the glass that were not laser treated. The laser treated areas are marked with rectangles (not in scale).

In this blue Cuenca glass, X-ray maps collected showed a clear distinction in the amount of crust forming elements (S, Ca and P) before and after laser treatment. As can be seen in figure 5.29, those areas in the three images characterized by high concentration of the three elements appear in regions that were not cleaned outside the squares where the laser cleaning process was performed. The surrounding areas show very low or no detection of these elements.

Green glass from Cuenca Cathedral

As reported in Chapter 3, this glass from Cuenca cathedral (fig.5.30) had its surface covered by a white coloured deterioration layer that showed a high level of non-uniformity with some regions having a very thin crust and others with bigger thickness. Needle-shaped crystals were identified by scanning electron microscope as part of crust formation with EDS analysis identifying these crystals as either gypsum ($CaSO_4 \cdot 2H_2O$) or anhydrite

($CaSO_4$) together with a formation of calcite (calcium carbonate) compounds. The glass surface also showed that it had a layer of red-brown grisaille.

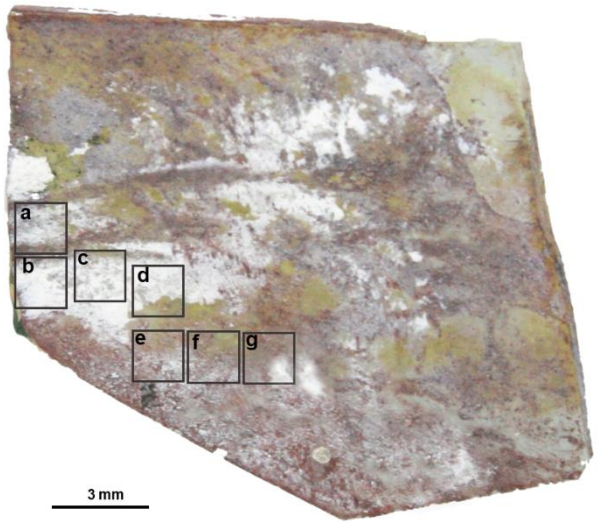

Figure 5.30: *Green glass from Cuenca cathedral. Squares indicate the seven sections that had been selected for treatment with the fs UV laser.*

Following a similar trend with that applied on the colourless and the blue glasses from Cuenca cathedral the laser treatments on the green Cuenca glass were performed with an energy per pulse of 2.02 μJ/pulse. Similarly, the protocol of increasing the number of laser irradiation series per treated area was adopted for this glass as well. The oscillator frequency was set at 200 kHz and a PPD value of 20 was selected. Laser scanning speed was fixed at 150 mm/s, giving a distance of 15 μm between pulses with a similar distance between lines to ensure a homogeneous cleaning with the beam size of this laser at the focal distance. A total of seven 1.5mm x 1.5mm squares were selected for laser cleaning (fig. 5.30). Table 5.7 lists the conditions that were applied in each of the squares during the laser treatments. Initial treatment began at section *a* applying 5 irradiation series with an energy per pulse of 2.02 μJ/pulse. As can be observed in figure 5.31 with the number of irradiation series applied (5 times) it was possible to remove the thin layer of the crust in this section but the conditions were insufficient to make any changes on the part that had a thick crust. Increasing the level of energy per pulse to try and eliminate the thick white crust was not an option since this level of laser energy would melt the underlying grisaille layer.

In section *b*, the number of irradiation series was increased to 10 while maintaining the energy per pulse at a safe level of 2.02 μJ/pulse. As was the case in section *a*, in spite of successful removal of the thinner crust, the thicker layer could not be removed at this laser energy level, and this similar trend was experienced in section *c* and *d* even after increasing the number of irradiation series to 15 and 35 respectively. In chapter 3, the crust was reported to be a matrix of gypsum or anhydrite and calcite, in this case it could be inferred that due to the complex combination of compounds in the matrix and its thickness it would require a higher number of irradiation series to remove while maintaining a safe laser energy level.

As observed in figure 5.30 section *e*, *f* and *g* had a thinner crust covering the surface. In this case treatment in section *e* was performed at the basic energy per pulse value of 2.02 μJ/pulse, with a single irradiation series (tab. 5.7). In figure 5.31, it is evident that at this laser energy level and with a single irradiation series it was possible to eliminate almost all of the thin white crust from the surface. In order to allow safe application of multiple irradiation series without inducing any damage to the underlying grisaille layer, subsequent laser treatments were performed at a lower energy per pulse values, in this case at 1.34 μJ/pulse. Laser treatment in section *f* were performed by a single irradiation series at 1.34 μJ/pulse leading to a successful removal of the crust as can be seen in figures 5.31 and 5.32. Section *g* was covered partly by a thinner crust and also by a thicker layer at the bottom right side. By applying 5 irradiation series at an energy per pulse value of 1.34 μJ/pulse it was possible to eliminate most of the thinner crust as well as part of the thicker crust as can be seen in figure 5.31 (bottom right corner of section *g*)

Green Cuenca glass	*Power (mW)*	*Energy per pulse (μJ)*	*Fluence (J/cm^2)*	*Irradiance (GW/cm^2)*	*No. of series*
a	405	2.02	0.29	1203.69	5
b	405	2.02	0.29	1203.69	10
c	405	2.02	0.29	1203.69	15
d	405	2.02	0.29	1203.69	35
e	405	2.02	0.29	1203.69	1
f	268	1.34	0.19	799.43	1
g	268	1.34	0.19	799.43	5

Table 5.7: *Green glass from Cuenca cathedral. Fs UV conditions that were applied to laser clean the different sections of the green Cuenca glass seen in figure 5.28.*

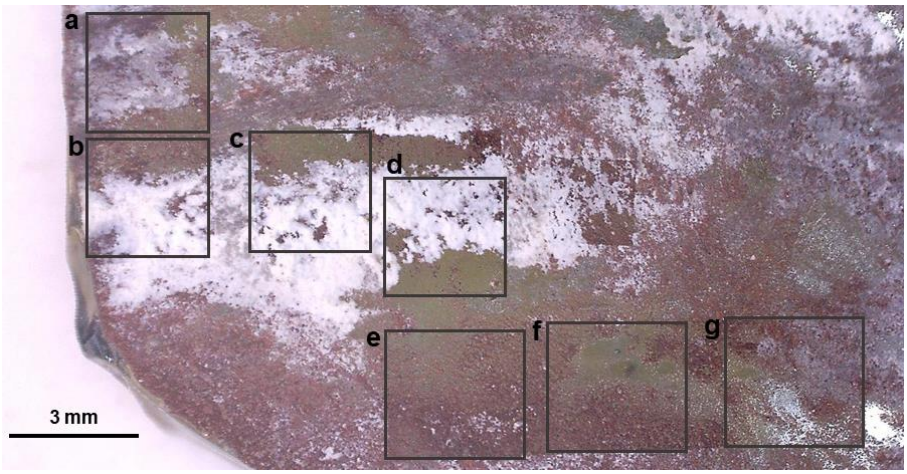

Figure 5.31: *Green glass from Cuenca cathedral. The seven selected sections after laser treatment with; a) 2.02 μJ/pulse, 5 times, b) 2.02 μJ/pulse, 10 times, c) 2.02 μJ/pulse, 15 times, d) 2.02 μJ/pulse, 35 times, e) 2.02 μJ/pulse, 1 time, f) 1.34 μJ/pulse, 1 time and g) 1.34 μJ/pulse, 5 times.*

Figure 5.32: *Green glass from Cuenca cathedral. A close up optical image of section f in figure 5.31 after laser cleaning at a laser energy value of 1.34 μJ/pulse with a single irradiation series. The top part is the laser cleaned area also showing the uneven distribution of the red-brown grisaille.*

Similarly, as it was observed with the blue glass, the XRF maps in the green glass indicated a reduction in the concentration of S, Ca and P that had been reported as responsible for the formation of the unwanted crust. Figure 5.33, shows these maps, and the laser treated areas, that are marked with a rectangle are clearly identified because they have been decontaminated.

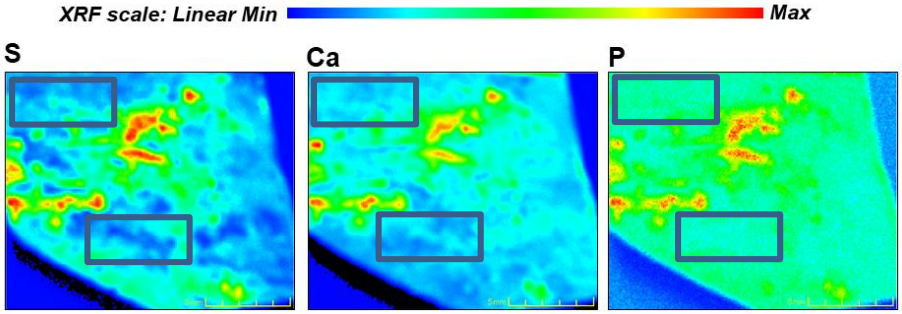

Figure 5.33: Green glass from Cuenca cathedral. XRF elemental map distribution of the crust forming compounds.

Red glass from Chartres cathedral

The red from Chartres cathedral had a thick white crust covering the entire surface apart from an outline on the edge, and this glass showed no evidence of having contained any grisaille. As a result of the thick crust, laser treatment conditions different from those applied on the glasses from Cuenca cathedral were selected. The distance between lines was kept at 15 µm, with a laser speed of 300 mm/s and a frequency of 20 kHz. Laser irradiation was applied, in this case not by series, but in a loop with the energy per pulse being increased from 1.12 µJ/pulse up to 6.47 µJ/pulse. The loop configuration meant that there was no any waiting time between two consecutive pulses. It was observed that below the energy per pulse of 1.12 µJ/pulse the crust was unaffected by the laser irradiation.

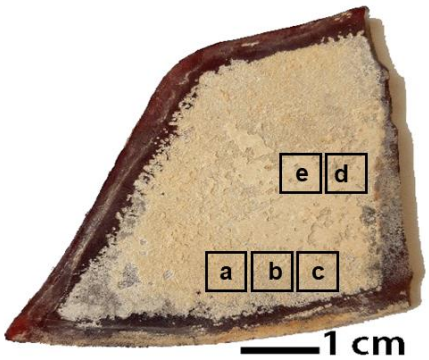

Figure 5.34: *Red glass from Chartres cathedral. The five selected 1.5 x 1.5mm squares that were irradiated with fs UV laser.*

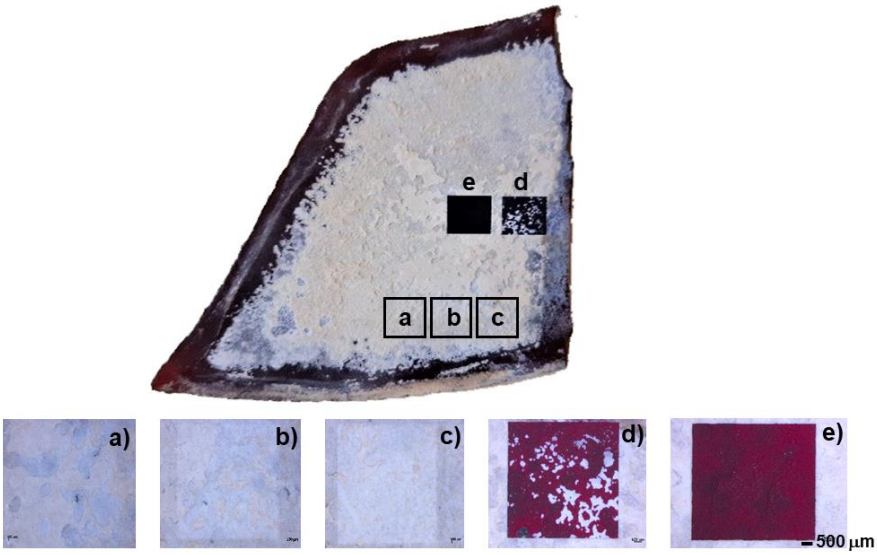

Figure 5.35: *Red glass from Chartres cathedral. The five squares after laser irradiation with; a) 1 loop of 10 series with 1.12* µJ/pulse, b) *1 loop of 10 series with 3.19* µJ/pulse, c) *1 loop of 10 series with 6.47* µJ/pulse, d) *1 loop of 200 series with 6.47* µJ/pulse and d) *1 loop of 300 series with 6.47* µJ/pulse.

Red Chartres glass	***a***	***b***	***c***	***d***	***e***
Power (mW)	224	638	1294	1294	1294
Energy per pulse (µJ)	1.12	3.19	6.47	6.47	6.47
Fluence (J/cm^2)	0.16	0.45	0.91	0.91	0.91
Irradiance (GW/cm^2)	665.75	1896.19	3833.99	3833.99	3833.99
No. of series in a loop	10	10	10	200	300

Table 5.8: *Red glass from Chartres cathedral. Laser conditions that were applied on the five selected areas of this glass.*

The laser treatment was performed in five selected areas of 1.5 × 1.5 mm^2 as shown in figure 5.34 targeting the white coloured crust covering the glass. The laser parameters applied here are listed in table 5.8.

The energy per pulse applied in the first three squares was in the following order; 1.12 µJ/pulse, 3.19 µJ/pulse and 6.47 µJ/pulse (tab. 5.8) while carefully observing the crust removal or any changes on the surface due to the laser irradiation. Treatment in square *a* begun by applying an energy per pulse of 1.12 µJ/pulse in a loop of 10 series and as can be seen in figure 5.35 (square *a*) a thin layer of the crust was removed. In square *b*, the energy per pulse was increased to 3.19 µJ/pulse and like in square *a*, the irradiation series

were performed in a loop of 10 times. Similarly, this level of energy per pulse was not sufficient enough and only a thin layer of crust was ejected. In square *c*, the energy per pulse was raised to 6.47 µJ/pulse applied in a 10 series loop and at this level of energy as seen in figure 5.35 (square *c*) a significant amount of crust was removed. Following this, it was evident that this level of energy per pulse (6.47 µJ/pulse) would be sufficient for subsequent laser irradiation to remove the crust and only the number of series in a loop needed to be increased. As can be observed in figure 5.35 (square *d*), the crust was almost completely eliminated when 200 irradiation series were applied in a loop. Complete removal of the crust without inducing any damage to the glass was achieved by applying 6.47 µJ/pulse energy per pulse with 300 irradiation series in a loop (fig. 5.35 square *e*).

EDS analysis of the laser cleaned areas showed a great reduction in the amount of crust forming elements such as Ca and S (tab. 5.9) when compared to their respective amount before any laser intervention. This is an indication that the set laser conditions were sufficient to successfully remove the crust even when the laser irradiation series were applied in a loop.

Chartres red glass: *White crust before laser*									
Elements	**O**	**Si**	**Ca**	**Na**	**K**	**Al**	**Mg**	**P**	**S**
%at	*54.9*	*13.7*	*6.8*	*0.6*	*1.3*	*0.9*	*0.4*	*0.7*	*6.3*
White surface crust after laser irradiation									
Elements	**O**	**Si**	**Ca**	**Na**	**K**	**Al**	**Mg**	**P**	**S**
%at	*61.7*	*29.9*	*2.2*	*0.4*	*1.8*	*1.4*	*0.8*	*0.7*	*1.1*

Table 5.9: *Red glass from Chartres cathedral. EDS analysis showing elemental differences before and after laser cleaning of the glass.*

CHAPTER 6: COMPARISONS OF TRADITIONAL CLEANING TECHNIQUES WITH LASER CLEANING PROTOCOLS

Mechanical and chemical cleaning experiments were performed to make a comparison with cleaning protocols that were carried out using laser technology. The traditional cleaning trials were carried at the *Maison-Lorin* Glass Conservation Workshop in Chartres France. A panel of stained-glass window covered with a thick corrosion crust was selected for this study (fig 6.1). Two glass pieces were detached from the original panel using mechanical tools. Figure 6.2 show photographs of both faces of the two glass pieces.

Two chemical products commonly used at the *Maison-Lorin* Glass Conservation Workshop were used in the restoration. These products are EDTA (Ethylenediaminetetraacetic acid) and Sodium thiosulfate. The two chemical products were applied using gels prepared using Carbopol and Carbogel. Carbopol is a water soluble polymer, used as a suspending and thickening in many industries and is also used as a gelling agent. The gelling effect is activated in two steps, first by the dispersion ad hydration of the product and second by neutralizing the solution by the addition of chemicals that increase the pH. These neutralizing chemicals include sodium hydroxide, potassium hydroxide and triethanolamine (https://www.silverson.com/us/resource-library/application-reports/dispersion-and-hydration-of-carbopol).

Figure 6.1: *Stained glass from Chartres cathedral, France. Original panel from which the samples were detached for the chemical treatments.*

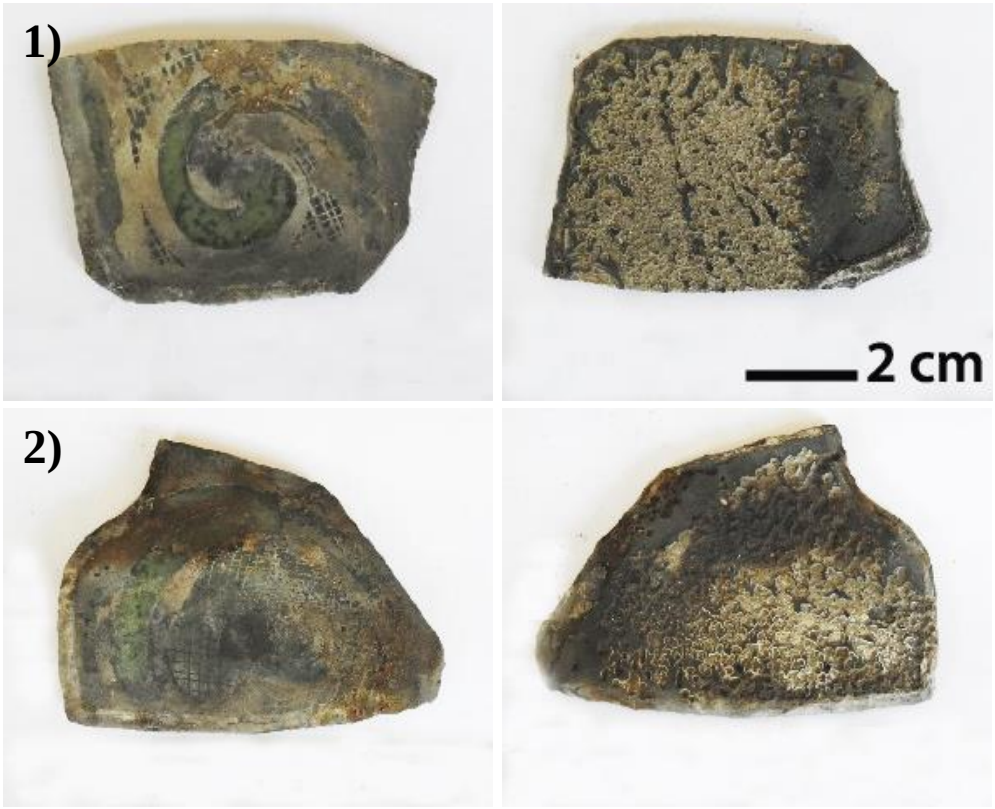

Figure 6.2: *Stained glass from Chartres cathedral, France. The two glass pieces before any interventions. The images on the right of each are the reverse side.*

Carbogel on the hand is formed from neutralized polyacrylic acid that allows the formation of a gel by simply adding water to achieve the desired viscosity. A sufficiently high viscosity gel can be obtained by using Carbogel in aqueous solution. The water retention capacity of Carbogel is quite high, which in turn evaporates very slowly. Carbogel modified polyacrylic acid can be added to EDTA to form a gel that can be applied on the glass surface that requires restoration (https://shop-espana.ctseurope.com/234-carbogel). Both Carbopol and Carbogel appear as white grains.

In this workshop mechanical interventions were being used as complementary techniques to the chemical cleaning. That is, soft brushes were being utilized to scrap off surface crusts that have already been loosened by chemical means. The scraping was done carefully taking care not to leave scratch marks on the glass or to destroy the underlying paint layer.

6.1. Cleaning stained-glasses with EDTA chemical product

EDTA is one of the chemical products commonly used for the removal of surface crusts from the surface of the stained-glass windows. EDTA is best used to dissolve and remove crusts on the glass surface that contains no paint/grisaille (mostly internal face of the window). EDTA reacts with oxides (iron, lead etc.) that are constituents of grisaille and paint), thus EDTA contact with grisaille is best avoided. Basically, EDTA is prepared and applied in about 5 series or until the surface crust is removed. The PH of the EDTA mixture has to be well measured to avoid potential damage to the glass substrate. Incorrect PH may also weaken the acting effect of the EDTA product.

During this study, the product was prepared by mixing EDTA with Ammonia biocarbonate (20g/L), carbopol ultrez 21 (20g/L) with de-mineralized water being used to make the solution. The PH of the mixture was tested with a litmus paper. The prepared mixture was applied on the glass surface and allowed to settle for about 2 hours before being wiped out followed by subsequent reapplication, to a maximum of 5 times. The results after the 5 series of EDTA chemical cleaning can be seen in figure 6.3 and figure 6.4.iii clearing showing that the product was effective at removing the dark crust that had previously covered the surface of the glass.

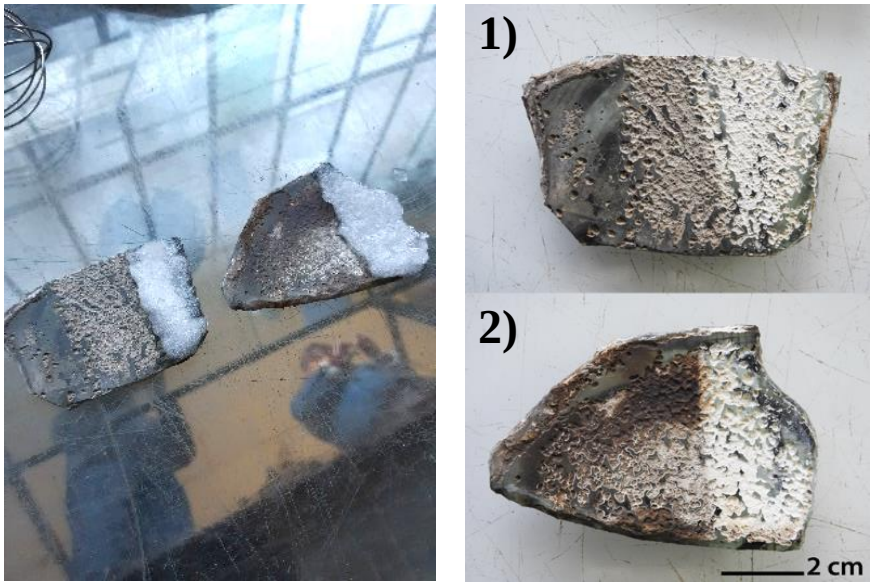

Figure 6.3: *Stained-glass from Chartres cathedral, France. Left: The glass pieces covered to allow the EDTA product to act. Right: The results after 2 subsequent treatments with the EDTA product.*

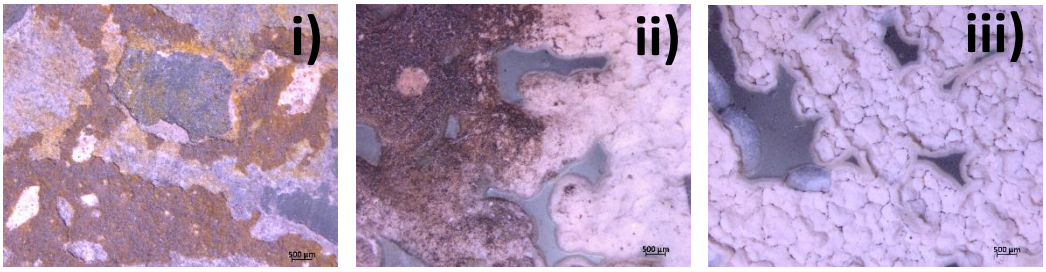

Figure 6.4: *Stained-glass from Chartres. i) The surface of glass 2 showing the extent of degradation before restoration. ii) An interface between a non-restored section and the one restored with 5 series with EDTA chemical in glass 2 and iii) The aspect of glass 2 surface after the 5 series of cleaning with EDTA product.*

6.2. Using Sodium thiosulfate chemical product to clean the stained-glasses

Sodium thiosulfate is best used to decontaminate glass surfaces that have paint/grisaille. In this study, carbogel was used instead of carbopol ultrez 21 in the preparation of the final chemical product to be used for the cleaning process.

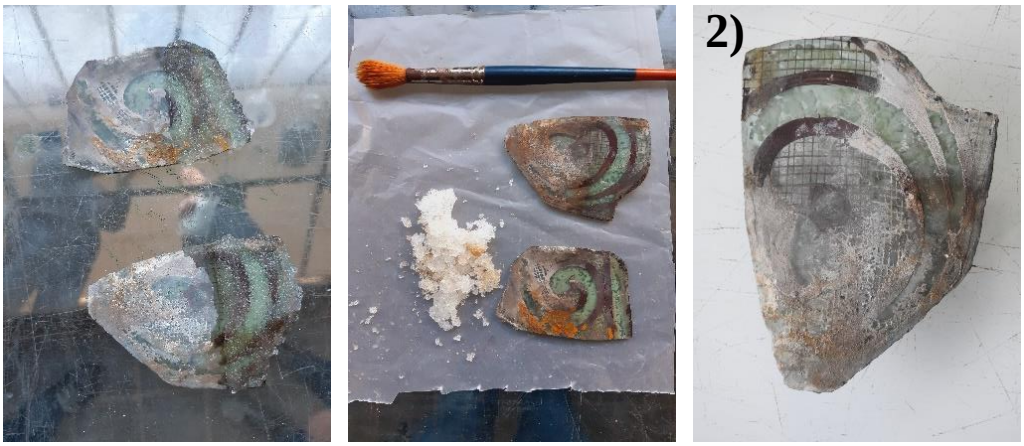

Figure 6.5: *Stained-glass from Chartres cathedral, France. Left: The glass pieces covered with Sodium thiosulfate product. Centre: After the product is wiped out with a soft brush. Right: The result after one treatment on glass 2 (top left part of the glass is after wiping out remnants of the dissolved white crust with a cotton swab wet with demineralized water).*

Sodium thiosulfate solution was prepared and applied on the glass side that had grisaille. As was the case when using EDTA, each application required a waiting time of about 2 h

before the subsequent application to allow the reacting agent to act. During this test, a single application was enough to dissolve the white crust without affecting the grisaille. The loosened white crust was scrubbed off mechanically with the use of a soft brush, softly stroking off the particles without leaving scratch marks (fig. 6.5). After, remnants of the white crust were removed using a cotton swab moistened with alcohol/acetone.

Tests in both cases using the two chemical products showed that the crust that had formed in the pores posed a challenge to remove with just a few chemical cleaning cycles. This crust often accumulating in the pores require more treatments combining both chemical and mechanical cleaning techniques to restore the glasses. Figure 6.6 show the results of the chemical and mechanical cleaning of the two glasses.

Figure 6.6: *Stained-glass from Chartres cathedral, France. Left: the two glasses after treatment with EDTA product. Right: After treatment with Sodium thiosulfate product.*

6.3. Using the fs UV laser to clean the Chartres glass

Laser interventions were considered in order to make a general comparison with the conventional restoration methods that were applied on the glasses from the Chartres. In this case, laser cleaning was performed on glass *2* using a fs UV laser. Due to the extent of the corrosion crust and the pitting affecting the glass, laser treatment conditions similar to those applied on the red glass from Chartres cathedral in Chapter 5 were selected. The distance between lines was kept at 15 µm, with a laser speed of 300 mm/s and a frequency of 20 kHz. The treatment was performed with the laser placed 4 cm above the focal plane. In these conditions the laser beam size has an elliptical shape with dimensions 2a= 90 µm and 2b= 50 µm. With this increase in the beam size, the levels of fluence and irradiance are similar to those used in the cleaning experiments used on the other glasses. Laser

cleaning was performed in six 5mm x 5mm squares as seen in figure 6.7. Table 6.1 shows the laser conditions that were applied in each of the squares. The irradiation series were applied in a loop, with a loop of 5 series taking approximately 1 minute to complete. However, initial treatment showed that the crust started to be removed when the laser energy per pulse reached 16.22 µJ/pulse (fluence 0.63 µJ/cm^2, irradiance 2635.3 GW/cm^2). In this case, further laser cleaning was performed mainting this laser energy level 16.22 µJ/pulse and only increasing the number of irradiation series in each loop.

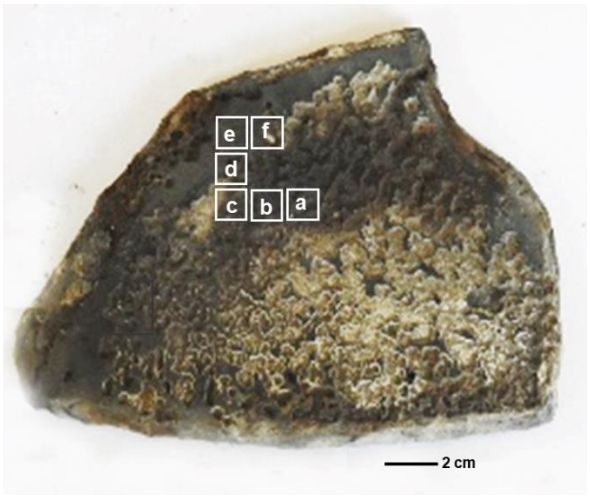

Figure 6.7: *Stained-glass from Chartres cathedral. The six selected sections for laser cleaning with fs UV laser in glass 2.*

Green Cuenca glass	*Power (W)*	*Energy per pulse (µJ)*	*Fluence (J/cm^2)*	*Irradiance (GW/cm^2)*	*No. of series in each loop*
a	3.24	16.22	0.63	2635.3	5
b	3.24	16.22	0.63	2635.3	20
c	3.24	16.22	0.63	2635.3	100
d	3.24	16.22	0.63	2635.3	20
e	3.24	16.22	0.63	2635.3	20
f	3.24	16.22	0.63	2635.3	50

Table 6.1: *Stained-glass from Chartres cathedral. fs UV laser conditions that were applied to clean the six sections in glass 2.*

Initial laser cleaning of glass 2 started by applying 5 irradiation series in a single loop in section *a*. At this amount of series there was a partial removal of the dark crust as can be seen in figure 6.8.a. The glass substrate did not show any signs of damage. The number of irradiation series in a loop were increased to 20 and with these conditions, the laser

cleaning process was more effective in the crust removal, as observed in figure 6.8.b, without signs of damage to the glass substrate. In section *c*, the number of irradiation series were increased to a total of 100 times. As seen in figure 6.8.c there was a complete and effective removal of the dark crust exposing a white coloured layer. This white coloured layer featured pits which are often a result of glass deterioration in a form of dissolution of glass elements resulting in creation of craters. Sufficient removal of the dark coloured crust was deemed complete with 100 series of irradiation taking approximately 18 minutes without inducing any damage to the glass surface.

Subsequent laser cleaning was targeted at glass regions that had the substrate exposed. In this case, the number of irradiation series were reduced to 20 in each loop to avoid any potential unforeseen damage to the glass itself. Laser cleaning on section *d* and *e* were performed by applying 20 series of irradiation each and even at this level of conditions the dark crust was sufficiently removed (figure 6.8.d and e). In figure 6.8.e it is observed that the laser was effective at removing the crust from the glass substrate with the surface of the glass left intact without any form of physical damage or any change of colour that is common with UV radiation. The same can be said of section f in figure 6.8, even after increasing the irradiation series to 50 times the integrity of the substrate is maintained and there is a greater improvement in the transparency of the glass.

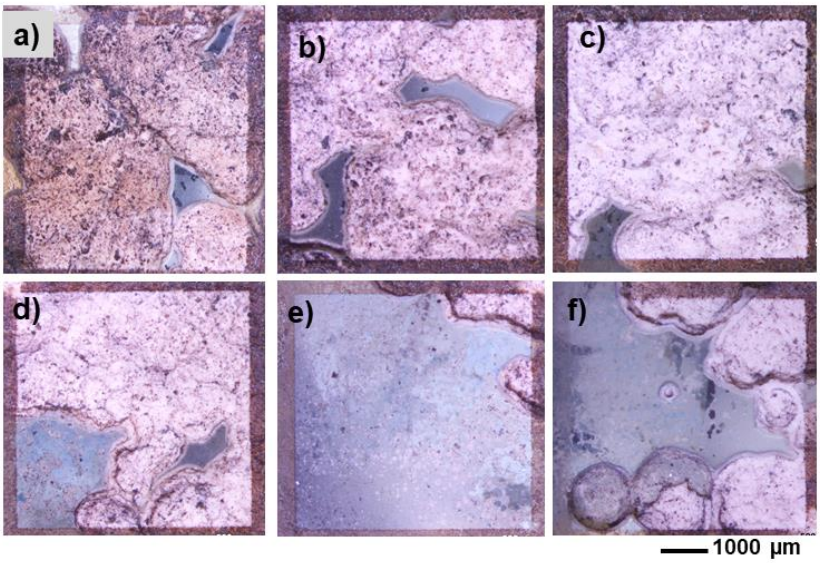

Figure 6.8: *Stained-glass from Chartres cathedral. The six sections in glass b after laser cleaning with fs UV laser at an energy per pulse value of 16.22 µJ/pulse for; a) 5 times, b) 20 times, c) 100 times, d) 20 times, e)20 times and f) 50 times in a loop.*

These two studies performed to remove corrosion crust from the glasses using chemical and mechanical methods and also by laser technique show that these techniques can effectively be applied to restore deteriorated glasses. In our case, we noted that the pits caused by long time dissolution of the glass poses a major challenge since the dark crust could be removed effectively even within the craters themselves. The long term effects of the chemical remnants on the glass after cleaning is an important aspect to be considered as this has been reported in literature to cause considered damage to the glasses and pigments (Altavilla *et al*., 2008; Murcia-Mascarós *et al*., 2008; Tennent & Newton, 1983). The same applies to mechanical removal of the crust that often remove microscopic scratch marks on the glass surface and which may also lead to lose of the part of the grisaille (Murcia-Mascarós *et al*., 2008). Also when using laser techniques, the parameters and conditions of operation have to be well defined to avoid problems that may occur some of which have been addressed in previous chapters of this work. The chemical cleaning combined with mechanical methods used in this study showed that to achieve a desirable removal of the crust it required a considered amount of time. In this, using the two chemical product mentioned in this chapter, it required a wait time of 2 hours for each application to take effect and this process would be repeated about 5 times or more leading to many hours for the whole process. The laser technique presented a comparatively shorter time of cleaning, about 18 minutes for the whole process.

CHAPTER 7: CONCLUSIONS

This research study has demonstrated that laser technology has gained great traction and is a powerful new tool in cultural heritage conservation offering vast possibilities in terms of its applicability when correct parameters are defined. This work has also shown that it is important to have an initial analyse of laser-material interactions to guarantee excellent results with laser cleaning.

This research work began with initial experiments using a set of different coloured contemporary stained glasses that are often used for restoration of historical stained-glass windows. This was in order to evaluate the influence of the different laser parameters and define a protocol that would later be applied when cleaning historical stained-glasses. Experiments were carried out on the contemporary glasses using three different short-pulsed laser operating in different wavelengths. Laser treatments were carried to evaluate the efficiency of using two different laser operating modes i.e. beam scan and burst mode. The glasses were coated with an artificial ink in order to evaluate and understand the phenomenology that occurs when this artificial layer is removed laser irradiation.

This work demonstrated that when laser cleaning is applied to remove contaminating layers from the surface of a glass, the limiting factor is the control of the maximum temperature reached within the outermost layer. Several experiments in this study showed that when laser energy levels are below the damage threshold, laser treatments that do not cause any direct damage to the glass can deteriorate it if they are applied to remove contaminants that are deposited on both glass surfaces. Using a thermocamera to record the temperature rise on the surface of the glasses during laser cleaning, it was determined that the heat generated on the contaminant material being cleaned induces a level of thermal stress which is high enough to cause thermal-mechanical cracks on the glass. In consequence, it was deduced that one of the main objectives of an ideal set of laser parameters to achieve an effective cleaning protocol is to minimize this heat input, referred in this case as heat accumulation.

Two different laser cleaning protocols were designed. When high frequency burst laser treatments are applied, the temperature reached is limited by selecting a maximum number of pulses at each position of the burst series and introducing a time lapse between each series. In the particular case of the n-IR 800 ps laser used in this work, pulses of 24 µJ (fluence 0.49 J/cm^2 and irradiance 0.61 GW/cm^2) in treatments with 200 pulses for 10

cycles or more, with non-irradiation time-lapse intervals between each treatment, resulted in a more observable and effective cleaning. This was also proved to be effective at avoiding micro-cracks and melting in the substrate, even if the glasses showed an important level of absorption if the time between toe consecutive cycles in a given position is higher than 30 s.

During this study a protocol using the burst mode to uniformly clean a select area was developed in order to avoid heat accumulation, a problem associated with the use of standard burst configuration. This protocol starts with the standard burst configuration, with this configuration being repeated by subsequently shifting the next lattices in a horizontal direction until a set of horizontal parallel lines are created. To completely clean a given area, the process is repeated moving all the created lattices a fraction vertically a number of times with a 10 s waiting time between each step until the whole area is covered. This protocol proved to be effective in cleaning a given surface without damaging the glass. However, this protocol had a limitation given the excessive number of waiting times in between each step. The option to avoid these problems was to increase the size of the area that was being treated. This proved to be a good option especially when the time required to complete a single series was longer than 30 s. This is because by the time the laser returns to the initial position to start the subsequent step this area of the sample has already cooled down after the previous treatment.

On the other hand, some new lasers have the possibility of reducing the effective pulse repetition frequency while maintaining the energy per pulse. In this case, the reduction of such frequency is sufficient to define safe cleaning protocols, even if scanning speeds are also reduced to maintain a desired pulse overlap. This was demonstrated in the present work with contemporary glass samples using a n-IR 228 fs laser-based treatment which provided irradiance values in the proximity of $10^4 GW/cm^2$. Safe laser treatments were achieved by limiting the pulse repetition frequency to 20 kHz or below.

This research work also showed that n-IR fs laser was very effective for removing contamination layers formed as a result of pollution and environmental factors, this layers are usually covering a patina of gypsum, anhydrite or calcite crust. Due to the high absorption level of this contamination layer, the n-IR laser was very effective in eliminating it. However, the efficacy of the fs IR laser cleaning is strongly reduced once this layer was eliminated exposing the underlying white patina. Therefore, the possibility of using fs UV radiation was also considered. Initial experiments using the a 238 fs UV

laser indicated that from a given level of energy, called optical damage threshold, there was a gradual lowering of transmittance values and browning of the colourless glass with the green glass showing faint darkening as the laser power was increased. These effects were associated with photo-oxidation of some of the elements that are present in the glass composition. It was concluded that when UV radiation is used, in addition to mechanical damage processes, these chemical damage processes have also to be considered. Further laser treatments using the burst and the beam scanning modes with the contemporary glasses implied that when using fs UV radiation, safe cleaning protocols would be realized by combining low frequency values that avoid heat accumulation, with pulse energy values lower than the optical damage threshold. It was also observed that changes induced by the UV laser were greater in the beam scanning configuration.

Finally, this initial work also demonstrated that because of the colour differences in the contemporary glasses and their chemical composition, these glasses exhibited different behaviour when exposed to laser radiation, an important factor that should be considered when laser cleaning historical stained-glasses that also have varied colours and chemistry. Usually, IR radiation generate higher thermal effects whereas UV radiation tend to cause chemical modifications on the material being processed.

The ideas established with the contemporary glasses proved essential in designing laser cleaning protocols that avoided glass damage when cleaning was carried out on the historic stained-glass windows from Cuenca and Chartres cathedrals. Prior to embarking on laser cleaning of the historical stained-glasses, a multi-characterization approach was applied to determine the chemical composition of the glasses as well as the type of compounds that were forming the corrosion products on the surface of these glasses. Through characterization it was established that the colourless and green glasses from Cuenca cathedral were glasses with high levels of K and Na, and the red glass from Chartres cathedral was a potash-lime glass, a category that was extensively used in the medieval times. The blue glass from Cuenca cathedral was a soda lime type. Further analysis showed that the corrosion crust covering the three glasses from Cuenca cathedral and the red one from Chartres cathedral was either a formation of gypsum or anhydrite with the colourless glass from Cuenca cathedral also having apatite in the crust matrix. The colourless glass had a dark-coloured external layer that was characterized as originating from a carbon compound. In addition, the green glass had calcite in the crust. Finally, the three glasses from Cuenca cathedral showed evidence of having a grisaille layer below the crust.

Given that the colourless glass from Cuenca cathedral had a dark-coloured layer of crust on the surface, laser cleaning was initially carried out using the fs IR following the same criteria of beam scanning protocol defined with the contemporary glasses. To avoid heat accumulation, the effective frequency was maintained at 10 kHz. The effectiveness of the cleaning was checked combining the energy of each pulse and the number of times that the cleaning process was repeated. When cleaning with the fs IR, it was observed that when inner layers of the putty or crust were reached, the efficiency of the cleaning process reduced because the absorption of the laser radiation became lower. However, with the fs UV it was possible to remove all the crust even with a low energy per pulse of 1.12 µJ/pulse without inducing any damage to the grisaille layer or to the glass substrate. Interestingly, due to an error with the laser control software an area of the colourless Cuenca glass irradiated with a high energy per pulse level of 46.6 µJ/pulse but did not cause any photo-oxidation effects as was the case with the colourless contemporary glass irradiated with the fs UV. However, this experience showed that at this level of laser energy it was possible to cause significant damage to the grisaille layer even with a single irradiation series as was later observed with the scanning electron microscope. This experience demonstrated the importance of adopting a double checking protocol in the laser system that ensures the restorer in charge double checks the emission parameters before the treatment is performed. Using the fs UV with the defined laser cleaning protocols, it was possible to remove the crusts from all the glasses.

The red Chartres glass was different given that the crust on the surface was thicker in comparison to the other glasses, in this case, an energy of 1.12 µJ/pulse applied on the other glasses was insufficient to remove the thick crust. Even multiple irradiation series were not sufficient to remove this crust. In this case, higher energy per pulse values with irradiation series being applied in a continuous loop were explored and this protocol was effective. Total removal of the thick crust was reached with energy per pulse value of 6.47 µJ/pulse with 300 series of irradiation in a loop.

Finally, experiments were carried to make a comparison of conventional cleaning techniques with laser cleaning protocols and this were performed to remove crust that was covering two glasses from the Chartres cathedral. Chemical cleaning was combined with mechanical methods where by the dark crust was eliminated by the application of reactive chemicals about 5 times with a wait time of 2 hours after each application. It was evident that the method was effective despite the longer time required for the whole process. However, as reported in previous chapters and in literature it is important to keep in mind

the long term effects of chemical remnants used as well as micro-scratches that might be left after mechanical interventions. It was also demonstrated that laser cleaning with the fs UV maintaining the laser fluence and irradiance values below the glass damage thresholds and frequencies lower than 20 kHz and only adjusting the irradiation series was effective in the removal of the crust without inducing any damage to the glass.

This work has demonstrated that ultra-short pulse lasers offer new opportunities to develop safe laser cleaning protocols that can be used in the restoration of stained-glass samples.

REFERENCES:

Aiello, D., Buccolieri, A., Buccolieri, G., Castellano, A., Di Giulio, M., Leo, L. S., Lorusso, A., Nassisi, G., Nassisi, V., & Torrisi, L. (2006). Selective laser cleaning of chlorine on ancient coins. *XVI International Symposium on Gas Flow, Chemical Lasers, and High-Power Lasers*, *6346*(63463), 63463H. https://doi.org/10.1117/12.739397

Al-Hassan, A. Y. (2009). An eighth century Arabic treatise on the colouring of glass: Kitāb al-Durra al-maknūna (the book of the hidden pearl) of Jābir ibn Hayyān (c. 721-c. 815). In *Arabic Sciences and Philosophy* (Vol. 19, Issue 1). https://doi.org/10.1017/S0957423909000605

Al Sekhaneh, W., El Serogy, A., & El-Bakri, M. (2015). Yag-laser cleaning of archaeological materials in Jordanian museums. *Mediterranean Archaeology and Archaeometry*, *15*(3), 157–164. https://doi.org/10.5281/zenodo.19297

Alberta, S., Gianmario, M., & Valentina, P. (2011). The stained glass window of the southern transept of St. Anthony's Basilica (Padova, Italy): Study of glasses and grisaille paint layers. *Spectrochimica Acta - Part B Atomic Spectroscopy*, *66*(1), 81–87. https://doi.org/10.1016/j.sab.2010.11.015

Alonso Abad, M. P., Peña Poza, J., Agua Martínez, F., Capel del Águila, F., García Heras, M., & Villegas, M. Á. (2019). Estudio histórico y arqueométrico de dos vidrieras de la Catedral de Astorga. *Ge-Conservacion*, *15*, 06–17. https://doi.org/10.37558/gec.v15i0.594

Altavilla, C., Ciliberto, E., La Delfa, S., Panarello, S., & Scandurra, A. (2008). The cleaning of early glasses: Investigation about the reactivity of different chemical treatments on the surface of ancient glasses. *Applied Physics A: Materials Science and Processing*, *92*(1), 251–255. https://doi.org/10.1007/s00339-008-4499-x

Andreotti, A., Colombini, M. P., Nevin, A., Melessanaki, K., Pouli, P., & Fotakis, C. (2006). Multianalytical Study of Laser Pulse Duration Effects in the IR Laser Cleaning of Wall Paintings from the Monumental Cemetery of Pisa. *Laser Chemistry*, *2006*, 1–11. https://doi.org/10.1155/2006/39046

Arif, S., & Kautek, W. (2015). Laser cleaning of paper: Cleaning efficiency and irradiation dose. *Studies in Conservation*, *60*, S97–S105. https://doi.org/10.1179/0039363015Z.000000000214

Asmus, J. F. (2010). Thirty-seven years of lasers in the conservation of art. *Rev. Cub. Fisica*, *27*(1), 3–8.

Bartoli, L., Pouli, P., Fotakis, C., Siano, S., & Salimbeni, R. (2006). Characterization of Stone Cleaning by Nd:YAG Lasers with Different Pulse Duration. *Laser Chemistry*, *2006*(May 2014), 1–6. https://doi.org/10.1155/2006/81750

Becherini, F., Bernardi, A., Daneo, A., Bianchini, F. G., Nicola, C., & Verità, M. (2014). Thermal Stress as a Possible Cause of Paintwork Loss in Medieval Stained Glass Windows. *Studies in Conservation*, *53*(4), 238–251. https://doi.org/10.1179/sic.2008.53.4.238

Bellendorf, P., Roemich, H., Gerlach, S., Mottner, P., López, E., & Wittstadt, K. (2010). Archaeological glass: the surface and beyond. *Glass and Ceramics Conservation*

2010: Interim Meeting of the ICOM-CC Working Group, October 3-6 2010 Corning, New York, U.S.A., February, 137–144.

Bernady, E., Kamińska, M., Płotek, M., & Walczak, M. (2018). The investigation of 15th century paint layers on two stained glass windows from the Dominican Monastery in Krakow, Poland. *Glass Technology: European Journal of Glass Science and Technology Part A*, *59*(2), 46–53. https://doi.org/10.13036/17533546.59.2.103

Bernardi, A., Becherini, F., Verità, M., Ausset, P., Bellio, M., Brinkmann, U., Cachier, H., Chabas, A., Deutsch, F., Etcheverry, M. P., Geotti Bianchini, F., Godoi, R. H. M., Kontozova-Deutsch, V., Lefèvre, R., Lombardo, T., Mottner, P., Nicola, C., Pallot-Frossard, I., Rölleke, S., … Van Grieken, R. (2013). Conservation of stained glass windows with protective glazing: Main results from the European VIDRIO research programme. *Journal of Cultural Heritage*, *14*(6), 527–536. https://doi.org/10.1016/j.culher.2012.11.009

Bhagavantam, S. (1938). Interpretation of Raman spectra in crystals: Anhydrite and gypsum. In *Proceedings of the Indian Academy of Sciences - Section A* (Vol. 8, Issue 5, pp. 345–348). https://doi.org/10.1007/BF03045904

Bilmes, G. M., Vallejo, J., Costa-Vera, C., & Garcia, M. E. (2018). High efficiencies for laser cleaning of glassware irradiated from the back: application to glassware historical objects. *Applied Physics A: Materials Science and Processing*, *124*(4). https://doi.org/10.1007/s00339-018-1761-8

Bordalo, R., Morais, P. J., Gouveia, H., & Young, C. (2006). Laser cleaning of easel paintings: An overview. *Laser Chemistry*, *2006*. https://doi.org/10.1155/2006/90279

Brems, D., & Degryse, P. (2014). Trace element analysis in provenancing Roman glass-making. *Archaeometry*, *56*(SUPPLS1), 116–136. https://doi.org/10.1111/arcm.12063

Brems, Dieter, Degryse, P., Hasendoncks, F., Gimeno, D., Silvestri, A., Vassilieva, E., Luypaers, S., & Honings, J. (2012). Western Mediterranean sand deposits as a raw material for Roman glass production. *Journal of Archaeological Science*, *39*(9), 2897–2907. https://doi.org/10.1016/j.jas.2012.03.009

Bumbrah, G. S., & Sharma, R. M. (2016). Raman spectroscopy – Basic principle, instrumentation and selected applications for the characterization of drugs of abuse. *Egyptian Journal of Forensic Sciences*, *6*(3), 209–215. https://doi.org/10.1016/j.ejfs.2015.06.001

Buzgar, N., Buzatu, A., & Sanislav, I. V. (2009). The Raman study on certain sulfates. *Analele Stiintifice Ale Universitatii " Al. I. Cuza" Din Iasi , Geologie*, *55*(1), 5–23. http://www.scopus.com/inward/record.url?eid=2-s2.0-84878729190&partnerID=tZOtx3y1%5Cnhttp://geology.uaic.ro/auig/article.php?id=26

Byrne, R. O. (2017). *Conservation of Historic Window Glass Author (s): Richard O . Byrne Source : Bulletin of the Association for Preservation Technology , Vol . 13 , No . 3 , Architectural Glass : History and Conservation (1981), pp . 3-9 Published by : Association for P*. *13*(3), 3–9.

Caldwell, Z. (2019). How was stained glass made in the Middle Ages ? *Art and Culture*, 2018–2020.

Capobianco, N., Hunault, M. O. J. Y., Loisel, C., Trichereau, B., Bauchau, F., Trcera, N.,

Galoisy, L., & Calas, G. (2021). The representation of skin colour in medieval stained glasses: The role of manganese. *Journal of Archaeological Science: Reports*, *38*(June), 103082. https://doi.org/10.1016/j.jasrep.2021.103082

Carmona, N., Villegas, M. A., & Navarro, J. M. F. (2006). Study of glasses with grisailles from historic stained glass windows of the cathedral of León (Spain). *Applied Surface Science*, *252*(16), 5936–5945. https://doi.org/10.1016/j.apsusc.2005.08.023

Carmona, Noemi, Wittstadt, K., & Römich, H. (2009). Consolidation of paint on stained glass windows: Comparative study and new approaches. *Journal of Cultural Heritage*, *10*(3), 403–409. https://doi.org/10.1016/j.culher.2008.12.004

Comite, V., Andreoli, M., Atzei, D., Barca, D., Fantauzzi, M., Russa, M. F. La, Rossi, A., Guglielmi, V., & Fermo, P. (2020). Degradation products on Byzantine glasses from Northern Tunisia. *Applied Sciences (Switzerland)*, *10*(21), 1–18. https://doi.org/10.3390/app10217523

Conchello, J. A., & Lichtman, J. W. (2005). Optical sectioning microscopy. *Nature Methods*, *2*(12), 920–931. https://doi.org/10.1038/nmeth815

Cooper, M. (2007). Lasers in the Preservation of Cultural Heritage: Principles and ApplicationsLasers in the Preservation of Cultural Heritage: Principles and Applications , C. Fotakis , D. Anglos , V. Zafiropulos , S. Georgiou and V. Tornari , Taylor & Francis, New York, 2. *Physics Today*, *60*(12), 58–59. https://doi.org/10.1063/1.2825073

Corrêa Pinto, A. M., Palomar, T., Alves, L. C., da Silva, S. H. M., Monteiro, R. C., Macedo, M. F., & Vilarigues, M. G. (2019). Fungal biodeterioration of stained-glass windows in monuments from Belém do Pará (Brazil). *International Biodeterioration and Biodegradation*, *138*(January), 106–113. https://doi.org/10.1016/j.ibiod.2019.01.008

Daher, C., Paris, C., Le Hô, A. S., Bellot-Gurlet, L., & Échard, J. P. (2010). A joint use of Raman and infrared spectroscopies for the identification ofnatural organic media used in ancient varnishes. *Journal of Raman Spectroscopy*, *41*(11), 1494–1499. https://doi.org/10.1002/jrs.2693

Dajnowski, A., & Dajnowski, B. A. (2017). *Using the new G.C. Laser Cleaning System for cleaning and surface preparation for re-gilding of a large outdoor bronze monument of Alexander Hamilton*. 217–228. https://doi.org/10.12775/3875-4.15

Danilatos, G. D. (1986). Colour micrographs for backscattered electron signals in the SEM. *Scanning*, *8*(1), 9–18. https://doi.org/10.1002/sca.4950080104

Davies, R. J., Burghammer, M., & Riekel, C. (2008). A combined microRaman and microdiffraction set-up at the European Synchrotron Radiation Facility ID13 beamline. *Journal of Synchrotron Radiation*, *16*(1), 22–29. https://doi.org/10.1107/S0909049508034663

de Cruz, A., Andreotti, A., Ceccarini, A., & Colombini, M. P. (2014). Laser cleaning of works of art: evaluation of the thermal stress induced by Er:YAG laser. *Applied Physics B: Lasers and Optics*, *117*(2), 533–541. https://doi.org/10.1007/s00340-014-5865-3

Degryse, P., & Schneider, J. (2008). Pliny the Elder and Sr-Nd isotopes: tracing the provenance of raw materials for Roman glass production. *Journal of Archaeological Science*, *35*(7), 1993–2000. https://doi.org/10.1016/j.jas.2008.01.002

Degryse, Patrick, Scott, R. B., & Brems, D. (2014). The archaeometry of ancient glassmaking: reconstructing ancient technology and the trade of raw materials. *Perspective*, *2*, 224–238. https://doi.org/10.4000/perspective.5617

Delgado, J. M., Nunes, D., Fortunato, E., Laia, C. A. T., Branco, L. C., & Vilarigues, M. (2017). The effect of three luminescent ionic liquids on corroded glass surfaces – A first step into stained-glass cleaning. *Corrosion Science*, *118*, 109–117. https://doi.org/10.1016/j.corsci.2017.01.027

Dickmann, K., Hildenhagen, J., Studer, J., & Müsch, E. (2005). *Archaeological Ironwork: Removal of Corrosion Layers by Nd:YAG-Laser*. 71–77. https://doi.org/10.1007/3-540-27176-7_9

Dickmann, Klaus, Klein, S., & Zafiropulos, V. (2001). Laser cleaning of marble: discoloration effects using various Nd:YAG laser wavelengths (ω, 2ω, 3ω). *Laser Techniques and Systems in Art Conservation*, *4402*, 54. https://doi.org/10.1117/12.445675

Drewello, U., Weißmann, R., Rölleke, S., Müller, E., Wuertz, S., Fekrsanati, F., Troll, C., & Drewello, R. (2000). Biogenic surface layers on historical window glass and the effect of excimer laser cleaning. *Journal of Cultural Heritage*, *1*(2), 161–171. https://doi.org/10.1016/S1296-2074(00)00183-7

Elnaggar, A., Mohamed, H., Mahgoub, G., & Fouad, M. (2010). Laser Cleaning of Excavated Greco-Roman Glass: Removal of Burial Encrustation and Corrosion Products. *Studies in Conservation*, *55*(sup2), 80–84. https://doi.org/10.1179/sic.2010.55.supplement-2.80

Fearn, S., McPhail, D. S., & Oakley, V. (2004). Room temperature corrosion of museum glass: An investigation using low-energy SIMS. *Applied Surface Science*, *231–232*, 510–514. https://doi.org/10.1016/j.apsusc.2004.03.205

Fekrsanati, F., Hildenhagen, J., Dickmann, K., Troll, C., Drewello, U., & Olaineck, C. (2000). UV-laser radiation: Basic research of the potential for cleaning stained glass. *Journal of Cultural Heritage*, *1*(2), 155–160. https://doi.org/10.1016/S1296-2074(00)00150-3

Fekrsanati, F., Klein, S., Hildenhagen, J., Dickmann, K., Marakis, Y., Manousaki, A., & Zafiropulos, V. (2001). Investigations regarding the behaviour of historic glass and its surface layers towards different wavelengths applied for laser cleaning. *Journal of Cultural Heritage*, *2*(4), 253–258. https://doi.org/10.1016/S1296-2074(01)01130-X

Fernandes, P., Vilarigues, M., Alves, L. C., & da Silva, R. C. (2008). Stained glasses from Monastery of Batalha: Non-destructive characterisation of glasses and glass paintings. *Journal of Cultural Heritage*, *9*(SUPPL.), 5–9. https://doi.org/10.1016/j.culher.2008.07.005

Ferrer, P., & Torres, A. R. De. (2013). *Molecular stratigraphic analysis with Raman spectroscopy of the shell of a mussel*. *34*, 82–84.

Frantzikinaki, K., Marakis, G., Panou, A., Vasiliadis, C., Papakonstantinou, E., Pouli, P., Ditsa, T., Zafiropulos, V., & Fotakis, C. (2007). The Cleaning of the Parthenon West Frieze by Means of Combined IR- and UV-Radiation. In *Lasers in the Conservation of Artworks*. https://doi.org/10.1007/978-3-540-72310-7_12

Freestone, I. C., Gorin-Rosen, Y., & Hughes, M. J. (2000). Primary glass from Israel and

the production of glass in late antiquity and the early Islamic period. *Travaux de La Maison de l'Orient*, *33*, 65–88.

Freestone, I., Greenwood, R., & Gorin-rosen, Y. (2002). Byzantine and Early Islamic Glassmaking in the Eastern Mediterranean: Production and Distribution of Primary Glass. In *1st Internatonal Conference Hylalos Vitrum Glass* (pp. 167–174).

García-Heras, M., Villegas, M. A., Caen, J. M. A., Domingo, C., & García-Ramos, J. V. (2006). Patination of historical stained windows lead cames from different European locations. *Microchemical Journal*, *83*(2), 81–90. https://doi.org/10.1016/j.microc.2006.03.001

García-Heras, Manuel, Carmona, N., Gil, C., & Villegas, M. A. (2005). Neorenaissance/Neobaroque stained glass windows from Madrid: A characterisation study on some panels signed by the Maumejean Fréres company. *Journal of Cultural Heritage*, *6*(2), 91–98. https://doi.org/10.1016/j.culher.2004.12.001

García-Heras, Manuel, Villegas, M. A., Cano, E., Pizano, F. C., & Bastidas, J. M. (2004). A conservation assessment on metallic elements from Spanish Medieval stained glass windows. *Journal of Cultural Heritage*, *5*(3), 311–317. https://doi.org/10.1016/j.culher.2004.01.003

Garcia-Vallès, M., Gimeno-Torrente, D., Martínez-Manent, S., & Fernández-Turiel, J. L. (2003). Medieval stained glass in a Mediterranean climate: Typology, weathering and glass decay, and associated biomineralization processes and products. *American Mineralogist*, *88*(11-12 PART 2), 1996–2006. https://doi.org/10.2138/am-2003-11-1244

Gemeda, B. T., Lahoz, R., Caldeira, A. T., & Schiavon, N. (2018). Efficacy of laser cleaning in the removal of biological patina on the volcanic scoria of the rock-hewn churches of Lalibela, Ethiopia. In *Environmental Earth Sciences* (Vol. 77, Issue 2). https://doi.org/10.1007/s12665-017-7223-3

Georgiou, S., Zafiropulos, V., Anglos, D., Balas, C., Tornari, V., & Fotakis, C. (1998). Excimer laser restoration of painted artworks: Procedures, mechanisms and effects. *Applied Surface Science*, *127–129*, 738–745. https://doi.org/10.1016/S0169-4332(97)00734-4

Guiheneuf, V., Delaleux, F., Riou, O., Logerais, P. O., & Durastanti, J. F. (2017). Investigation of damp heat effects on glass properties for photovoltaic applications. *Corrosion Engineering Science and Technology*, *52*(3), 170–177. https://doi.org/10.1080/1478422X.2016.1234803

Hunault, M. O. J. Y., Bauchau, F., Boulanger, K., Hérold, M., Calas, G., Lemasson, Q., Pichon, L., Pacheco, C., & Loisel, C. (2021). Thirteenth-century stained glass windows of the Sainte-Chapelle in Paris: An insight into medieval glazing work practices. *Journal of Archaeological Science: Reports*, *35*(August 2020). https://doi.org/10.1016/j.jasrep.2020.102753

Iglesias-Campos, M. A. (2014). Effects of mechanical cleaning by manual brushing and abrasive blasting on lime render coatings on Architectural Heritage. *Materiales de Construccion*, *64*(316), 1–8. https://doi.org/10.3989/mc.2014.08313

Janssens, K., Vittiglio, G., Deraedt, I., Aerts, A., Vekemans, B., Vincze, L., Wei, F., Deryck, I., Schalm, O., Adams, F., Rindby, A., Knöchel, A., Simionovici, A., & Snigirev, A. (2000). Use of Microscopic XRF for Non-destructive Analysis in Art

and Archaeometry. *X-Ray Spectrometry*, *29*(1), 73–91. https://doi.org/10.1002/(SICI)1097-4539(200001/02)29:1<73::AID-XRS416>3.0.CO;2-M

Joyce, A. M., & Kane, D. M. (2006). Comparison of front and back laser irradiation in laser cleaning of silica particles from silica glass. *PICALO 2006 - 2nd Pacific International Conference on Applications of Laser and Optics - Conference Proceedings*, *299*, 299–304. https://doi.org/10.2351/1.5056947

Kautek, W., & Pentzien, S. (2005). *Laser Cleaning System for Automated Paper and Parchment Cleaning*. *January*, 403–410. https://doi.org/10.1007/3-540-27176-7_51

Kerse, C., Kalaycloğ Lu, H., Elahi, P., Çetin, B., Kesim, D. K., Akçaalan, Ö., Yavaş, S., Aşlk, M. D., Öktem, B., Hoogland, H., Holzwarth, R., & Ilday, F. Ö. (2016). Ablation-cooled material removal with ultrafast bursts of pulses. *Nature*, *537*(7618), 84–88. https://doi.org/10.1038/nature18619

Koh, Y. S. (2006). *Laser Cleaning as a Conservation Technique for Corroded Metal Artifacts*. 144. http://epubl.ltu.se/1402-1544/2006/02/LTU-DT-0602-SE.pdf

Kontozova-Deutsch, V., Deutsch, F., Godoi, R. H. M., Van Grieken, R., & De Wael, K. (2011). Urban air pollutants and their micro effects on medieval stained glass windows. *Microchemical Journal*, *99*(2), 508–513. https://doi.org/10.1016/j.microc.2011.07.003

Koob, S. P., & Davison, S. (2004). Conservation and Restoration of Glass. In *Journal of the American Institute for Conservation* (Vol. 43, Issue 3). https://doi.org/10.2307/4129645

Koussi, E. K., Jung, H. J., Faure, N., Donnet, C., Mauclair, C., & Sedao, X. (2020). Comparative Study of Ultraviolet and Infrared Femtosecond Laser Irradiation on Textile Polymers PET and PA66. *Journal of Laser Micro Nanoengineering*, *15*(3), 245–251. https://doi.org/10.2961/jlmn.2020.03.2015

Krok, F., M.Walczak, Karaszkiewicz, P., Szelagowska, K., Szymonski, M., & Prauzner-Bechcicki, J. (2010). Comparative study of historic stained glass by LIBS and SEM/EDX. *Lasers in the Conservation of Artworks*, *June 2017*, 141–145. https://doi.org/10.1201/9780203882085.ch22

Lapczyna, M., Chen, K. P., Herman, P. R., Tan, H. W., & Marjoribanks, R. S. (1999). Ultra high repetition rate (133 MHz) laser ablation of aluminum with 1.2-ps pulses. *Applied Physics A: Materials Science and Processing*, *69*(7), 1–5. https://doi.org/10.1007/s003390051552

Legrand, S., Van der Snickt, G., Cagno, S., Caen, J., & Janssens, K. (2019). MA-XRF imaging as a tool to characterize the 16th century heraldic stained-glass panels in Ghent Saint Bavo Cathedral. *Journal of Cultural Heritage*, *40*(2019), 163–168. https://doi.org/10.1016/j.culher.2019.06.003

Lentjes, M. (2007). *Controlled Laser Cleaning of Artworks Via Low Resolution Plasma Spectroscopy and Linear*.

Litasov, K. D., & Podgornykh, N. M. (2017). Raman spectroscopy of various phosphate minerals and occurrence of tuite in the Elga IIE iron meteorite. *Journal of Raman Spectroscopy*, *48*(11), 1518–1527. https://doi.org/10.1002/jrs.5119

Liu, J. M. (1982). Simple technique for measurements of pulsed Gaussian-beam spot sizes. *Optics Letters*, *7*(5), 196. https://doi.org/10.1364/ol.7.000196

Liu, Y. (2009). RAMAN, MIR, AND NIR SPECTROSCOPIC STUDY OF CALCIUM SULFATES: GYPSUM, BASSANITE, AND ANHYDRITE. *40th Lunar and Planetary Science Conference*, *50*(2).

Lu, Y. F., Komuro, S., & Aoyagi, Y. (1994). Laser-induced removal of fingerprints from glass and quartz surfaces. *Japanese Journal of Applied Physics*, *33*(8 R), 4691–4696. https://doi.org/10.1143/JJAP.33.4691

M. Corrêa Pinto, A., Macedo, M. F., & G. Vilarigues, M. (2018). The conservation of stained-glass windows in Latin America: A literature overview. *Journal of Cultural Heritage*, *34*, 172–181. https://doi.org/10.1016/j.culher.2018.04.019

Mahamood, R. M. (2018). *Laser Basics and Laser Material Interactions*. https://doi.org/10.1007/978-3-319-64985-6_2

Maingi, E. M., Alonso, M. P., Angurel, L. A., Rahman, M. A., Chapoulie, R., Dubernet, S., & de la Fuente, G. F. (2022). Historical stained-glass window laser preservation: The heat accumulation challenge. *Boletin de La Sociedad Espanola de Ceramica y Vidrio*, *1*, 69–82. https://doi.org/10.1016/j.bsecv.2021.12.003

Marucci, G., Beeby, A., Parker, A. W., & Nicholson, C. E. (2018). Raman spectroscopic library of medieval pigments collected with five different wavelengths for investigation of illuminated manuscripts. *Analytical Methods*, *10*(10), 1219–1236. https://doi.org/10.1039/c8ay00016f

Mateo, M. P., Nicolas, G., Piñon, V., Ramil, A., & Yañez, A. (2005). Laser cleaning: An alternative method for removing oil-spill fuel residues. *Applied Surface Science*, *247*(1–4), 333–339. https://doi.org/10.1016/j.apsusc.2005.01.086

Matteini, M., Lalli, C., Tosini, I., Giusti, A., & Siano, S. (2003). Laser and chemical cleaning tests for the conservation of the Porta del Paradiso by Lorenzo Ghiberti. *Journal of Cultural Heritage*, *4*(SUPPL. 1), 147–151. https://doi.org/10.1016/s1296-2074(02)01190-1

McMullan, D. (1995). Scanning electron microscopy 1928–1965. *Scanning*, *17*(3), 175–185. https://doi.org/10.1002/sca.4950170309

Merino, R. I., Laguna-bercero, M. A., Lahoz, R., Larrea, Á., Luisa, M., Sola, D., Oliete, P. B., Orera, A., & Pe, J. I. (2021). *Laser processing of ceramic materials for electrochemical and high temperature energy applications*. 1–21.

Murcia-Mascarós, S., Foglia, P., Santarelli, M. L., Roldán, C., Ibañez, R., Muñoz, A., & Muñoz, P. (2008). A new cleaning method for historic stained glass windows. *Journal of Cultural Heritage*, *9*(SUPPL.). https://doi.org/10.1016/j.culher.2008.08.008

Murphy, D. B. (2001). and Electronic. In *Imaging* (Vol. 83, Issue 991). http://www.ncbi.nlm.nih.gov/pubmed/20701335

Navarro, J. M. F. (1996). Procesos de alteración de las vidrieras medievales: estudio y tratamientos de protección TT - Alteration processes of Medieval stained glass windows: study and protection treatments. *Materiales de Construcción*, *46*(242–243), 5–25.

News, A. M., Organizations, A., Memoriam, I., Noting, W., Programs, C. T., Columns, S. G., & Columns, N. (2017). *Update on Laser Ablation Technology : Conservation Applications for In-Situ Objects and Architecture within the United States*. *42*(1), 1–28.

Ngo, C. C., Nguyen, Q. H., Nguyen, T. H., Quach, N. T., Dudhagara, P., Vu, T. H. N., Le, T. T. X., Le, T. T. H., Do, T. T. H., Nguyen, V. D., Nguyen, N. T., & Phi, Q.-T. (2021). Identification of Fungal Community Associated with Deterioration of Optical Observation Instruments of Museums in Northern Vietnam. *Applied Sciences*, *11*(12), 5351. https://doi.org/10.3390/app11125351

Op, E., & Halogen-free, T. (2019). *CLOSURES , DOORS AND WINDOWS*. 1–17.

Osticioli, I., Mencaglia, A. A., & Siano, S. (2017). Temperature-controlled portable Raman spectroscopy of photothermally sensitive pigments. *Sensors and Actuators, B: Chemical*, *238*, 772–778. https://doi.org/10.1016/j.snb.2016.07.104

Oujja, M., Rebollar, E., Castillejo, M., Domingo, C., Cirujano, C., & Guerra-Librero, F. (2005). Laser cleaning of terracotta decorations of the portal of Palos of the Cathedral of Seville. *Journal of Cultural Heritage*, *6*(4), 321–327. https://doi.org/10.1016/j.culher.2005.05.001

Paddock, S. W. (1999). Confocal laser scanning microscopy. *BioTechniques*, *27*(5), 992–1004. https://doi.org/10.2144/99275ov01

Palomar, T., Grazia, C., Pombo Cardoso, I., Vilarigues, M., Miliani, C., & Romani, A. (2019a). Analysis of chromophores in stained-glass windows using Visible Hyperspectral Imaging in-situ. *Spectrochimica Acta - Part A: Molecular and Biomolecular Spectroscopy*, *223*, 117378. https://doi.org/10.1016/j.saa.2019.117378

Palomar, T., Grazia, C., Pombo Cardoso, I., Vilarigues, M., Miliani, C., & Romani, A. (2019b). Analysis of chromophores in stained-glass windows using Visible Hyperspectral Imaging in-situ. *Spectrochimica Acta - Part A: Molecular and Biomolecular Spectroscopy*, *223*. https://doi.org/10.1016/j.saa.2019.117378

Papanikolaou, A., Siozos, P., Philippidis, A., Melessanaki, K., Pouli, P., & Vi, V. I. (2008). Towards the understanding of the two wavelength laser cleaning in avoiding yellowing on stonework: a micro-Raman and LIBS study. In *Lasers in the Conservation of Artworks* (Issue January). https://doi.org/10.1201/9780203882085

Peterson, D. A. (2010). Confocal Microscopy. *Encyclopedia of Movement Disorders*, 250–252. https://doi.org/10.1016/B978-0-12-374105-9.00230-6

Pinto, A. M. C., Sanjad, T. A. B. C., Angélica, R. S., Da Costa, M. L., Paiva, R. S., & Palomar, T. (2018). 19th century stained-glass windows from Belém do Pará (Brazil): Analytical characterisation and pathology. *Boletin de La Sociedad Espanola de Ceramica y Vidrio*, *57*(4), 133–141. https://doi.org/10.1016/j.bsecv.2017.10.005

Popović, L., Manoun, B., De Waal, D., Nieuwoudt, M. K., & Comins, J. D. (2003). Raman spectroscopic study of phase transitions in Li3PO4. *Journal of Raman Spectroscopy*, *34*(1), 77–83. https://doi.org/10.1002/jrs.954

Pouli, P., Bounos, G., Georgiou, S., & Fotakis, C. (2007). Femtosecond Laser Cleaning of Painted Artefacts; Is this the Way Forward? *Lasers in the Conservation of Artworks*, 287–293. https://doi.org/10.1007/978-3-540-72310-7_33

Pouli, Paraskevi, Paun, I. A., Bounos, G., Georgiou, S., & Fotakis, C. (2008). The potential of UV femtosecond laser ablation for varnish removal in the restoration of painted works of art. *Applied Surface Science*, *254*(21), 6875–6879. https://doi.org/10.1016/j.apsusc.2008.04.106

Reynolds, E. (Aislin). (2013). The Development of Stained Glass in Gothic Cathedrals.

JCCC Honors Journal, *4*(1), 3.

Richet, P. (2007). *Une brève histoire du verre*. *13*, 4–8.

Roemich, H., Gerlach, S., Mottner, P., Mees, F., Jacobs, P., Van Dyck, D., & Doménech Carbó, T. (2003). Results from burial experiments with simulated medieval glasses. *Materials Research Society Symposium - Proceedings*, *757*(January), 97–108. https://doi.org/10.1557/proc-757-ii2.3

Römich, H., Dickmann, K., Mottner, P., Hildenhagen, J., & Müller, E. (2003a). Laser cleaning of stained glass windows - Final results of a research project. *Journal of Cultural Heritage*, *4*(SUPPL. 1), 112–117. https://doi.org/10.1016/s1296-2074(02)01187-1

Römich, H., Dickmann, K., Mottner, P., Hildenhagen, J., & Müller, E. (2003b). Laser cleaning of stained glass windows – Final results of a research project. *Journal of Cultural Heritage*, *4*, 112–117. https://doi.org/10.1016/s1296-2074(02)01187-1

Römich, H., & Weinmann, A. (2000). Laser cleaning of stained glass windows. Overview on an interdisciplinary project. *Journal of Cultural Heritage*, *1*(2), 151–154. https://doi.org/10.1016/S1296-2074(00)00186-2

Sadezky, A., Muckenhuber, H., Grothe, H., Niessner, R., & Pöschl, U. (2005). Raman microspectroscopy of soot and related carbonaceous materials: Spectral analysis and structural information. *Carbon*, *43*(8), 1731–1742. https://doi.org/10.1016/j.carbon.2005.02.018

Salimbeni, R., Zafiropulos, V., Radvan, R., Verges-Belmin, V., Kautek, W., Andreoni, A., Sliwinski, G., Castillejo, M., & Ahmad, S. R. (2005). <title>Lasers in conservation of artworks: the European Community research</title>. *Advanced Laser Technologies 2004*, *5850*(September 2016), 33–42. https://doi.org/10.1117/12.633536

Schalm, O., Janssens, K., & Caen, J. (2003). Characterization of the main causes of deterioration of grisaille paint layers in 19th century stained-glass windows by J.-B. Capronnier. *Spectrochimica Acta - Part B Atomic Spectroscopy*, *58*(4), 589–607. https://doi.org/10.1016/S0584-8547(02)00282-3

Schalm, Olivier, Janssens, K., Wouters, H., & Caluwé, D. (2007). Composition of 12-18th century window glass in Belgium: Non-figurative windows in secular buildings and stained-glass windows in religious buildings. *Spectrochimica Acta - Part B Atomic Spectroscopy*, *62*(6-7 SPEC. ISS.), 663–668. https://doi.org/10.1016/j.sab.2007.03.006

Schalm, Olivier, Janssens, K., Wouters, H., Caluwé, D., Römich, H., Dickmann, K., Mottner, P., Hildenhagen, J., Müller, E., Weinmann, A., Carmona, N., Villegas, M. Á. A., Navarro, J. M. F., Godoi, R. H. M. H. M., Kontozova, V., Van Grieken, R., Pinto, A. M. C., Sanjad, T. A. B. C., Angélica, R. S., … Olaineck, C. (2011). 19th century stained-glass windows from Belém do Pará (Brazil): Analytical characterisation and pathology. *Journal of Cultural Heritage*, *9*(2), 133–141. https://doi.org/10.1016/j.bsecv.2017.10.005

Schreiner, M. (1991). Glass of the past: The degradation and deterioration of medieval glass artifacts. *Mikrochimica Acta*, *104*(1–6), 255–264. https://doi.org/10.1007/BF01245513

Shackley, M. S. (2011). X-Ray Fluorescence Spectrometry (XRF) in Geoarchaeology. In

X-Ray Fluorescence Spectrometry (XRF) in Geoarchaeology. https://doi.org/10.1007/978-1-4419-6886-9

Shugar, A., Lough, K., & Chen, J. J. (2017). Characterization of a Surface Tarnish Found on Daguerreotypes Revealed under Shortwave Ultraviolet Radiation. *MRS Proceedings*, *1656*, 319–333. https://doi.org/10.1557/opl.2014.706

Siano, S., Agresti, J., Cacciari, I., Ciofini, D., Mascalchi, M., Osticioli, I., & Mencaglia, A. A. (2012). Laser cleaning in conservation of stone, metal, and painted artifacts: State of the art and new insights on the use of the Nd:YAG lasers. *Applied Physics A: Materials Science and Processing*, *106*(2), 419–446. https://doi.org/10.1007/s00339-011-6690-8

Smith, K. C. A., & Oatley, C. W. (1955). The scanning electron microscope and its fields of application. *British Journal of Applied Physics*, *6*(11), 391–399. https://doi.org/10.1088/0508-3443/6/11/304

Stokes, D. J. (2008). Principles and Practice of Variable Pressure/Environmental Scanning Electron Microscopy (VP-ESEM). In *Principles and Practice of Variable Pressure/Environmental Scanning Electron Microscopy (VP-ESEM)*. https://doi.org/10.1002/9780470758731

Strassl, M., Wieger, V., Brodoceanu, D., Beer, F., Moritz, A., & Wintner, E. (2008). Ultra-short pulse laser ablation of biological hard tissue and biocompatibles. *Journal of Laser Micro Nanoengineering*, *3*(1), 30–40. https://doi.org/10.2961/jlmn.2008.01.0007

Striova, J., Fontana, R., Barbetti, I., Pezzati, L., Fedele, A., & Riminesi, C. (2021). Multisensorial assessment of laser effects on shellac applied on wall paintings. *Sensors*, *21*(10). https://doi.org/10.3390/s21103354

Suzuki. (2002). *High resolution scanning electron microscopy of immunogold labelled cells by the use of thin plasma coating of osmium.*

Tang, N. (2009). ARCHAEOMETRICAL INVESTIGATION OF SOME MEDIEVAL GLASS SAMPLES FROM ALANYA REGION. *Master Thesis*. http://dx.doi.org/10.1016/B978-0-12-849873-6.00001-7%0Ahttp://saber.ucv.ve/ojs/index.php/rev_venes/article/view/1112%0Ahttps://www.bps.go.id/dynamictable/2018/05/18/1337/persentase-panjang-jalan-tol-yang-beroperasi-menurut-operatornya-2014.html

Tennent, N. H., & Newton, R. G. (1983). The Deterioration and Conservation of Painted Glass: A Critical Bibliography. In *Studies in Conservation* (Vol. 28, Issue 4). https://doi.org/10.2307/1505971

Terry, A. D. (2006). A history of Stained Glass and its techniques from Medieval to Modern times. *The Grove Encyclopedia of Decorative Arts. Oxford University Press.*, *5*(23), 1–15.

Teule, R., Scholten, H., van den Brink, O. F., Heeren, R. M. A., Zafiropulos, V., Hesterman, R., Castillejo, M., Martín, M., Ullenius, U., Larsson, I., Guerra-Librero, F., Silva, A., Gouveia, H., & Albuquerque, M. B. (2003). Controlled UV laser cleaning of painted artworks: S systematic effect study on egg tempera paint samples. *Journal of Cultural Heritage*, *4*(SUPPL. 1), 209–215. https://doi.org/10.1016/s1296-2074(02)01137-8

Tomasini, E. P., Gómez, B., Halac, E. B., Reinoso, M., Di Liscia, E. J., Siracusano, G., &

Maier, M. S. (2015). Identification of carbon-based black pigments in four South American polychrome wooden sculptures by Raman microscopy. *Heritage Science*, *3*(1), 4–11. https://doi.org/10.1186/s40494-015-0049-y

Torrero, E., Sanz, D., Arroyo, M. N., & Navarro, V. (2015). The cathedral of Santa María (Cuenca, Spain): Principal stone characterization and conservation status. *International Journal of Conservation Science*, *6*(4), 625–632.

Ueda, M., Makino, R., Kagawa, K. ichiro, & Nishiyama, B. ichi. (1991). Laser cleaning of glass. *Optics and Lasers in Engineering*, *15*(4), 275–278. https://doi.org/10.1016/0143-8166(91)90065-2

Van der Snickt, G., Legrand, S., Caen, J., Vanmeert, F., Alfeld, M., & Janssens, K. (2016). Chemical imaging of stained-glass windows by means of macro X-ray fluorescence (MA-XRF) scanning. *Microchemical Journal*, *124*(2016), 615–622. https://doi.org/10.1016/j.microc.2015.10.010

Vandenabeele, P. (2007). B. Stuart: Analytical techniques in materials conservation. *Analytical and Bioanalytical Chemistry*, *389*(7–8), 2035–2036. https://doi.org/10.1007/s00216-007-1658-4

Vandenabeele, P. (2013). *Practical Raman spectroscopy*.

Vogel, N. A., & Achilles, R. (n.d.). *Preservation briefs*.

Vondráčková, T., Nývlt, V., & Němec, F. (2016). Characteristics of Gothic Cathedrals in France and their Structural Elements. *Procedia Engineering*, *161*, 1751–1756. https://doi.org/10.1016/j.proeng.2016.08.771

Webb, E. K. (2020). UV-induced visible luminescence for conservation documentation. *UV-Vis Luminescence Imaging Techniques*, 35–60.

Weber, R., Graf, T., Berger, P., Onuseit, V., Wiedenmann, M., Freitag, C., & Feuer, A. (2014). Heat accumulation during pulsed laser materials processing. *Optics Express*, *22*(9), 11312. https://doi.org/10.1364/oe.22.011312

White, S. N. (2009). Laser Raman spectroscopy as a technique for identification of seafloor hydrothermal and cold seep minerals. *Chemical Geology*, *259*(3–4), 240–252. https://doi.org/10.1016/j.chemgeo.2008.11.008

Winer, I. M. (1966). A Self-Calibrating Technique Measuring Laser Beam Intensity Distributions. *Applied Optics*, *5*(9), 1437. https://doi.org/10.1364/ao.5.001437

Wittstadt, K., Maas-diegeler, G., Bellendorf, P., & Dirsch, C. (2008). *A Special Kind of Crack Pattern on Historic Glass – Exploring the Causes of ' Sugaring . '* 21–30.

Yariv, A. (1975). *Yariv A. - Quantum Electronics.pdf*.

Zanini, A., Trafeli, V., & Bartoli, L. (2018). The laser as a tool for the cleaning of Cultural Heritage. *IOP Conference Series: Materials Science and Engineering*, *364*(1). https://doi.org/10.1088/1757-899X/364/1/012078

Zheng, J., Cheng, C., Fang, W., Chen, C., & Yan, R. (2014). *1. Introduction*. *8*(1959), 3960–3964.